

INTERPLANETARY COLLISIONLESS SHOCK WAVES

BY

JIH-KWIN CHAO

B. S., National Taiwan University
1962

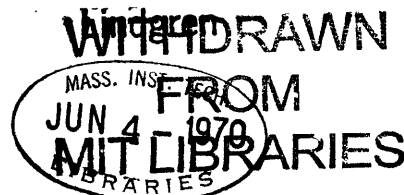
M. S., University of Alaska
1965

SUBMITTED IN PARTIAL FULFILLMENT OF THE
REQUIREMENTS FOR THE DEGREE OF
DOCTOR OF SCIENCE
AT THE
MASSACHUSETTS INSTITUTE OF TECHNOLOGY

Signature of Author _____
Department of Meteorology, 8 January 1970

Certified by _____ Thesis Supervisor

Accepted by _____
Chairman, Departmental Committee
on Graduate Students



INTERPLANETARY COLLISIONLESS SHOCK WAVES

BY

JIH-KWIN CHAO

Submitted to the Department of Meteorology on 8 January 1970 in partial fulfillment of the requirement for the degree of Doctor of Science.

ABSTRACT

Mathematical Relations for MHD shocks in the interplanetary plasma are investigated. The possibility for the presence of the thermal anisotropy is allowed for. The obtained set of equations represents a generalization of the MHD Rankine-Hugoniot relations for isotropic plasma. The so-called "coplanarity theorem" is proven to be valid also for anisotropic plasmas. The experimental data from Pioneer 6, Pioneer 7 and Mariner V referring to both the positive ions of the solar wind and the interplanetary magnetic field have been searched through for a combined period of about ten months for shock-like discontinuities. Seven discontinuities have been discovered and analyzed in detail. Advantage was taken of the following two facts: (a) experimental knowledge of all three components of the magnetic field and the solar wind velocity on both sides of the shock, as well as the knowledge of the density jump across the shock; (b) The simultaneous presence of other satellites in the interplanetary space at the time of observation of the seven shocks. The first fact implies that the data are more complete than those available to other investigators of the interplanetary shocks, and render, for the first time, an opportunity for testing the validity of MHD shock relations. The second fact permit us to develop a new method for determining the shock normal and the shock speed. The transit time of the shock between two spacecraft, offers an additional test for the validity of shock relations. All seven discontinuities are demonstrated as MHD shocks: five of them turn out to be "fast" and two "slow" shocks. The slow shocks are believed to be the first experimental examples ever observed. Finally, the effects of the thermal anisotropies on the shock relations and differences between electron and ion temperatures are discussed. It is found that the plasma behind the shock is more isotropic than that ahead of the shock.

Thesis Supervisor: Stanislaw Olbert

Title: Professor of Physics

TABLE OF CONTENTS

Title Page

Abstract

Table of Contents

List of Tables

List of Figure Captions

1. Introduction
2. Magnetohydrodynamic Model of the Collisionless Shock Waves
 - 2.1 Basic Equations of Collisionless Shocks--Fluid Description
 - 2.2 General Jump Conditions in MHD Discontinuities
 - 2.2.1 The coplanarity theorem
 - 2.2.2 Simplified shock equations for scalar pressures
 - 2.2.3 Review of various discontinuities in isotropic plasmas
 - 2.2.4 Anisotropic plasma
3. Detailed Study of the Jump Conditions for Anisotropic Pressure
 - 3.1 On the Choice of the Proper Root of Shock Equations
 - 3.2 The Concept and the Role of the Anisotropy Parameter in the Jump Conditions
 - 3.3 The Numerical Solutions
4. A Method of Identification of the Shock Frames with the Help of the Transit Time
 - 4.1 Analytical Expressions for Shock Normal
 - 4.2 Analytical Expressions for Magnetic Field Components in Shock Frame of Reference
5. Experimental Evidence of the Interplanetary Collisionless Shocks
 - 5.1 Introductory Remarks
 - 5.2 Results of the Analysis of the Seven Shock-like Events
 - 5.3 Spatial Distribution of the Shock Normals
6. The Two-Fluid Character and Pressure Anisotropy of the Interplanetary Shocks

- 6.1 General Remarks About Differences Between Positive-Ion and Electron Anisotropies
- 6.2 Relations Between M_S , P'/P , ξ' and ξ Derivable from Equations (2.79), (2.80), (4.27) and Experimental Data of a Given Shock
- 6.3 Results of Numerical Computations of ξ' , M_S and P'/P as Functions of ξ
- 6.4 Attempts to Estimate the Electron Temperature from Available Data

7. Summary of the Results

- 7.1 Critical Review of Observational Findings
- 7.2 Resume of Analytical Investigations

Appendix A Shock Equations for Anisotropic Plasmas

Appendix B Proof for Common Intersection Point in the Family of Curves Shown in Figures (3.1) to (3.5)

Appendix C The "Best-Fit" Procedure for Matching the MHD Shock Relations with the Data

References

Acknowledgement

Biographical Note

LIST OF TABLES

- Table 2-1 Basic MHD Shocks and Discontinuities .
- Table 3-1 The Numerical Ranges of Constants M_A , M_S , Θ_B , ξ and ξ' .
- Table 5-1 The Primary and Secondary Spacecraft and the Identified Shock-like Discontinuities .
- 5-2 Measured Averages of Magnetic Field and Plasma Parameters Across (The Shocks of March 22, 1966).
- 5-3 Measured Averages of Magnetic Field and Plasma Parameters Across (The Shocks of March 23, 1966).
- 5-4 Physical Parameters Associated with March 22, 1966 Shock and Obtained from the "Best-Fit Matching Procedure".
- 5-5 Physical Parameters Associated with March 23, 1966 Shock and Obtained from the "Best-Fit Matching Procedure".
- 5-6 Measured Averages of Magnetic Field and Plasma Parameters Across the Shock of August 29, 1966.
- 5-7 Measured Averages of Magnetic Field and Plasma Parameters Across the Shock of June 26, 1967.
- 5-8 Measured Averages of Magnetic Field and Plasma Parameters Across the Shock of August 29, 1967.
- 5-9 Physical Parameters Associated with August 29, 1966 Shock and Obtained from the "Best-Fit Matching Procedure".
- 5-10 Physical Parameters Associated with June 26, 1967 Shock and Obtained from the "Best-Fit Matching Procedure".
- 5-11 Physical Parameters Associated with August 29, 1967 Shock and Obtained from the "Best-Fit Matching Procedure".

- Table 5-12 Measured Averages of Magnetic Field and Plasma Parameters Across the Shock of July 20, 1967.
- 5-13 Measured Averages of Magnetic Field and Plasma Parameters Across the Shock of August 30, 1967.
- 5-14 Physical Parameters Associated with July 20, 1967 Shock and Obtained from the "Best-Fit Matching Procedure".
- 5-15 Physical Parameters Associated with August 30, 1967 Shock and Obtained from the "Best-Fit Matching Procedure".
- 5-16 Shock Normals and Possible Solar Flares Associated with Them.
- Table 6-1 Best-Fit Values of η and the Measured Parameters, w_0 and $P^{(i)}/(B^2/2\mu_0)$.
- 6-2 The Ion and Electron Temperature Ratios (under the assumption that $P^{(e)} = P^{(i)}$).

LIST OF ILLUSTRATIONS

- Figure 2-1: A "pill box" with thickness δ and lateral dimension L associated with the shock front. The vectors indicated by solid (dotted) lines represent the magnetic field (wind velocity projection) in the (x_1, x_3) plane. The unprimed (primed) quantities refer to the pre-shock (post-shock) state of the plasma.
- Figure 3-1: The ratio of density in the pre-shock state to that in the post-shock state, y , vs. anisotropy parameter ξ' , for various values of the angle Θ_B (at fixed M_A , M_S and ξ).
- Figure 3-2: The same plot of y vs. ξ' as in Figure 3-1, but with different values of ξ ; M_A and M_S are held fixed.
- Figure 3-3: The same plot of y vs. ξ' as in Figure 3-1, but with different values of M_A ; ξ and M_S are held fixed.
- Figure 3-4: Same plot of y vs. ξ' as in Figure 3-1, but with different values of M_S ; ξ and M_A are held fixed.
- Figure 3-5: The same plot of y vs. ξ' as in Figure 3-1 at a large value of M_A (1, 2, 3) and at a large value of M_S (4, 5, 6).
- Figure 4-1: Contours of constant $D1$ in the (k, β) plane, for various values of ξ and ξ' .
- Figure 4-2: Contours of constant $D1$, $D2$, and $D3$ in the (k, β) plane for the case of isotropic pressure.
- Figure 5-1: Trajectories of Pioneer 6 and Pioneer 7 projected onto the ecliptic plane, as viewed from the earth.
- Figure 5-2: Trajectory of Mariner V projected onto the ecliptic plane, as viewed from the earth.
- Figure 5-3: The definition of the RTN and solar ecliptic coordinates (θ, φ) .
- Figure 5-4: The measured values of physical parameters as functions of time (for a time interval of 90 minutes), associated with the shock of March 22, 1966. The first column on the left, going from top to bottom, represents, respectively, the thermal velocity (km/sec) w_0 , the magnitude of the wind velocity (km/sec) and the ion number density (per cc). The second column shows the angles φ_v and θ_v as defined in Figure 5-3, and measured in degrees. The third column, from top to bottom, shows, respectively, the magnitude of the magnetic field (γ) and the two angles φ_B and θ_B measured in degrees and identifying the direction of \underline{B} -

vector in the solar ecliptic coordinates. All quantities are plotted vs. time measured in minutes (with arbitrary origin). The vertical bars on both sides of the discontinuities indicate the combined error due both to the experimental uncertainties and to the statistical fluctuations. The dotted horizontal lines indicate the best fit values for each parameter.

- Figure 5-5: The same plot as Figure 5-4 for the March 23, 1966 shock.
- Figure 5-6: The best fit value of magnetic field (dotted line) and velocity vector (solid line) as seen in the Σ^* frame for the March 22, 1966 shock.
- Figure 5-7: The same plot as Figure 5-6 for the March 23, 1966 shock.
- Figure 5-8: The same plot as Figure 5-4 for the August 29, 1966 shock.
- Figure 5-9: The same plot as Figure 5-4 for the June 26, 1967 shock.
- Figure 5-10: The same plot as Figure 5-4 for the August 29, 1967 shock.
- Figure 5-11: The same plot as Figure 5-6 for the August 29, 1966 shock.
- Figure 5-12: The same plot as Figure 5-6 for the June 26, 1967 shock.
- Figure 5-13: The same plot as Figure 5-6 for the August 29, 1967 shock.
- Figure 5-14: The same plot as Figure 5-4 for the July 20, 1967 shock.
- Figure 5-15: The same plot as Figure 5-4 for the August 30, 1967 shock.
- Figure 5-16: The same plot as Figure 5-6 for the July 20, 1967 shock.
- Figure 5-17: The same plot as Figure 5-6 for the August 30, 1967 shock.
- Figure 5-18: The distribution of the individual values of the polar (θ_S) and azimuthal (ϕ_S) angles, of the seven shock normals. The shorter line segments refer to the slow shocks.
- Figure 6-1: The pressure ratios, P'/P , the temperature ratios, T'/T , the sound Mach number, M_S , and the post-shock anisotropy parameter, plotted as functions of the pre-shock anisotropy parameter, ξ . The curves are based on equations (6.3), (2.79), (2.80) and experimental data referring to the March 22, 1966 shock.
- Figure 6-2: The same as Figure 6-1, for March 23, 1966 shock.
- Figure 6-3: The same as Figure 6-1, for August 29, 1966 shock.
- Figure 6-4: The same as Figure 6-1, for June 26, 1967 shock.

Figure 6-5: The same as Figure 6-1 for the July 20, 1967 shock.

Figure 6-6: The same as Figure 6-1 for the August 29, 1967 shock.

Figure 6-7: The same as Figure 6-1 for the August 30, 1967 shock.

Chapter 1 .

INTRODUCTION

It is well known that compressional waves in ordinary fluids can develop into shock waves when the velocity of the fluid exceeds the speed of propagation of these waves (Landau & Lifshitz, 1959). If one studies the shock from its own frame of reference, then, on each side of the shock, the density, the velocity and the pressure may be treated as steady and uniform. The part of the fluid streaming toward the shock surface is usually referred to as being in a "pre-shock state"; the part on the other side of the shock surface is correspondingly referred to as being in a "post-shock state". Between the two states there exists a very thin transition layer of the order of one mean free path for collisions between molecules of the fluids. The density, pressure and velocity may be considered as discontinuous across this layer. The conservation laws of mass, momentum, and energy lead to the Rankine-Hugoniot relations, which relate the density, pressure, and velocity on one side of the shock to those on the other.

The existence of shocks in a fully ionized gas with a mean free path for particle-particle collisions much smaller than the length scale of the system (collision-dominated plasma) can be inferred along similar lines of reasoning as in ordinary fluids. However, the presence of the magnetic field may modify and complicate the character of the plasma

shock waves considerably in comparison with ordinary shocks. Nonetheless, generalized Rankine-Hugoniot relations may still be derived. Most standard textbooks on Magnetohydrodynamics (e. g. Shercliff, 1965, Hughes & Young, 1966, etc.) discuss MHD shock waves.

The recent discovery of the phenomenon of solar wind by means of direct satellite and deep space probe observations offers an excellent opportunity for the search of shocks in the interplanetary medium. In an attempt to describe quantitatively the behavior of solar wind, it is tempting to approach the problem via simplest possible model ; E. N. Parker (1963) has done this using macroscopic description in the MHD approximation. Although, the application of MHD approximation for the case of the solar wind is not readily justifiable, the hydromagnetic equations have proven useful for predicting the supersonic behavior of the solar wind (Parker, 1963), the existence of the bow shock (Axford, 1962; Spreiter, 1963; etc.). In the more recent years, large- as well as small- scale properties of the solar wind have been studied using a more accurate forms of the magnetohydrodynamic equation (Colburn & Sonett, 1966) and the kinetic equation for collisionless plasmas (Scarf, 1969). Although the kinetic plasma equations give a more precise description of the reality, the mathematical difficulties associated with their solutions prevent us from obtaining useful experimentally verifiable results. On the other hand, a fluid description in the magnetohydrodynamic approximation gives us, in general, fewer mathematical difficulties. In addition, the

fluid equations have been utilized in various branches of sciences for a long time, so that techniques of their solutions are better understood.

In the solar wind, the mean free path for the binary Coulomb interactions between particles may be comparable to, or larger than the scale length. Therefore, the interplanetary plasma in contrast to collision-dominated plasma, is practically collisionless. The relationships derived for ordinary MHD shocks may not be applicable here. Thus, a careful re-examination of the problem is necessary.

The usual collision mechanism which generates randomness and allows a description of the system in terms of the fluid variables (pressure, density and velocity) in a collision-dominated plasma is absent in a collisionless plasma. However, Chew, Goldberger and Low (1956) have shown that the presence of a strong magnetic field replaces to some degree the randomizing tendency of collisions so that fluid concepts again are valid. More generally, if the scale length is much larger than the characteristic lengths such as the Debye length, electron and ion gyroradius of the plasma, then the fluid concepts are applicable (Rossi and Olbert, 1970). In the solar wind, the scale length of interest is much larger than these characteristic lengths. Therefore, the macroscopic fluid variables of the solar wind (see Chapter 2) may be considered as meaningful.

The solar wind is fully ionized, containing mainly electrons and protons with about 5 per cent (by number) of helium ions. It streams

radially from the sun into interplanetary space. The stream velocity near the earth ranges from 300 km/sec to 700 km/sec, with densities from 1 to 10 ions per cm^3 (Lazarus et al. 1966). The temperatures or pressures (as defined in Chapter 2) have been observed to be anisotropic (Hundhausen, 1967). More specifically, the ion temperature ($T_{\parallel i}$) parallel to the magnetic field differs from the ion temperature ($T_{\perp i}$) transverse to the magnetic field. The commonly observed value of $T_{\parallel i} / T_{\perp i}$ is about 2.5 (Hundhausen, 1968). The sound velocity (using the average temperature between $T_{\parallel i}$ and $T_{\perp i}$) and Alfvén velocity are about of the same order of magnitude, ranging from 20 to 60 km/sec. Hence, the solar wind represents a supersonic flow. The mean Coulomb collision time between electrons and protons of the solar wind is of the order 10^4 to 10^7 sec. The strength of the interplanetary magnetic field at 1 A. U. lies in the neighborhood of 5 gamma (1 gamma = 10^{-5} gauss) during quiet solar conditions and may be intensified up to a few tens of gammas during active, solar conditions (Ness, 1967).

The large-scale interplanetary magnetic field has an Archimedes spiral configuration (Wilcox, 1968). The density decreases radially from the sun approximately as an inverse square dependence.

During disturbed conditions on the sun, bursts of plasma are ejected into the interplanetary space. The bursts comprise the so-called "enhanced solar wind". They interact not only with the quiet solar wind component, but also with each other. These interactions may generate

propagating shock waves in the interplanetary space.

Gold (1955) and Parker (1963) suggested that solar flares generate interplanetary shocks. Using the hydrodynamic equation, Parker (1963) computed how a blast wave would propagate in an interplanetary medium under various model conditions. The effect of magnetic field was neglected for simplicity. Colburn and Sonett (1966), and Wilkerson (1969) discuss the MHD shocks propagating in the interplanetary space. Sonett et al. (1964) have applied the MHD model to one event in deep interplanetary space where both plasma and field information were available. They found very good agreement between the computed and measured parameters. However, they measured the solar wind velocity only in the antisolar direction. In order to check experimentally the computed parameters from the MHD model of shocks, more measurements are needed. Ogilvie and Burlaga (1969) found that six shock-like discontinuities obey the MHD Rankine-Hugoniot relation within the accuracy of the observations. Again, their measurements lack the directions of solar-wind velocity; additional information is needed to check the computed values. All the computations given by these authors are based on the assumption of an isotropic pressure. Observations of events where either the plasma parameters or the magnetic field were available, have been reported by Gosling et al. (1967 a, b), Taylor (1968), Ness (1967). Shock velocities have been deduced using conservation relations by several of these authors.

Anisotropic pressures were incorporated into the MHD model of collisionless shocks by Abraham-Shrauner (1967), and Lynn (1967). However, CGL (Chew, Goldberger and Low) double-adiabatic-hypothesis was used for those studies. It is very difficult to justify the CGL approximation across the shock layer.

In order to study the effect of the anisotropic pressure on the MHD shocks without any ad hoc assumptions, it is necessary to reformulate the conservation laws for momentum, and energy. The available system of equations is no longer closed. It turns out (see Chapter 2) that the number of unknowns exceeds the number of equations by one. However, when we are able to measure necessary physical parameters on both sides of the shock then we can use this "over-determined" set of equations to check the validity of the "theoretical" solutions. We can also determine parameters, which are not accessible by measurements but are important from the theoretical point of view.

We have at our disposal the plasma data from various satellite experiments conducted by the MIT space physics group. The direction of the bulk velocity of solar wind as well as the bulk speed, the density and the thermal speed of positive ions are available on both sides of the shock surface, together with the complete magnetic fields provided by Goddard Space Flight Center (GSFC) (Ness et al.) and Jet Propulsion Laboratory (JPL) (Davis et al.). A complete check of the validity of MHD model of collisionless shock waves in the interplanetary space is

thus now possible. When discontinuities satisfying MHD shock model are verified, the solutions, such as the electron pressure, anisotropy of the plasmas both in the pre- and post-shock states, can be also obtained.

In Chapter 2, the mathematical model of the MHD shock for isotropic pressures is reviewed. Shock jump conditions are derived with the consideration of anisotropic pressures. In Chapter 3, a detailed study of the developed theory and the numerical results are presented. The ratios of the densities across the shock are given as families of curves in terms of various parameters. In Chapter 4, a new method for finding the shock normal and the shock speed without the knowledge of the total pressures of plasma is developed in detail. In Chapter 5, the experimental data are used to test the validity of the shock equations derived in Chapters 2 and 4. The possible shock-like discontinuities have been searched from the data of Pioneer 6, 7 and Marinar V during the period of 1966 to 1967. Among many candidates, seven have been identified as shocks. They satisfy the generalized Rankine-Hugoniot relations. The results are presented in the form of tables and graphs. In Chapter 6, the necessity of the two-fluid description of the solar wind for more precise interpretation of the data is discussed. The differences between the electron pressures and ion pressures across the shocks are studied. Some rough estimates of the expected values for the electron pressures are given. In Chapter 7, a summary of all the findings

is given. The discussion of the results and suggestions for further future studies are presented.

Chapter 2

MAGNETOHYDRODYNAMIC MODEL OF
THE COLLISIONLESS SHOCK WAVES

2.1 Basic Equations of Collisionless Shocks -- Fluid Description

To begin with, let us discuss in general the laws of conservation of mass, momentum and energy for an ionized gas.

Starting from the microscopic point of view, we write down the Boltzmann Equation (Chapman & Cowling, 1961; Spitzer, 1962) for each species of ions and electrons using the Einstein summation convention over j . ($j = 1, 2, 3$)

$$\frac{\partial f_{\alpha}}{\partial t} + v_j \frac{\partial f_{\alpha}}{\partial x_j} + \frac{F_{\alpha j}}{m_{\alpha}} \frac{\partial f_{\alpha}}{\partial v_j} = \left(\frac{\delta f_{\alpha}}{\delta t} \right)_{coll.} \quad (2.1)$$

where $f_{\alpha}(\underline{r}, \underline{v}, t)$ is the distribution function in six-dimensional phase space composed of the velocity space \underline{v} , the ordinary space \underline{r} and the time t ; m_{α} is the mass of species α ; $F_{\alpha j}$ is the j th component of force acting on the particles of species α ; $\left(\frac{\delta f_{\alpha}}{\delta t} \right)_{coll.}$ represents the rate of change of f_{α} due to collisions between particles.

For a collisionless plasma, such as the solar wind, the collision term may be neglected. The equation (2.1) may be interpreted as the rate of change of $f_{\alpha}(\underline{r}, \underline{v}, t)$ along the trajectory of a particle in phase space (Liouville Theorem).

If the region has a scale length L which is very large compared

with the various characteristic lengths of the plasmas, a one fluid model can be applied to the collisionless plasmas under the quasi-stationary condition (Rossi & Olbert, 1970).

The characteristic lengths of a given plasma depend on such quantities as the number density, pressure, magnetic field strength, mass of the ions etc. In solar wind, the largest characteristic length is of the order of the gyroradius of ions (based on their thermal speed), and the scale lengths we are interested in are much larger than this characteristic length. Therefore, we may use the one-fluid equations for approximate macroscopic description of the solar wind.

The macroscopic equations of continuity, momentum and energy can be obtained by moment formation of Boltzmann equation, i. e. by multiplying the Boltzmann equation separately by $\sum_{\alpha} m_{\alpha}$, $\sum_{\alpha} m_{\alpha} v_i$ and $\frac{1}{2} \sum_{\alpha} m_{\alpha} v^2$ then integrating each equation over the velocity space respectively. (\sum_{α} denotes the summation over species α .) For detail derivation of these equations, see Rossi and Olbert (1970), Spitzer (1962).

Let us define the following macroscopic quantities:

(1) The density: The total mass of all species in unit volume

$$\rho(r, t) = \sum_{\alpha} m_{\alpha} \int f_{\alpha} d^3v \quad (2.2)$$

(2) The average streaming velocity of the plasma as a whole

$$\underline{V}(\underline{r}, t) = \frac{(\sum_{\alpha} m_{\alpha} \int \underline{v} f_{\alpha} d^3v)}{\rho} \quad (2.3)$$

(3) The average kinetic energy density of the particles

$$K(\underline{r}, t) = \frac{1}{2} \sum_{\alpha} m_{\alpha} \int v^2 f_{\alpha} d^3v \quad (2.4)$$

(4) The kinetic stress tensor

$$\pi_{ij}(\underline{r}, t) = \sum_{\alpha} m_{\alpha} \int v_i v_j f_{\alpha} d^3v \quad (2.5)$$

Define the velocity \underline{v}^* of a particle in a system Σ^* moving with the plasma streaming velocity \underline{V} . Hence;

$$\underline{v}^* = \underline{v} - \underline{V} \quad (2.6)$$

Substituting \underline{v}^* into (2.5), the kinetic tensor can be written in the following form

$$\pi_{ij} = P_{ij} + \rho V_i V_j \quad (2.7)$$

(5) The pressure tensor is defined as

$$P_{ij} = \sum_{\alpha} m_{\alpha} \int v_i^* v_j^* f_{\alpha}^* d^3v^* \quad (2.8)$$

P_{ij} thus represents the kinetic tensor in the system Σ^* . In the case of ordinary gases, P_{ij} is isotropic and represents the ordinary thermal pressure. In the case of collision dominated plasma the assumption of a

scalar pressure is well justified. When the mean free path for coulomb interactions between particles is comparable to the scale length of the problem, P_{ij} is, in general, an-isotropic. In the presence of a strong magnetic field, one can show that the pressure tensor has the following form (Rossi and Olbert, 1969)

$$P_{ij} = P_{\perp} \delta_{ij} + (P_{\parallel} - P_{\perp}) b_i b_j \quad (2.9)$$

where the subscripts "parallel" (\parallel) and "perpendicular" (\perp) refer to the direction with respect to the magnetic field vector. b_i, b_j are the projection of the unit vector, \underline{B} / B , in the i, j , axes, respectively. (i. e. $b_i = \frac{B_i}{B}$.)

In solar wind, the distribution functions of ions in the system \sum^* may be roughly approximated by a "bi-Maxwellian form" (Hundhausen, 1968):

$$f_{\alpha}^*(\underline{r}, \underline{v}^*, t) = \frac{n_{\alpha} \alpha_{\perp} \alpha_{\parallel}^{1/2}}{\pi^{3/2}} e^{-\alpha_{\parallel} v_{\parallel}^{*2} - \alpha_{\perp} v_{\perp}^{*2}} \quad (2.10)$$

Substituting this form of the distribution function, and using the normalization condition of $f_{\alpha}^*(\underline{r}, \underline{v}^*, t)$, into (2.8), the following relations can be found:

$$\alpha_{\parallel} = \frac{n_{\alpha} m_{\alpha}}{2 P_{\parallel}} = \frac{n_{\alpha} m_{\alpha}}{2 n k \Theta_{\parallel}} ; \quad \alpha_{\perp} = \frac{n_{\alpha} m_{\alpha}}{2 P_{\perp}} = \frac{n_{\alpha} m_{\alpha}}{2 n k \Theta_{\perp}}$$

n_{α} is the number density of species α , and n is the total number den-

sity (i. e., $n = \sum_{\alpha} n_{\alpha}$). k is the Boltzmann's Constant ($k = 1.380 \times 10^{-16}$ erg deg $^{-1}$). Pressure tensor, P_{ij} , has the form of (2.9), and relates to temperature tensor, Θ_{ij} , by the relation

$$P_{ij} = n k \Theta_{ij} \quad (2.11)$$

If we rotate the coordinate system in such a way that the z-axis is parallel to the magnetic field \underline{B} , the pressure tensor becomes

$$\underline{P} = \begin{pmatrix} P_{\perp} & 0 & 0 \\ 0 & P_{\perp} & 0 \\ 0 & 0 & P_{\parallel} \end{pmatrix} \quad (2.12)$$

(6) The thermal energy

$$\epsilon_T = \frac{1}{2} \sum_{\alpha} m_{\alpha} \int v^{*2} f_{\alpha}^{*} d^3 v^{*} \quad (2.13)$$

ϵ_T equals one half of the trace of P_{ij}

(7) The heat flux

$$\underline{q} = \frac{1}{2} \sum_{\alpha} m_{\alpha} \int v^{*2} \underline{v}^{*} f_{\alpha}^{*} d^3 v^{*} \quad (2.14)$$

This quantity has been measured (Hundhausen, 1968) in the solar wind, and has been shown to be very small, thus justifying the approximate validity of Eq. (2.10). (Note that Eq. (2.10) makes the heat flux vanish identically.)

In terms of the above defined quantities, the laws of conservation of mass, momentum and energy are summarized as follows (Rossi and

Olbert, 1970):

(1) Equation of Continuity

$$\frac{\partial \rho}{\partial t} + \frac{\partial (\rho V_i)}{\partial x_i} = 0 \quad (2.15)$$

(2) Equation of Momentum

$$\frac{\partial (\rho V_j)}{\partial t} + \frac{\partial}{\partial x_i} (\rho_{ij} + \rho V_i V_j) = \rho_c \underline{E}_j + (\underline{j} \times \underline{B})_j + \rho g_j \quad (2.16)$$

where $\rho_c = \sum_{\alpha} n_{\alpha} (z_{\alpha} e)$ is the charge density of the plasma, \underline{g} is the gravitational acceleration, \underline{E} is the electric field and \underline{j} is the current density. Applying the Maxwell's Equations, the above equation can be written in the following form:

$$\frac{\partial G_i}{\partial t} + \frac{\partial A_{ij}}{\partial x_j} + \rho g_i = 0 \quad (2.17)$$

Define

$$G_i = \rho V_i + \frac{S_i}{c^2} \quad (2.18)$$

And

$$A_{ij} = \rho_{ij} + \rho V_i V_j - T_{ij} \quad (2.19)$$

where

$$\underline{S} = \frac{\underline{E} \times \underline{B}}{\mu_0} \quad (2.20)$$

is the Poynting vector,

$$T_{ij} = \epsilon_0 \epsilon_i \epsilon_j + \frac{B_i B_j}{\mu_0} - \left(\frac{1}{2} \epsilon_0 \epsilon^2 + \frac{1}{2} \frac{B^2}{\mu_0} \right) \delta_{ij} \quad (2.21)$$

is the Maxwell's stress tensor, ϵ_0 is the dielectric permittivity and the magnetic permeability of vacuum. \underline{S}/c^2 represents the electromagnetic momentum density. When the Alfvén speed is much smaller than the speed of light c , this term can be neglected in comparison with the $\rho \underline{v}$ in (2.18)

(3) Equation of Energy

$$\frac{d\epsilon_T}{dt} + \epsilon_T \frac{\partial v_i}{\partial x_i} + P_{ij} \frac{\partial v_j}{\partial x_i} = (\underline{j} - \rho \underline{v}) \cdot (\underline{\epsilon} + \underline{v} \times \underline{B}) - \text{div } \underline{g} \quad (2.22)$$

Again by virtue of Maxwell's equations, the energy equation can be re-written as

$$\frac{\partial \epsilon}{\partial t} + \frac{\partial F_j}{\partial x_j} = 0 \quad (2.23)$$

where

$$\epsilon = \epsilon_T + \frac{1}{2} \rho v^2 + \rho \varphi + \frac{1}{2} \epsilon_0 \epsilon^2 + \frac{1}{2} \frac{B^2}{\mu_0} \quad (2.24)$$

and

$$F_j = \left(\frac{1}{2} \rho v^2 + \rho \varphi + \epsilon_T \right) v_j + P_{ji} v_i + \mathcal{F}_j + S_j \quad (2.25)$$

φ is the gravitational potential ($\underline{g} = -\nabla \varphi$) which may be assumed to be time independent. From a scale analysis, one can show (Rossi and

Olbert, 1970) that, in solar wind, the electric field may be adequately approximated by

$$\underline{\xi} = -\underline{V} \times \underline{B} \quad (2.26)$$

Using this approximation one can show that the ratio of magnetic field stress to the electric field stress $\frac{B^2}{\mu_0 \epsilon_0 \xi^2}$ is of the order of $\frac{c^2}{V^2}$. Hence, one can neglect the influence of the electric field stress in (2.21) and (2.24).

Maxwell's equations allow us to state two additional relations which are necessary for the study of the shock jump conditions:

(A) The divergent free character of the magnetic field

$$\frac{\partial B_i}{\partial x_i} = 0 \quad (2.27)$$

(B) In a steady state ($\frac{\partial}{\partial t} = 0$), the curl free character of the electric field

$$\text{curl } \underline{\xi} = 0 \quad (2.28)$$

(2.15), (2.17), (2.23), (2.26), (2.27) and (2.28) form the basic equations for the fluid description of the collisionless shock waves.

2.2 General Jump Conditions in MHD Discontinuities

The solar plasma streams radially from the Sun; past a critical distance of several solar radii, the wind velocity, \underline{V} , is supersonic. Shocks or discontinuities may propagate in this plasma; their speed of

propagation, \underline{V}_s , as seen by satellites, will be different from \underline{V} . In order to apply the conservation equations given in the previous section, it is convenient to define the reference frame moving with the shock or discontinuity. Then, the bulk velocities of the solar wind with respect to the shock or discontinuity frame of reference are called \underline{V}^* , where $\underline{V}^* = \underline{V} - \underline{V}_s$. In the non-relativistic case, the magnetic fields and solar wind densities are invariant with respect to the Galilean transformation. In the following, we will consider an infinite plane shock propagating in the solar wind. All the parameters are defined with respect to this shock frame. (i. e. $\underline{V}^* = \underline{V} - \underline{V}_s$)

Let us assume that the infinite shock plane in Σ^* is parallel to the x_2, x_3 plane, and its normal is in the x_1 -direction. The plasma state on one side of the shock front is called the pre-shock state where the plasma flows toward the shock front, and the state on the other side of the front is called the post-shock state where the plasma flows away from it. Both the pre- and post- shock states are assumed uniform and steady. The effect of gravitation will cancel out because the gravitational force doesn't change across the shock front.

Let us consider a "pill box" as shown in Figure 2-1, the thickness of this "pill box", δ , is much smaller than the size, L , in the x_2 and x_3 directions. The flux of mass, momentum, or energy into the "pill box" must balance the respective flux out of the "pill box", provided there is no source or sink in the box. Since δ is much smaller than L , we can assume that all the flux through the "pill box"

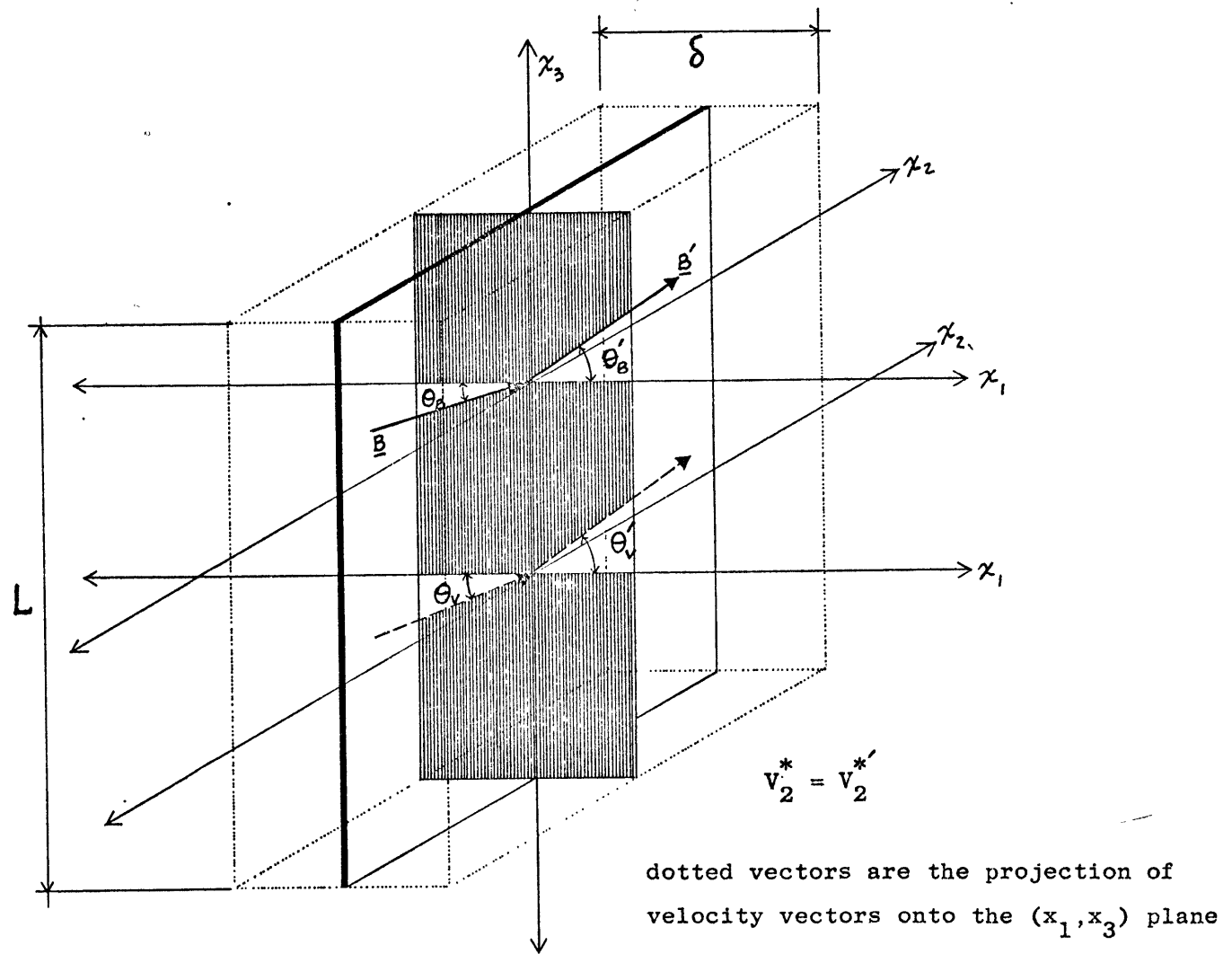


Figure 2-1

involves only the lateral face surfaces. (i. e. there is no flux leak in the x_2 , x_3 directions.)

We take the volume integral of the following equations in the steady state. (i. e. $\frac{\partial}{\partial t} = 0$.)

- (1) The zero divergence of the magnetic field (2.27).
- (2) The curl free character of the electric field (2.28).
- (3) Equation of continuity (2.15).
- (4) Equation of momentum (2.16) which consists of the equations for the three components.
- (5) Equation of energy (2.23).

Using Gauss's theorem, the volume integral can be transformed into the surface integral over the "pill box". Then, we obtain the following equations:

$$\left[B_1 \right] = 0 \quad (2.29)$$

$$\left[\rho V_1^* \right] = 0 \quad (2.30)$$

$$\left[V_3^* B_1 - V_1^* B_3 \right] = 0 \quad (2.31)$$

$$\left[V_1^* B_2 - V_2^* B_1 \right] = 0 \quad (2.32)$$

$$\left[\rho V_1^* V_2^* - \zeta \frac{B_1 B_2}{\mu_0} \right] = 0 \quad (2.33)$$

$$\left[\rho V_1^* V_3^* - \zeta \frac{B_1 B_3}{\mu_0} \right] = 0 \quad (2.34)$$

$$\left[\rho V_1^{*2} + P + \frac{1}{3} \left(\xi + \frac{1}{2} \right) \frac{B^2}{\mu_0} - \xi \frac{B_1^2}{\mu_0} \right] = 0 \quad (2.35)$$

$$\left[\left[\frac{1}{2} \rho V^{*2} + \epsilon_T + P + \frac{1}{3} (\xi + 2) \frac{B^2}{\mu_0} \right] V_1^* - \xi \frac{B_1 B_2}{\mu_0} V_2^* - \xi \frac{B_1 B_3}{\mu_0} V_3^* \right] = 0 \quad (2.36)$$

where the bracket [] indicates the difference of the enclosed quantity on the two sides of the shock. Equations (2.29), (2.30), and (2.36) are derived from (2.27), (2.15), and (2.23), respectively, (2.31), (2.32) are derived from (2.28) with the MHD approximation (2.26), and (2.33), (2.34), (2.35) are derived from (2.16).

Note that these eight equations contain nine variables: the density ρ , the three components of the velocity, \underline{V}^* , and the magnetic field, \underline{B} , and the two pressures, P_{\parallel} and P_{\perp} , for both the pre- and the post-shock states. Note also that instead of P_{\parallel} and P_{\perp} we have introduced two related quantities:

$$\xi = 1 - \frac{P_{\parallel} - P_{\perp}}{B^2/\mu_0} \quad (2.37)$$

and

$$P = \frac{1}{3} (2 P_{\perp} + P_{\parallel}) \quad (2.38)$$

We can see that P equals one third of the trace of P_{ij} , and thus is a scalar quantity independent of the rotation of coordinate axes. ξ is a

dimensionless parameter measuring the degree of "thermal" anisotropy in plasma. Notice also the relation

$$\epsilon_T = P_{\perp} + \frac{1}{2} P_{\parallel} \quad (2.39)$$

We see from (2.37), that when P_{ij} is a scalar, (i. e. $P_{\parallel} = P_{\perp}$) ξ becomes unity. Then, the above eight equations reduce to the ordinary MHD shock wave relations, (Anderson, 1963). There are then only eight variables, namely ρ , \underline{V} , \underline{B} , and P and eight equations (2.29) to (2.36). Thus, for scalar pressure, these equations form a closed system, where the state on one side of the shock can be computed from the state on the other side. However, for the case of solar plasma P_{ij} is known not always to be a scalar. The knowledge of P_{ij} introduces two parameters (i. e. P_{\parallel} and P_{\perp}) for the eight equations. Then, the system of the equations is not closed because the unknowns exceed the equations by one. This difficulty is discussed later (see Chapter 5).

2.2.1 The coplanarity theorem

For an isotropic pressure plasma, the coplanarity theorem is well known and can be stated as follows: the magnetic field vectors on both sides of the shock and the normal to the shock lie in the same plane. In this section, we shall show that the coplanarity theorem still holds for anisotropic plasmas.

Let us write explicitly the jump conditions that are needed to prove the general coplanarity theorem. Unprimed and primed quantities refer

to the pre- and post- shock states respectively. The subscripts, 1, 2, and 3, refer to the directions x_1, x_2, x_3 , respectively.

$$B_1 = B_1' \equiv B_1 \quad (2.40)$$

$$\rho V_1^* = \rho' V_1^{*'} \equiv C \quad (2.41)$$

$$V_3^* B_1 - V_1^* B_3 = V_3^{*'} B_1' - V_1^{*'} B_3' \quad (2.42)$$

$$\rho V_1^* V_3^* - \xi \frac{B_1 B_3}{\mu_0} = \rho' V_1^{*'} V_3^{*'} - \xi' \frac{B_1' B_3'}{\mu_0} \quad (2.43)$$

$$V_1^* B_2 - V_2^* B_1 = V_1^{*'} B_2' - V_2^{*'} B_1' \quad (2.44)$$

$$\rho V_1^* V_2^* - \xi \frac{B_1 B_2}{\mu_0} = \rho' V_1^{*'} V_2^{*'} - \xi' \frac{B_1' B_2'}{\mu_0} \quad (2.45)$$

Substituting (2.40), (2.41) into (2.42), we obtain

$$\left(\frac{B_3'}{\rho'} - \frac{B_3}{\rho} \right) C = B_1 (V_3^{*'} - V_3^*) \quad (2.46)$$

where C is a constant defined by (2.41)

Substituting (2.40), (2.41) into (2.43), we obtain

$$C (V_3^{*'} - V_3^*) = (\xi' B_3' - \xi B_3) \frac{B_1}{\mu_0} \quad (2.47)$$

By eliminating $(V_3^{*'} - V_3^*)$ between (2.46) and (2.47) we obtain

$$\left(\frac{B_3'}{\rho'} - \frac{B_3}{\rho} \right) \frac{c}{B_1} = \left(\xi' B_3' - \xi B_3 \right) \frac{B_1}{\mu_0 c} \quad (2.48)$$

(2.48) can be written in the following form:

$$\left(M_A'^2 - \xi' \right) B_3' = \left(M_A^2 - \xi \right) B_3 \quad (2.49)$$

Define

$$M_A = \frac{V_i^*}{V_A} \quad (2.50)$$

and

$$V_A = \frac{B_1}{\sqrt{\mu_0 \rho}} \quad (2.51)$$

where V_A is the Alfvén speed based on the normal component of the magnetic field B_1 , and M_A is the Alfvén Mach number based on V_A .

Similarly, we obtain the following equation for B_2 and B_2' from (2.41), (2.45), and (2.44)

$$\left(M_A'^2 - \xi' \right) B_2' = \left(M_A^2 - \xi \right) B_2 \quad (2.52)$$

As long as $(M_A'^2 - \xi')$ and $(M_A^2 - \xi)$ do not vanish, we can divide (2.49) by (2.52), and obtain:

$$\frac{B_3'}{B_2'} = \frac{B_3}{B_2} \quad (2.53)$$

This is the mathematical expression of the coplanarity theorem for an anisotropic pressure plasma. Let us define the vector \underline{B}_t , and \underline{B}_t' as

the projection of the magnetic field vectors, \underline{B} and \underline{B}' , respectively on the shock plane. Equation (2.53) implies that \underline{B}_t and \underline{B}'_t point in the same direction. Therefore, we can always choose a coordinate system such that the B_2 component on both sides of the shock front vanishes. This simplifies the original system of the jump conditions across the shock front considerably.

In the case of the isotropic pressure plasma (i. e. $\xi' = \xi = 1$), the equation (2.49) and (2.52) still hold. This leads to the same equation (2.53). Thus, as we have indicated previously the coplanarity theorem is valid for the isotropic as well as the anisotropic pressure plasmas.

2.2.2 Simplified shock equations for scalar pressures

Using the coplanarity theorem, we may choose $B_2 = B'_2 = 0$; then the system of equations (2.29) to (2.36) simplifies into :

$$[B_1] = 0 \quad (2.54)$$

$$[V_2^*] = 0 \quad (2.55)$$

$$[\rho V_1^*] = 0 \quad (2.56)$$

$$[V_3^* B_1 - V_1^* B_3] = 0 \quad (2.57)$$

$$[\rho V_1^* V_3^* - \frac{B_1 B_3}{\mu_0}] = 0 \quad (2.58)$$

$$\left[\rho V_1^{*2} + P + \frac{B^2}{2\mu_0} \right] = 0 \quad (2.59)$$

$$\left[\left(\frac{1}{2} \rho V_1^{*2} + E_T + P + \frac{B^2 - B_1^2}{\mu_0} \right) V_1^* - \frac{B_1 B_3}{\mu_0} V_3^* \right] = 0 \quad (2.60)$$

It is convenient in the analysis of the shock to use the ratio $\frac{\rho'}{\rho}$, $\frac{V_1^*}{V_1^*}$, $\frac{B_2'}{B_2}$, $\frac{V_3^*}{V_3^*}$ and $\frac{P_3'}{P_3}$, instead of the actual variables ρ' , V_1^* , etc. These five ratios can be solved for in terms of the non-dimensional quantities characteristic of the pre-shock state (see Appendix A). These non-dimensional quantities are : the Alfven Mach number M_A (2.50), the sound Mach number, M_s , is defined as

$$M_s = \frac{V_1^*}{V_s} \quad (2.61)$$

where

$$V_s = \sqrt{\gamma \frac{P}{\rho}} \quad (2.62)$$

In what follows, we shall assume that the polytropic index γ is 5/3. The two angles θ_B and θ_V are formed respectively by \underline{B} and \underline{V}^* with the shock normal in the pre-shock state.

Putting for short :

$$\begin{aligned} x &= \frac{\rho'}{\rho} ; & y &= \frac{V_1^{*'}}{V_1^*} ; & u &= \frac{B_3'}{B_3} \\ z &= \frac{V_3^{*'}}{V_3^*} & \text{and} & & v &= \frac{P'}{P} \end{aligned} \quad (2.63)$$

We find from the equations (2.54) through (2.60) :

$$y = \frac{1}{x} \quad (2.64)$$

$$z = \frac{\tan \theta_B}{\tan \theta_v} \left(\frac{1-y}{M_A^2 y - 1} \right) + 1 \quad (2.65)$$

$$u = \frac{M_A^2 - 1}{M_A^2 y - 1} \quad (2.66)$$

$$(y-1) + \frac{1}{\gamma M_s^2} (v-1) + \frac{u^2}{2 M_A^2} \tan^2 \theta_B - \frac{\tan^2 \theta_B}{2 M_A^2} = 0 \quad (2.67)$$

$$C_4 y^4 + C_3 y^3 + C_2 y^2 + C_1 y + C_0 = 0 \quad (2.68)$$

where

$$\begin{aligned} C_4 &= -4 M_A^4 \\ C_3 &= 5 M_A^4 + \frac{5 M_A^4}{\gamma M_s^2} + 8 M_A^2 + \frac{5}{2} M_A^2 \tan^2 \theta_B \\ C_2 &= - \left(10 M_A^2 + 2 M_A^2 \tan^2 \theta_B + \frac{10 M_A^2}{\gamma M_s^2} + M_A^4 \right. \\ &\quad \left. + \frac{5 M_A^4}{\gamma M_s^2} + 4 \tan^2 \theta_B + 4 \right) \end{aligned} \quad (2.69)$$

$$C_1 = 2 M_A^2 \left(1 + \frac{5}{\gamma M_s^2} \right) + 5 \left(1 + \frac{1}{\gamma M_s^2} \right) + 5 \tan^2 \theta_B - \frac{1}{2} \tan^2 \theta_B M_A^2$$

$$C_0 = - \left(1 + \frac{5}{\gamma M_s^2} + \tan^2 \theta_B \right)$$

2.2.3 Review of various discontinuities in isotropic plasmas

For an isotropic pressure plasma, the theory and jump conditions of the hydromagnetic shocks have been studied extensively (Anderson, 1963 ; Bazer and Ericson, 1959). We do not intend to give the mathematical derivation nor a detailed review on this subject. However, we feel that a brief summary of the results which are pertinent to our analysis of the interplanetary shocks is advisable at this point.

Let us classify the discontinuities into two categories resulting from the solutions of the conservation equations (2.29) to (2.36). The first class refers to the discontinuities which are identified by the condition that there is no flow across the surface of discontinuity, i. e. ρv_1^* vanishes. These again can be divided into contact and tangential discontinuities depending on whether there is a normal component of magnetic field B_1 or not. The second class refers to the case when $\rho v_1^* \neq 0$, and is called shock. The shocks can be divided again into three kinds :

(1) Alfven shock, or the so-called rotational discontinuity. This shock is not a true shock because there is no density change across it. It represents the singular case when $M_A^2 = M_A'^2 = 1$. From this condition it follows immediately that the Alfven shock propagates at the Alfven velocity

and can be thought of as a large amplitude Alfvén wave. A reversal of \underline{B} may occur across a rotational discontinuity.

(2) Fast shock. This shock is closely related to the fast mode of the MHD wave propagating in an infinite homogeneous plasma with infinite conductivity. Across the fast shock not only the density but also the magnetic field strength increases.

(3) Slow shock. This shock is closely related to the slow mode of the MHD wave. Across the slow shock the density increases but the magnetic field strength decreases.

Among the three kinds of shock waves, only the fast and slow shocks obey the coplanarity theorem.

Neither the fast nor the slow shock will exist if the plasma is incompressible. There are good reasons to expect that the fast and slow mode of the MHD waves can develop into the corresponding fast and slow shocks. Kantrowitz and Petschek (1966) give a detail explanation of this matter.

We do not intend to make further remarks on the subject of the tangential and contact discontinuities. Burlaga (1968), Burlaga & Ness (1969), have given a detail description on this subject related to the observations in interplanetary space. Certain properties of these discontinuities and of the shocks are summarized in Table 2-1.

Table 2-1

Basic MHD Shocks and Discontinuities

	Velocity	Density	Field
Fast Shock	$V_n^* \neq 0$	$[\rho] > 0$	$[B] > 0$
Slow Shock	$V_n^* \neq 0$	$[\rho] > 0$	$[B] < 0$
Alfvén Shock or Rotational Discontinuity	$V_n^* = \pm \frac{B_n}{\sqrt{\mu_0 \rho}}$	$[\rho] = 0$	$[B] = 0 ; B_n \neq 0$
Tangential Discontinuity	$V_n^* = 0$ $[V_t^*] \neq 0$	$[\rho] \neq 0$	$[B] \neq 0 ; B_n = 0$
Contact Discontinuity	$V_n^* = 0$ $[V] = 0$	$[\rho] \neq 0$	$[B] = 0 ; B_n \neq 0$

It can be shown that the fast and slow shocks are "evolutional"

(Kulikovskiy and Lyubimov, 1965). Shocks are called "evolutional" if they are stable against small perturbations. Denoting by a_{fast} and a_{slow} the propagation velocity of the fast and slow magnetosonic waves in the direction of the shock wave, respectively, we have the following criteria :

(i) For a fast shock :

a. Pre-shock state

$$V_1^* > a_{fast} \quad (2.70)$$

b. Post-shock state

$$a'_{fast} > V_1^{*'} > V_A' \quad (2.71)$$

(ii) For a slow shock :

a. Pre-shock state

$$V_A > V_1^* > a_{slow} \quad (2.72)$$

b. Post-shock state

$$a'_{\text{slow}} > V_1^{*'} \quad (2.73)$$

For a detailed derivation of the above inequalities, we refer the reader to the works by Bazer and Ericson, (1959) and Shercliff, (1960). We see that in a fast shock the normal velocity jumps from supersonic to subsonic relative to the fast magnetosonic velocity and that in a slow shock it jumps from supersonic to subsonic relative to the slow magnetosonic velocity. In the fast shock the values of V_1^* and $V_1^{*'}$ are both "super-Alfvenic" and in the slow shock V_1^* and $V_1^{*'}$ are both "sub-Alfvenic".

Across a fast shock the direction of \underline{B} is rotated away from the normal and in a slow shock \underline{B} is rotated toward the normal.

The magnitudes of the magnetic field \underline{B} rise across a fast shock and drop across a slow shock. It can be shown that across both a fast and slow shock the component \underline{B}_t of \underline{B} tangent to the shock front does not change sign.

When \underline{B}_t is created or wiped out across a shock, we have the extreme cases of a fast and slow shock, respectively, named "switch-on" and "switch-off" shocks, respectively.

2.2.4 Anisotropic plasma

In analogy the isotropic pressure plasma, the three kinds of shock waves as well as the tangential and contact discontinuity are also expected to exist in the case of anisotropic plasmas. However, the anisotropy of the plasma will modify the various kinds of discontinuities reviewed in

the preceding section. It is also possible that new kinds of discontinuities may appear.

Since, only the shock waves are of the main interest to us here, we will restrict ourselves to the problems related to the shock solutions and investigate how the anisotropy of the plasma will modify the solutions of an isotropic plasma.

As mentioned before in the case of anisotropic pressures we have nine unknowns but only eight equations, the solution of this system of equations is therefore not unique. We may specify one of the unknowns as a "free parameter". For a given value of this parameter the remaining eight unknowns can be computed with the help of equations (2.29) to (2.36).

As in the case of isotropic pressures the eight equations can be reduced into five equations by choosing an appropriately orientated coordinate system. From the coplanarity theorem derived in section 2.2.1, we always can orient our coordinate system such that B_2 vanished on both sides of the shock.

As in the previous case, it is required from equation (2.32) and (2.33), that V_2^* is continuous (i. e. $V_2^* = V_2^{*'}), and from (2.29) that B_1 is continuous (i. e. $B_1 = B_1')$ across the shock front. There are now six unknowns : ρ' , $V_1^{*'} , B_3' , V_3^{*'} , P'$ and ξ' , they can be reduced to dimensionless variables if one measures in terms of their given values in the pre-shock state.$

Replacine $P_{||}'$ and P_{\perp}' by anisotropy parameter ζ' and the scalar

pressure P' , i. e., putting , accordingly to equations (2.37) and (2.38),

$$P'_{\parallel} = P' - \frac{2}{3} (\xi' - 1) \frac{B'^2}{\mu_0} \quad (2.74)$$

$$P'_{\perp} = P' + \frac{1}{3} (\xi' - 1) \frac{B'^2}{\mu_0} \quad (2.75)$$

and using the symbols defined by (2.63). We find now (for details, see Appendix A) :

$$\chi = \frac{1}{y} \quad (2.76)$$

$$\zeta = \frac{\tan \theta_B}{\tan \theta_v} \left(\frac{\xi' - y \xi}{M_A^2 y - \xi'} \right) + 1 \quad (2.77)$$

$$u = \frac{M_A^2 - \xi}{M_A^2 y - \xi'} \quad (2.78)$$

$$(y-1) + \frac{1}{3M_A^2} (v-1) + \frac{u^2}{6M_A^2} \tan^2 \theta_B (2\xi' + 1) \quad (2.79)$$

$$- \frac{2}{3M_A^2} (\xi' - \xi) - \frac{\tan^2 \theta_B}{6M_A^2} (2\xi + 1) = 0$$

$$C_4 y^4 + C_3 y^3 + C_2 y + C_1 y + C_0 = 0 \quad (2.80)$$

where

$$C_4 = -4M_A^4 \quad (2.81)$$

$$C_3 = 10 \xi' M_A^2 - \frac{10}{3} \xi M_A^2 + 5 \left(1 + \frac{1}{\gamma M_s^2}\right) M_A^4 + \frac{4}{3} M_A^2 + \frac{5}{6} (2\xi + 1) M_A^2 \tan^2 \theta_B \quad (2.82)$$

$$C_2 = \frac{20}{3} \xi \xi' - \frac{8}{3} \xi' - 8 \xi'^2 - 10 M_A^2 \xi' \left(1 + \frac{1}{\gamma M_s^2}\right) - M_A^4 \left(1 + \frac{5}{\gamma M_s^2}\right) - \frac{4}{3} M_A^2 (1 - \xi) - \left[\frac{5}{3} \xi' (2\xi + 1) + \frac{2}{3} M_A^2 (\xi + 2) - \xi'^2 \right] \tan^2 \theta_B \quad (2.83)$$

$$C_1 = \frac{8}{3} \xi' (1 - \xi) + 5 \xi'^2 \left(1 + \frac{1}{\gamma M_s^2}\right) + 2 \xi' M_A^2 \left(1 + \frac{5}{\gamma M_s^2}\right) + \frac{2}{3 M_A^2} \xi'^2 (3\xi' - 5\xi + 2) + \tan^2 \theta_B \left[\left(\frac{8}{3} \xi' - \xi + \frac{10}{3} \xi \xi'\right) + M_A^2 \left(\frac{1}{2} - \xi'\right) + \frac{1}{6 M_A^2} (3\xi^2 + 5\xi'^2 + 10\xi \xi'^2 - 18\xi' \xi^2) \right] \quad (2.84)$$

$$C_0 = -\xi'^2 \left(1 + \frac{5}{\gamma M_s^2}\right) - \frac{4}{3 M_A^2} (1 - \xi) \xi'^2 - \left[\frac{4}{3 M_A^2} \xi'^2 (1 - \xi) + \xi'^2 \right] \tan^2 \theta_B \quad (2.85)$$

If one treats not only ξ but also ξ' as a known parameter, then (2.80) determines γ unambiguously. (One may note that by putting $\xi = \xi' = 1$, the above equations reduce to the ordinary MHD shock relations as given in section 2.2.2).

Chapter 3

DETAILED STUDY OF THE JUMP CONDITIONS
FOR ANISOTROPIC PRESSURE

3.1 On the Choice of the Proper Root of Shock Equations

Equations (2.76), (2.77), (2.78), (2.79) and (2.80) represent a complete set if the quantities M_A , M_S , ξ , Θ_B and Θ_V of the pre-shock state as well as the anisotropy parameter ξ' of the post-shock are assumed to be given. The first four equations are simple, single-valued functions of y . Once, the normal component of velocity jump, y , or the inverse of the density jump, $1/x$, is known, the values of u , v , and z can be evaluated easily provided the denominator $(M_A^2 y - \xi')$ of u and z does not vanish. The case $(M_A^2 y - \xi') = 0$ is singular and it is possible to prove that the solutions correspond to the so called "switch-on" or "switch-off" shocks. These two kinds of singular shocks will not be discussed here. Theoretical studies on this subject can be found in Anderson, (1963) and Bazer & Ericson, (1959).

Equation (2.80) allow us to determine the value of y . The complete set of solutions of (2.80) lead to four roots. One has to decide by independent arguments which of these four roots is physically meaningful. The necessary condition for the solutions to be physically meaningful is that they be real and positive.

In ordinary gas-dynamic and MHD shocks, the density increase

across the shock follows directly from the requirement that the entropy increases across the shock. However, in the case of collisionless plasmas, the plasma, in general, is not in the state of thermal equilibrium, the entropy cannot be defined in the same fashion as ordinary gases. We require that the density increases across the collisionless shock as the basic criterion to choose the proper γ . In order to fulfill the requirement that the density increases across the shock, the solution γ has to be less than one. Therefore, only those solutions for which γ lies between zero and one are physically meaningful. For certain given pre-shock states there may be no solution of (2.80) which is physically meaningful. In such cases we will not expect any shock to exist in nature. On the other hand, it is not possible to have more than one physically meaningful root which would lie between zero and one, because the post-shock state has to be uniquely determined in terms of a given pre-shock state. If there is more than one root of (2.80) which lie between zero and one, usually it is possible to distinguish the one which is physically meaningful from the condition that z , u , and v are positive, and the system of equations (2.76) to (2.80) is evolutionary (i. e. stable against perturbations). Therefore, if the shock exists we will have one and only one root of γ which is physically meaningful.

The chosen root of γ may correspond to a fast or a slow shock depending on the numerical values of pre-shock parameters. Strictly speaking, the terms "fast" and "slow" shock have been defined precisely

only for isotropic pressure. In that case, for the fast shock, the Alfvén Mach numbers M_A and M'_A have to be greater than one on both sides of the shock, while for slow shock, M_A and M'_A have to be less than one on both sides of the shock. These conditions come from the evolutionary requirements and were discussed in section 2.2.3. As can be seen from (2.66) this implies also that the ratio of tangential component of the magnetic field u is greater than one for a fast shock and less than one for a slow shock. Consequently, the values of M_A and u give us a direct information whether we deal with a fast or a slow shock.

For an anisotropic pressure plasma, the identification of fast and slow shocks is not so obvious because the problem of evolutionary condition for the anisotropic shocks has not yet been solved. Rather than to attempt a general solution to this problem within the scope of the present work, we introduce the following hypothetical criteria for distinguishing a fast shock from a slow one for the anisotropic plasma.

(1) We shall call shocks "fast" when u and M_A are larger than one and $(M_A^2 y - \xi')$ is positive, and (2) we shall call the shocks "slow", when u and M_A are less than one and $(M_A^2 y - \xi')$ is negative. These conditions are believed to be necessary but not sufficient for precise identification of fast and slow shocks in anisotropic plasmas. Note that if $\xi = \xi' = 1$, then our criteria coincide with the familiar MHD case discussed above.

There is still another way of identification of the fast and slow

shocks. Equation (2.68) can be factored in the following fashion:

$$(y-1) [C_4 y^3 + (C_4 + C_3) y^2 + (C_4 + C_3 + C_2) y + (C_4 + C_3 + C_2 + C_1)] = 0 \quad (3.1)$$

The identity root of (3.1) (i. e. $y = 1$) is the trivial solution, the remaining cubic equation of y , if looked upon as a function of the Alfvén Mach number, can be written in the following way:

$$e_6 M_A^6 + e_4 M_A^4 + e_2 M_A^2 + e_0 = 0 \quad (3.2)$$

where

$$e_6 = y^2 - 4y^3 \quad (3.3)$$

$$e_4 = (8 + 5R_e + \frac{5}{2} \tan^2 \theta_B) y^2 + (\frac{1}{2} \tan^2 \theta_B - 2) y \quad (3.4)$$

$$e_2 = (1 + \tan^2 \theta_B) - (4 \tan^2 \theta_B + 4 + 10R_e) y \quad (3.5)$$

$$e_0 = 5R_e \quad (3.6)$$

In the above equations we have put for short:

$$R_e = \frac{M_A^2}{(\gamma M_s^2)}$$

In the limit of weak shocks (i. e. $y = 1$), (3.2) reduces to

$$(M_A^2 - 1) [e_6 M_A^4 + (e_6 + e_4) M_A^2 + (e_6 + e_4 + e_2)] = 0 \quad (3.7)$$

It is apparent that the first factor represents the Alfvén wave and the second represents the fast and slow magnetoacoustic waves. This shows that three finite-amplitude shocks are possible, corresponding, respectively, to the slow, intermediate and fast shocks discussed in 2.2.3.

In the case of anisotropic plasma, (2.80) if looked upon as a function of Alfvén Mach number, is a bicubic equation for M_A^2 . As in the case for isotropic pressures, we have three roots of M_A^2 which may be defined as the slow, Alfvén and fast shocks for the anisotropic plasmas. Therefore, the equation (2.80) shows that there are no more than three kinds of shocks in the case of anisotropic plasmas as well.

3.2 The Concept and the Role of the Anisotropy Parameter in the Jump Conditions

The anisotropy parameter ξ has been defined by (2.37); its value is predicted by the structure of the velocity distribution of plasma (see Eq. 2.8). The more the ξ deviates from unity, the more anisotropic is the plasma.

An important problem for the collisionless shock is how to obtain the anisotropy changes across the shock front. The conservation equations alone are of no help in this respect. As mentioned before, there are nine unknowns but eight equations. If one takes higher moments from the Vlasov Equation, one still ends up with an underdetermined system of equations, because each next moment formation introduces

more unknowns. Some authors made special ad hoc assumptions on ξ and ξ' in order to obtain a closed system. In contrast to these early attempts we will try to obtain the values of ξ and ξ' by empirical means.

Without adopting any special assumption to close the system, it is still possible to obtain some information about the anisotropy change across the shock by studying the equations of the underdetermining system in a different light.

In the case of the actual experimental situation, when the parameters, ρ , \underline{V} , \underline{B} and P_i (where P_i is the ion pressure) are measured on both sides of the shock, then, we have to our disposal an over-specified set of equations. In principle, we can use this set to draw some quantitative or at least qualitative conclusions on those parameters which are not directly measured, such as the anisotropy parameter, ξ , the electron pressure, P_e , and the shock velocity, \underline{V}_s .

3.3 The Numerical Solutions

It is clear from (2.80) that the quantity y depends on the quantities M_A , M_S , Θ_B , ξ and ξ' but is independent of the angle Θ_v . The only quantity that depends on Θ_v is z .

In the following analysis, only the solution of (2.80) for y will be studied in detail. The values of the other variables can be readily computed from (2.76), (2.77), (2.78) and (2.79).

In the calculation, the numerical range of the constants M_A , M_S , Θ_B , ξ and ξ' have been selected in such a way as to cover their probable values expected from observations in interplanetary space, they are:

Table 3-1

The Numerical Ranges of Constants M_A , M_S , Θ_B , ξ and ξ'

constant	The ranges of the constants used in our calculations
M_A	0.5 - 10
M_S	0.5 - 10
Θ_B	$0^\circ - 90^\circ$
ξ	-0.5 - 2.5
ξ'	-0.5 - 2.5

For a given set of values of M_A , M_S , Θ_B , and ξ the quantity y has been calculated as a function of ξ' ; ξ' was allowed to vary from -0.5 to +2.5 at an interval of 0.1. If we fix the quantities M_A , M_S , and ξ in a given plot, a family of curves of y vs. ξ' for different Θ_B are obtained. Figure 3-1 shows the plot of y vs. ξ' for various Θ_B at fixed M_A , M_S and ξ . The numerical values chosen for M_A , M_S and ξ are 6.3, 12.0 and 1.0, respectively.

Closer examination of Figure 3-1 permits us to draw the following con-

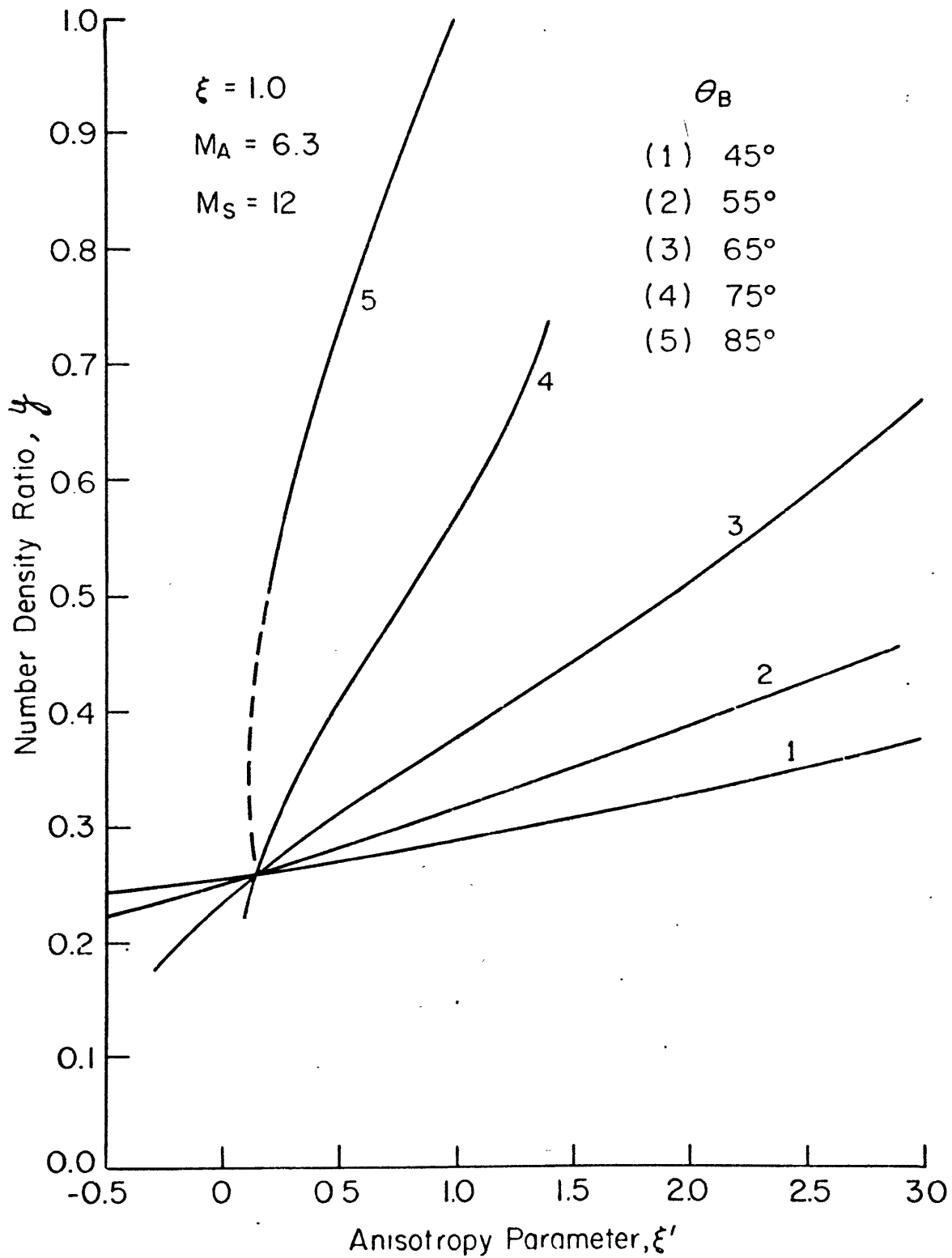


Figure 3-1

clusions:

(1) All curves referring to various values of Θ_B intersect at one point in the vicinity of $\xi' = 0.15$. This implies that for $\xi' = 0.15$ the density ratios (or normal velocity ratios) are independent of the tangential component of the magnetic field with respect to the shock normal. The occurrence of common intersection points is not accidental and can be shown to exist in general. For detail study of these interesting special values of ξ' , see Appendix B.

(2) The values of y are rather sensitive functions of Θ_B for $\xi' = 1$. (i. e. isotropic pressure in the post-shock state.) This implies that magnetic field orientation has important influence on the shock relations for this ξ' .

(3) Each curve of y vs. ξ' is a monotonically increasing function of ξ' .

(4) For certain range of values of ξ' , y may become less than 0.25, that is, the density ratio across the shock front may be larger than 4, which is the largest density jump allowed for isotropic MHD shock.

(5) The values of y become less dependent on ξ' when the angles Θ_B become less than 45° . In the extreme case when Θ_B approaches zero, the y values become independent of ξ' .

A large number of families of curves for different values of M_A , M_S and ξ have been investigated and most of them show similar character to that of Figure 3-1.

Let us discuss now the dependence of y on the remaining quantities, namely, ξ , M_A and M_S . Varying only one quantity at the time, we arrive at the following conclusions;

(A) Varying ξ

Figure 3-2 shows four plots of y vs. ξ' with constant M_A and M_S but for different values of the anisotropy parameter ξ . The set refers to $M_A = 8.6$, $M_S = 2.25$, and $\xi = 1.0, 0.8, 0.4$, and 0.2 respectively. It is found that y is almost independent of ξ , provided the angle Θ_B is not very large. For Θ_B less than 60° , no appreciable difference between various y 's for different ξ 's is found.

(B) Varying M_A

Figure 3-3 is similar to Figure 3-2 but the Alfvén Mach number M_A is allowed to vary instead. The set refers to $\xi = 0.75$ and $M_S = 2.45$, and $M_A = 10, 2.85, 1.5$ and 0.85 , respectively. The plots show the similar features as Figure 3-1 for M_A larger than 2.85 . The slope of y vs. ξ' at the same Θ_B and the y -value of the intersection point decrease as the Alfvén Mach number M_A increases. Note that for $M_A = 1.5$, the shape of the curves is quite different from those for which M_A are larger than 2.85 . For a certain range of ξ' , y becomes double-valued. Thus, additional conditions have to be introduced to choose the physically proper solution. Note further that for $M_A = 0.85$, the y - vs. ξ' - curve becomes again a monotonic, decreasing function of ξ' . These curves represent examples for slow shocks.

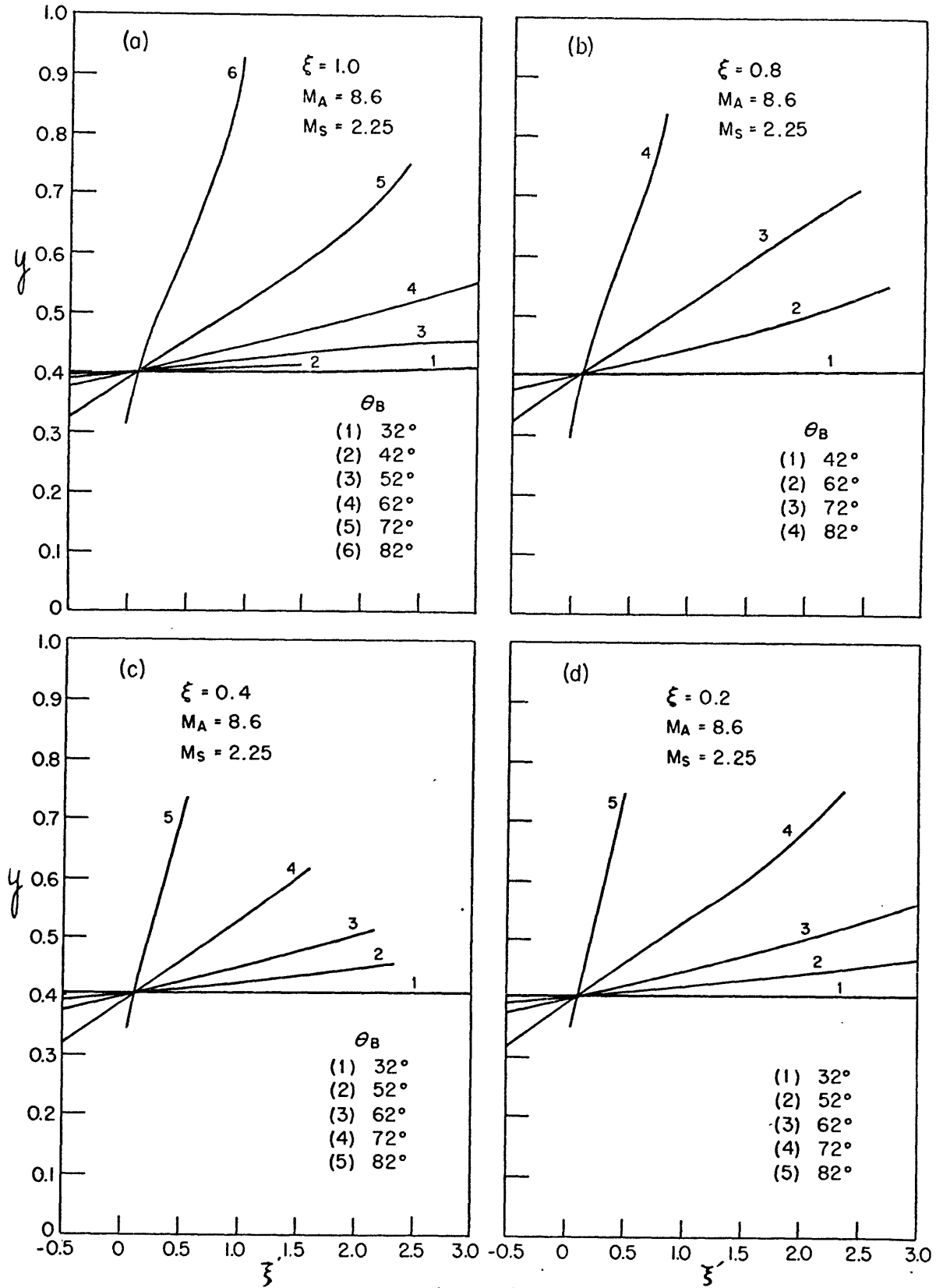


Figure 3-2

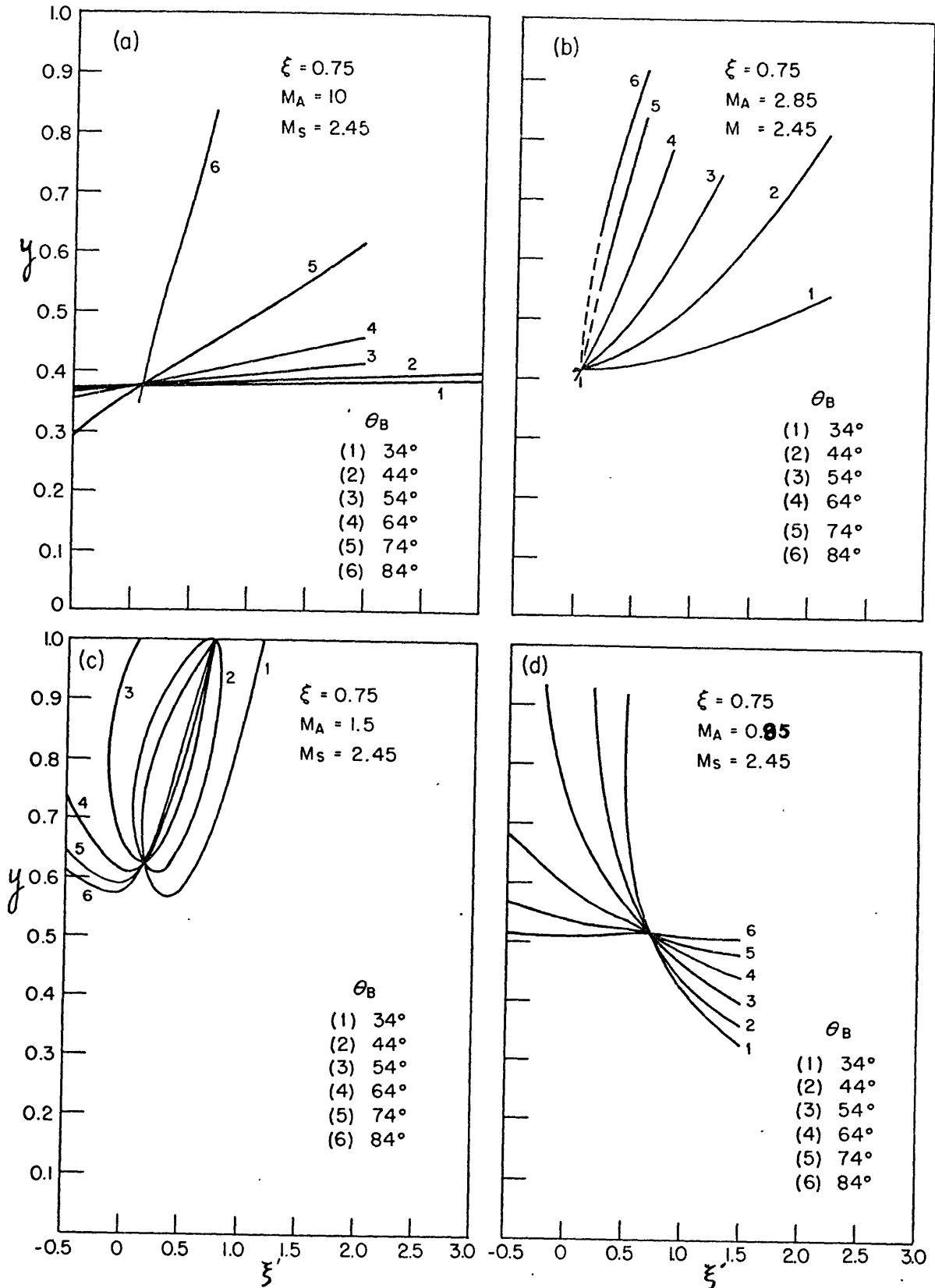


Figure 3-3

(C) Varying M_S

Figure 3-4 is similar to the previous Figures, but now the sound Mach number M_S is varied. The set refers to $\xi = 0$, $M_A = 3.7$, and $M_S = 10, 4.1, 1.5$ and 0.8 , respectively. The plots show again features similar to those in Figure 3-1 provided M_S is larger than 1.5. When $M_S = 0.85$, the general shape of the curves changes completely. As in Figure 3-4 (d), the y - vs. - ξ' - curves become highly dependent on ξ' for Θ_B larger than 70° and, moreover, y becomes quite small for certain values of ξ' when Θ_B is larger than 80° .

Finally, we should like to present results in two limiting cases: one involving very large Alfvén Mach number and the other, very large sound Mach number. The results are shown in Figure 3-5. It is interesting to note that y does not approach the limiting value of 0.25 as is the case in very strong shocks in isotropic plasmas. For large M_A , the values of y are almost independent of ξ' and Θ_B . On the other hand, for large M_S , the values of y depend strongly on ξ' and moderately on Θ_B . As both M_S and M_A become very large, one can show from (2.80) that the values y approach 0.25 for any given Θ_B and ξ' .

The results concerning y obtained in this chapter and the associated results concerning x , z , u and v , will be utilized in Chapters 5 and 6, where we undertake to analyze actual shocks observed in the interplanetary space.

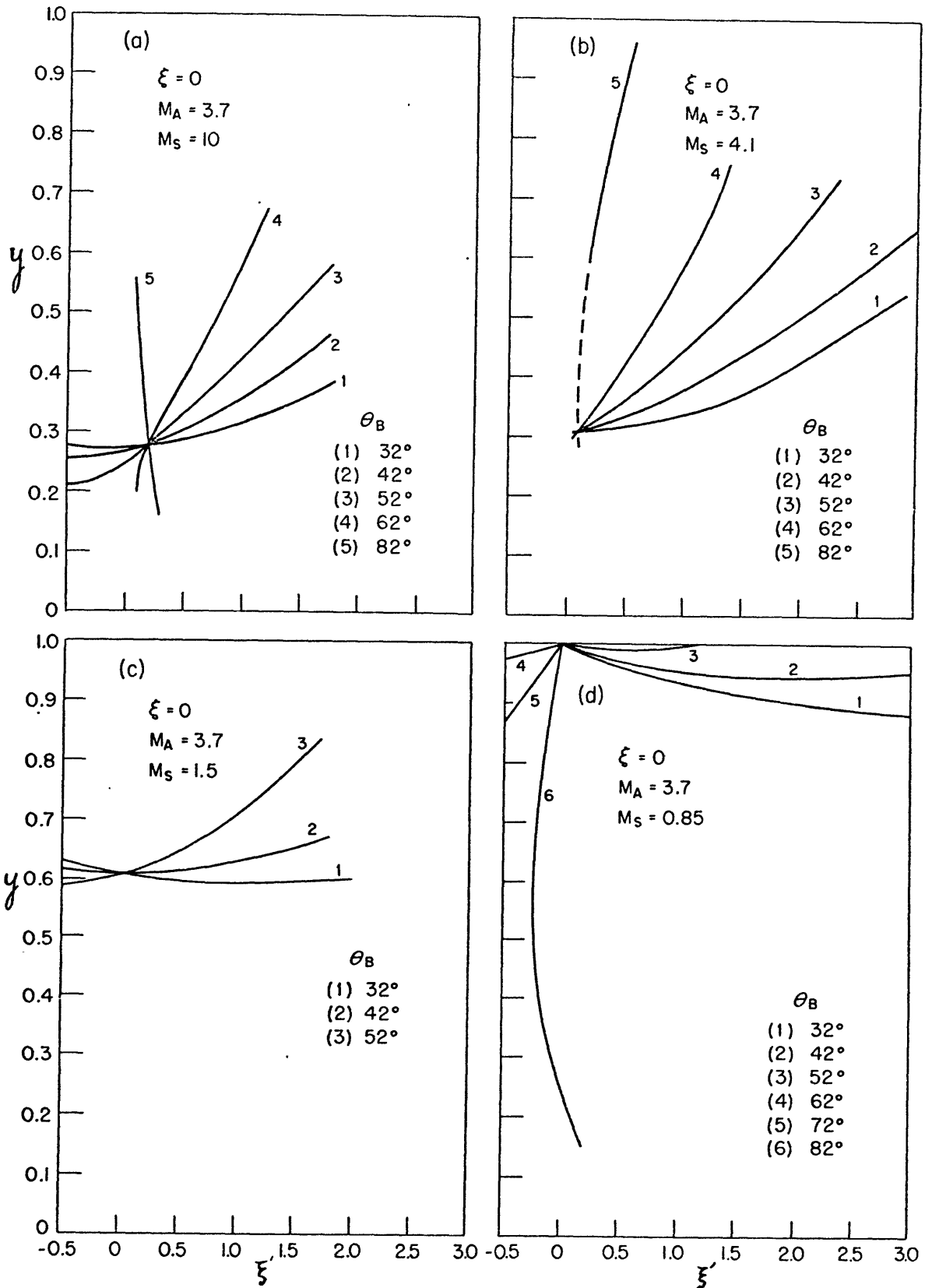


Figure 3-4

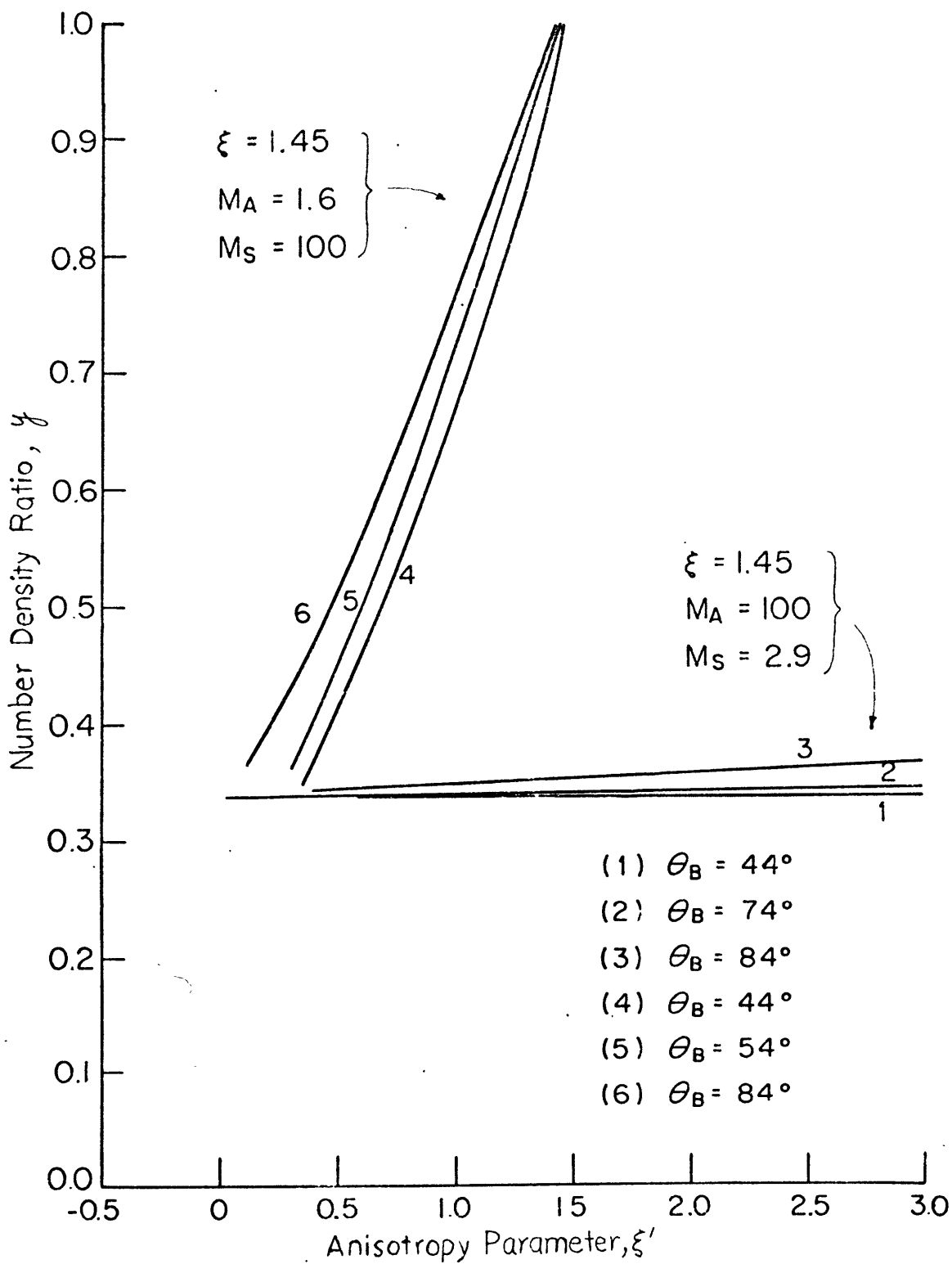


Figure 3-5

Chapter 4

A METHOD OF IDENTIFICATION OF THE SHOCK FRAMES WITH THE HELP OF THE TRANSIT TIME

4.1 Analytical Expressions for Shock Normal

Since the velocity vector of the interplanetary shocks is unknown, it is necessary first to compute this vector in order to define the shock frame. All the measured velocities, then, can be transformed into the shock frame. The magnetic field is the same in both the shock frame and the satellite frame (as long as the shock velocity stays non-relativistic). Hence, the magnetic field measured in the satellite frame may be used unmodified by the observer in the shock frame. The coplanarity theorem proven in section 2.2.1 requires that the magnetic fields on both sides of the shock and the shock normal vector lie in the same plane. Thus, when the shock is not propagating along the magnetic field nor perpendicular to it, the vectors $(\underline{B}' - \underline{B})$ and $(\underline{B}' \times \underline{B})$ must stay in the plane of the shock. Therefore, the shock normal, \hat{n} , is given by

$$\hat{n} = \pm \frac{(\underline{B}' - \underline{B}) \times (\underline{B}' \times \underline{B})}{(\underline{B}' - \underline{B}) \times (\underline{B}' \times \underline{B})} \quad (4.1)$$

The sign of the shock normal has to be determined from the measured plasma data. Thus, the coplanarity theorem enables us to determine the shock normal from the magnetic field data on both sides of the shock

alone; in other words, no additional information on other plasma parameters is needed in principle.

The determination of the shock normal \hat{n} , by this method is severely restricted due to two kinds of errors. The first kind of error is due to the fact that the magnetic fields are often observed to fluctuate, especially in the post-shock state. The shock normal \hat{n} determined from such unsteady magnetic fields will be subjected to large uncertainty. The second kind of error is due to the fact that the angle between \underline{B} and \underline{B}' is often very small. The above formula for \hat{n} shows that a few degrees of uncertainty in the direction of \underline{B}' or \underline{B} causes a large uncertainty in \hat{n} . In the extreme case when the shock propagates along or perpendicular to the magnetic field \underline{B} , the equation (4.1) is of no use for determining the shock normal.

Because of these practical difficulties, equation (4.1) can often be used only for guiding purposes as to the very approximate behavior of \hat{n} . In order to improve the determination on \hat{n} , one must resolve to iteration procedures which employ not only equation (4.1) but various other available shock equations. In other words, one uses (4.1) as a first step in the iteration processes and insists that not only (4.1) but also other pertinent shock equations be simultaneously satisfied. This procedure is quite involved and requires help of digital computers. The details of the iteration methods for the determining \hat{n} are present in the Appendix C.

Due to the complexity of the above mentioned process, it is impor-

tant to search for other means to determine the shock normal. Such opportunity offers itself in the interplanetary space when it so happens that, simultaneously with the primary satellite, there is present another satellite or a deep space probe capable of detecting, at least qualitatively the passage of the same shock. In practice, one always has precise information as to the position of the secondary vehicle relative to the primary one. In addition, one also knows well the time interval which the shock needs for the passage from the primary to the secondary vehicle. We shall refer, in what follows, to this time interval as the transit time, τ . If the distance between the two vehicles in question is not excessively large, say relatively small fraction of one astronomical unit (1 A. U.), then, it is plausible to assume that the shock front is planar and is propagating at a constant speed.

It is interesting to note that the earth itself can often replace the role of the secondary vehicle. This is so due to the fact that the passage of the interplanetary shock through the earth's magnetosphere causes observable sudden changes in the magnetic field measured on the surface of the earth (the so-called "storm sudden commencement," often abbreviated as ssc.) This functional relation between ssc-events and interplanetary shocks is a fairly well established fact, both on theoretical and experimental ground (Nishida, 1969; Hirshberg, 1963). Of course, the earth may be used as such a secondary detector only if the primary satellite is located well ahead of the earth magnetosphere. More specifically,

we must require that the transit time of the shock between the primary vehicle and the earth is substantially greater than the transit time for the passage of that shock through the frontal part of the magnetosphere.

[Since the distance from the subsolar point of the bow shock (or of the magnetopause) to the earth surface is of the order of ten earth radii, and, since the shock speed is typically of the order 500 km/sec, the transit time through the magnetosphere may be expected to be of the order of 3 minutes, i. e. $\tau \gg 3 \text{ min.}$]

We now proceed to discuss in detail how the availability of the secondary satellite can be utilized to derive an analytical expression for the shock normal. For this purpose, we will find convenient to make use of the following directly measurable quantities:

(1)

$$\hat{e}_B = \frac{\underline{B}}{|\underline{B}|} \quad (4.2)$$

\hat{e}_B represents the unit vector of the magnetic field in the pre-shock state. This quantity is assumed to be given directly from the data. As it will become clear later on, this is the only information about the magnetic field which we shall need for the present procedure. In other words, we do not require the knowledge of either the magnitude of the magnetic field in the pre-shock state or any of the three components of the magnetic field in the post-shock state.

(2)

$$\underline{W} = \underline{V}' - \underline{V} \quad (4.3)$$

\underline{W} represents the difference between the solar wind velocity before and after the shock. If the plasma measurements are complete, \underline{W} is a known vector (i. e. completely specified by three numbers) and is independent of any specific frame of references in which it was determined. In all the cases discussed in Chapter 5, this vector is known with a relatively high accuracy. Associated with this vector is the unit vector

$$\hat{e}_w = \frac{\underline{W}}{|\underline{W}|} \quad (4.4)$$

In the MHD approximation, either for isotropic or anisotropic pressures, the vector \underline{W} has the following important property: it lies in the plane containing \hat{n} , \underline{B} and \underline{B}' , i. e., it has no component at right angles to the plane formed by (\hat{e}_B, \hat{n}) . The proof of this follows directly from (2.45). Because of this property of \underline{W} , we have evidently

$$(\hat{e}_w \times \hat{e}_B) \cdot \hat{n} = 0 \quad (4.5)$$

(3)

$$\underline{u} = \frac{\underline{r}}{\tau} - \frac{\rho' \underline{V}' - \rho \underline{V}}{\rho' - \rho} \quad (4.6)$$

where \underline{r} represents the instantaneous position vector of the secondary satellite measured from the primary satellite. (By the "primary

satellite" we mean that satellite which provides the detailed information about \underline{W} , and \hat{e}_B .) The eight quantities ρ , ρ' , \underline{V} and \underline{V}' are all measured in the frame of reference of the primary satellite and may, for our purposes, be considered as given. Note that the quantity defined by (4.6) has the dimensions of a velocity and it possesses the important property that its component normal to the shock front vanishes. i. e.,

$$\underline{U} \cdot \hat{n} = 0 \quad (4.7)$$

To prove this, consider first that, by virtue of the law of mass conservation (2.30), the expression for the shock speed, V_s is given by:

$$V_s = \left(\frac{\rho V' - \rho V}{\rho' - \rho} \right) \cdot \hat{n} \quad (4.8)$$

Secondly, if we recall our assumption of the uniform propagation of the planar shock within the time interval τ , the expression $\frac{\underline{r} \cdot \hat{n}}{\tau}$ also represents (empirically) the shock speed. These two facts imply (4.7).

Associated with \underline{U} is the known unit vector:

$$\hat{e}_u = \frac{\underline{U}}{|\underline{U}|} \quad (4.9)$$

which identifies the direction of \underline{U} .

The usefulness of the above defined quantities for the construction of the shock normal is now apparent. Since, according to equations (4.5)

and (4.7), \hat{n} is perpendicular to both $\hat{e}_W \times \hat{e}_B$ and \hat{e}_U , it follows that:

$$\hat{n} = \frac{(\hat{e}_W \times \hat{e}_B) \times \hat{e}_U}{|(\hat{e}_W \times \hat{e}_B) \times \hat{e}_U|} \quad (4.10)$$

or, written out in a more explicit form:

$$\hat{n} = \frac{\hat{e}_B - k \hat{e}_W}{(1 - 2k\beta + k^2)^{1/2}} \quad (4.11)$$

where we have put for short

$$\beta = \hat{e}_W \cdot \hat{e}_B \quad (4.12)$$

$$k = \frac{\hat{e}_U \cdot \hat{e}_B}{\hat{e}_U \cdot \hat{e}_W} \quad (4.13)$$

Thus, we have obtained the shock normal in terms of two unit vectors \hat{e}_B and \hat{e}_W , and two scalars k and β .

Once the spatial orientation of the shock plane has been determined, the identification of the frame of reference moving with the shock, Σ^* , is trivial. One simply has to recall (4.8) which is readily computable from the data and (4.11).

The explicit specification of the remaining two axes of the Cartesian coordinates of Σ^* , is now very simple. For example, the unit vector,

* The above derivation of \hat{n} ^{was} ~~was~~ ~~been~~ suggested to me by Professor S. Olbert.

\hat{m} , indicating the direction of the component of \hat{e}_B tangential to the shock plane, is evidently given by:

$$\hat{m} = \frac{(\hat{n} \times \hat{e}_B) \times \hat{n}}{|(\hat{n} \times \hat{e}_B) \times \hat{n}|} \quad (4.14)$$

or written out explicitly, after simple algebra,

$$\hat{m} = \frac{(1 - k\beta)\hat{e}_w - (\beta - k)\hat{e}_B}{(1 - 2k\beta + k^2)^{1/2}(1 - \beta^2)^{1/2}} \quad (4.15)$$

4.2 Analytical Expressions for Magnetic Field Components in

Shock Frame of Reference

Once the speed and the orientation of Σ^* are known, as mentioned already previously, we may convert various physical quantities measured in the frame of the satellite to the corresponding quantities referring to Σ^* .

Here we are particularly interested in the computation of the magnitude of \underline{B} field in the pre-shock state, the normal component of \underline{B} and the tangential component of \underline{B}' after the shock. Recall that, out of the available information on the magnetic fields across the shock (six measured numbers in all), we have used up so far only two (\hat{e}_B). Thus, the remaining four numbers, (i. e., B and three components of \underline{B}') are now overdetermined. The comparison of the theoretical results with the observed ones gives us the opportunity of testing the validity of the MHD

shocks.

For this purpose, let us recall equations (2.30), (2.34) and (2.31).

Adjusting to notation so that the subscripts 1 and 3 of Chapter 2 are replaced by the subscripts n and m , respectively, we have:

$$[\rho V_n^*] = 0 \quad (4.16)$$

$$[\rho V_n^* V_m^* - \xi \frac{B_n B_m}{\mu_0}] = 0 \quad (4.17)$$

$$[V_m^* B_n - B_m V_n^*] = 0 \quad (4.18)$$

Using the definition of \underline{W} , we can write (4.17) and (4.18) also as:

$$\frac{\mu_0 \rho V_n^* V_n^{*'} W_m}{B_n \xi'} = (B_m' - B_m) V_n^{*'} - \frac{B_m V_n^{*'} (\xi' - \xi)}{\xi'} \quad (4.19)$$

$$W_m B_n = (B_m' - B_m) V_n^{*'} + B_m W_n \quad (4.20)$$

Since,

$$B_n = B (\hat{e}_B \cdot \hat{n})$$

$$B_m = B (\hat{e}_B \cdot \hat{m})$$

$$V_n^{*'} = -\frac{\rho}{\rho' - \rho} (\underline{W} \cdot \hat{n})$$

$$V_n^* = -\frac{\rho'}{\rho' - \rho} (\underline{W} \cdot \hat{n})$$

$$W_n = W(\hat{e}_w \cdot \hat{n})$$

$$W_m = W(\hat{e}_w \cdot \hat{m})$$

we obtain, by virtue of (4.11) through (4.15),

$$B = (\mu_0 m_p D)^{1/2} \frac{W(k-\beta)}{(1-k\beta)^{1/2} g \eta} \quad (4.21)$$

$$B_n = (\mu_0 m_p D)^{1/2} \frac{W(k-\beta)(1-k\beta)^{1/2}}{g \eta^{1/2}} \quad (4.22)$$

$$B'_m = (\mu_0 m_p D)^{1/2} \frac{W(1-\beta^2)^{1/2} [(k-\beta)k + \mathcal{A}g]}{(1-k\beta)^{1/2} g \eta^{1/2}} \quad (4.23)$$

where, for the sake of brevity, we have put:

$$D \equiv \frac{n^2 n'}{(n' - n)} \quad (4.24)$$

$$\mathcal{A} \equiv \frac{n' - n}{n} \quad (4.25)$$

$$g \equiv 1 - 2k\beta + k^2 \quad (4.26)$$

$$\eta \equiv \xi' + \frac{k(k-\beta)(\xi' - \xi)}{\mathcal{A}g} \quad (4.27)$$

In (4.24) and (4.25), n and n' are defined as the number densities of

ions in the pre- and post-shock states, respectively.

It is interesting to note that the ratios B'_m / B_m and B'^2 / B^2 which according to (4.19) through (4.23) are given by:

$$\frac{B'_m}{B_m} = 1 + \frac{\alpha g}{k(k-\beta)} \quad (4.28)$$

$$\frac{B'^2}{B^2} = \frac{1}{g} \left[\left(k + \frac{\alpha g}{k-\beta} \right)^2 (1-\beta^2) + (1-k\beta)^2 \right] \quad (4.29)$$

are independent of ξ and ξ' .

Thus, we can predict the above two ratios in terms of the experimentally known quantities α , k and β alone, without any knowledge of the degree of the anisotropy present in the plasma.

One may start the test of the theoretical results with the simplest assumption that the plasma is isotropic (i. e., $\xi = \xi' = 1$). If, under this assumption, the value of B as computed on the basis of (4.21) agrees with the observed one, we may tentatively conclude that the plasma is isotropic. On the other hand, if the assumption of isotropy leads to disagreements between the predicted and observed value of B , we have strong indication for an anisotropic character of the plasma.

When the assumption on isotropy is abandoned, ξ and ξ' can be looked upon as varying parameters, determined in such a way as to bring the computed B and B' into agreement with the measured values.

This procedure, which leads to empirical determination of the pressure anisotropies on both sides of the shock will be discussed in detail in Chapter 6.

Closer inspection of the equations (4.21), (4.22), and (4.23) shows that the analytical results can be conveniently represented in a graphical form. Among various representations, the following seems to be compact and useful.

To this end, introduce the dimensionless quantity: $(B^2 / (\mu_0 m_p D W^2))$, look upon it as a function of two variables k and β and, treat ξ and ξ' as fixed parameters. Let us define

$$D1 \equiv \frac{B^2}{\mu_0 m_p D W^2}$$

Figures 4-1 and 4-2 show the results.

We notice from Figure 4-1 that D1 decreases monotonically as one travels radially away from the origin of the β - k plane for all quoted combinations of ξ and ξ' . Note also the steepness of this relief is much more pronounced for the physically implausible case when the pre-shock plasma is more isotropic than the post-shock plasma.

Figure 4-2 shows, in addition to D1, also two other dimensionless quantities, namely

$$D2 \equiv \frac{B_n^2}{\mu_0 m_p D W^2}$$

$$D3 \equiv \frac{B_n'^2}{\mu_0 m_p D W^2}$$

given by equation (4.22) and (4.23) for the case of isotropy. D1 behaves in a very similar manner to those discussed in Figure 4-1.

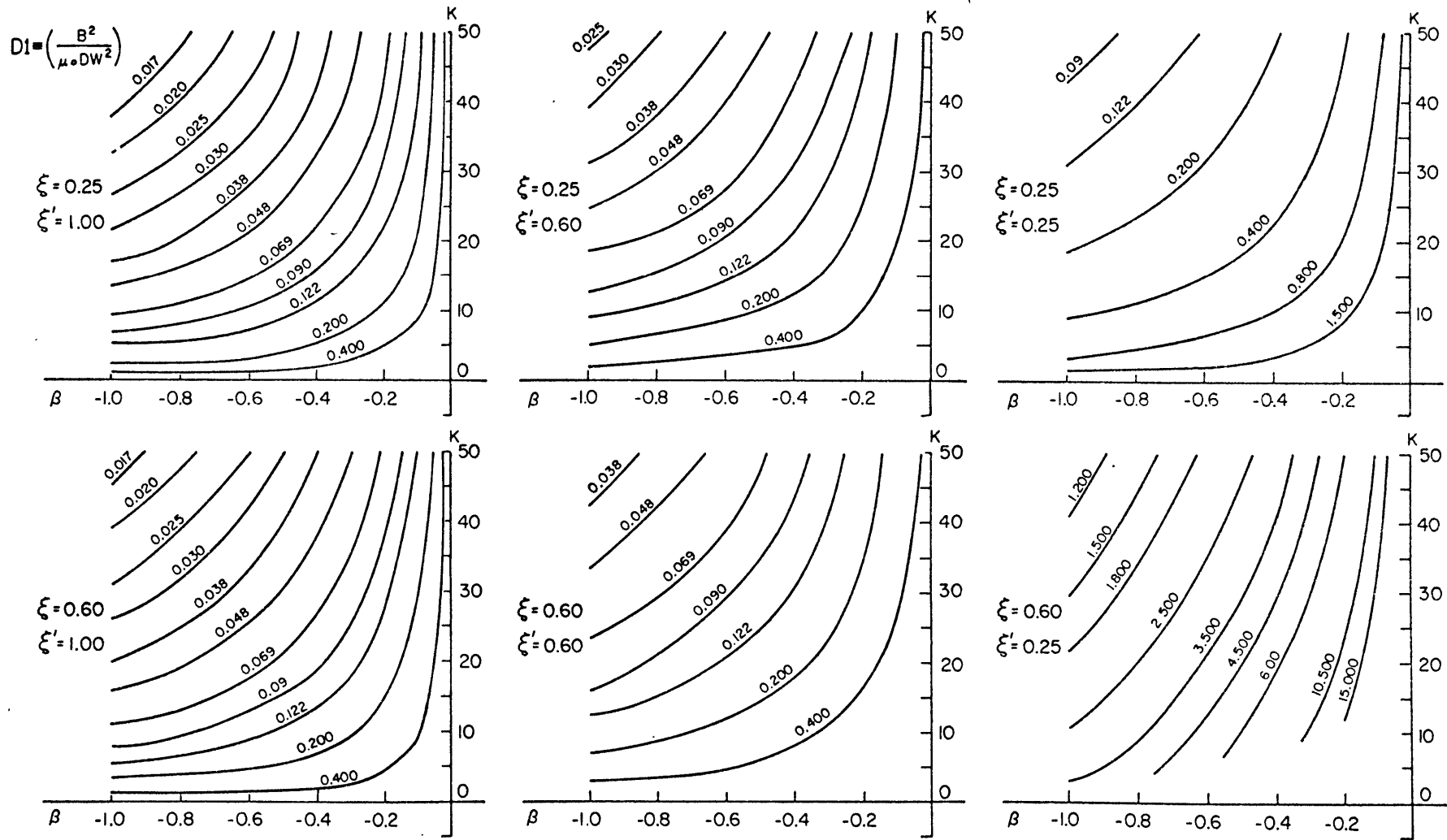


Figure 4-1

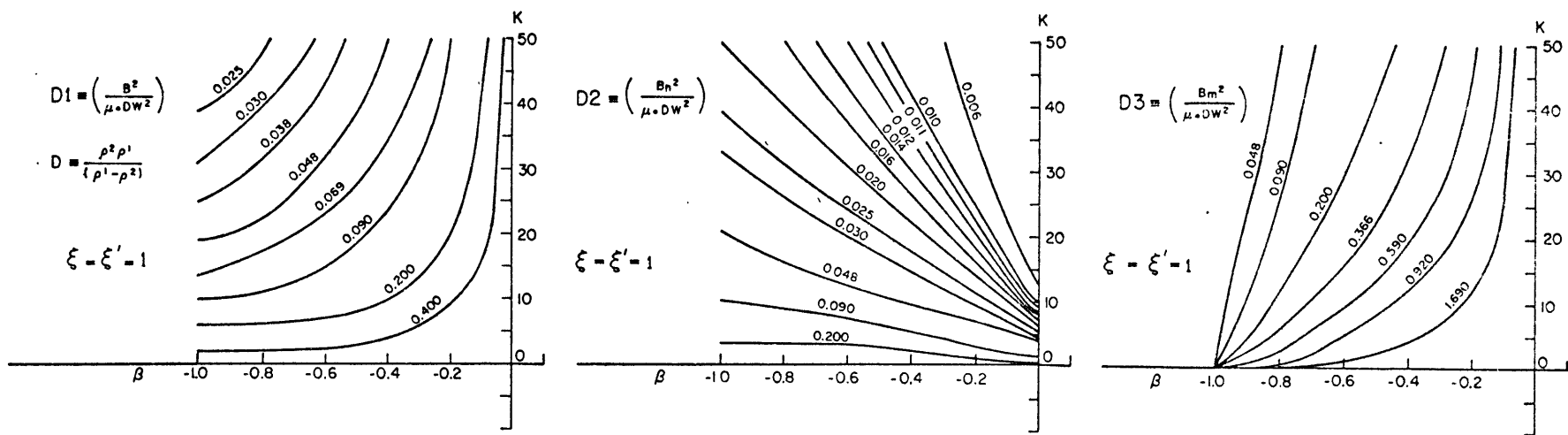


Figure 4-2

Chapter 5

EXPERIMENTAL EVIDENCE OF THE INTERPLANETARY COLLISIONLESS SHOCKS

5.1 Introductory Remarks

The plasma measurements in the interplanetary medium by means of deep space probes underwent substantial quantitative improvement in recent years. In particular, the MIT detectors onboard Mariner V, Pioneers 6 and 7 were capable of measuring reliably not only the densities of positive ions, n , but also all three components of their streaming velocities, \underline{V} . In addition, the MIT detectors were able to provide some information about the thermal motion of the ions. The description of the mode of operation and of the method of data reduction can be found by the reader elsewhere (Lazarus, et. al., 1966; Vasyliunas, 1969). The data from the above quoted spacecrafts have been made available in the reduced form to this author by Dr. A. Lazarus. In addition to the MIT plasma data, we were fortunate to have available also the magnetic field data. Thus, we have measurements of the magnetic fields simultaneous with our plasma measurements on Mariner V from the Jet Propulsion Laboratory (JPL) (under the supervision of Drs. L. Davis Jr. and E. Smith). Similarly complete magnetic field data are available to us in the case of Pioneers 6 and 7 from Drs. N. Ness

and L. Burlaga of Goddard Space Flight Center.

All data were available either on graphs or on magnetic tapes in the reduced form, i. e., in the form yielding directly the physical parameters of interest to us (for examples, three Cartesian components of the magnetic fields, ion number densities, etc.).

Pioneers 6 and 7, and Mariner V were launched respectively, on December 16, 1965, August 17, 1966, and June 14, 1967. The time spans with almost continuous data records for each of these spacecraft, which we searched through are as follows:

Pioneer 6:	From December, 1965 to April, 1966
Pioneer 7:	From August, 1966 to October, 1966
Mariner 8:	From June, 1967 to September, 1967

As a result of this extensive search we were able to identify seven well defined discontinuities which appeared to be plausible candidates for MHD shocks. These events identified by the universal time of their occurrence and their association with the given spacecraft (the "primary" spacecraft), are listed in Table 5-1. The secondary spacecraft as well as the approximate distance (in A. U.) between the primary and the secondary spacecraft (or the Earth), denoted by Υ , are also given in Tables 5-1 for each shock.

Table 5-1

The Primary and Secondary Spacecraft, and the Identified Shock-like Discontinuities

Primary Spacecraft	Shock Number	Universal Time	Secondary Spacecraft or ssc	Relative Distance
Explorer 6	1	20:58, March 22, '66	no ssc	none
	2	04:20, March 23, '66	ssc	1/100
Explorer 7	3	14:16, August 29, '66	Explorer 33	1/100
Explorer V	1	13:46, June 26, '67	Explorer 34	1/50
	2	05:25, July 20, '67	no ssc	none
	3	07:10, August 29, '67	Explorer 34	1/100
	4	13:24, August 30, '67	no ssc	none

Before we embark on a detailed discussion of these discontinuities we should like to make a few comments about the rates of data acquisition. These rates are different for different detectors and for different locations of the spacecraft relative to the earth. For example, as far as the magnetic field data are concerned, the time intervals between two consecutive measurements range from 1 up to 5 seconds depending on the distance of the spacecraft from the earth. On the other hand, the time span between two plasma measurements is much wider: For the initial flight period of Pioneers 6 and 7 this time span was 1 minute. Later in the flight, when the spacecraft were far from the earth, this time span jumped to as much as 20 minutes. For the initial flight period of Mariner V, the time span was 5 minutes, but for the later part of the flight, the time span became 20 minutes.

For the convenience of the reader we show in Figures 5-1 and 5-2 the trajectories of the three spacecraft as viewed by the observer on earth.

5.2 Results of the Analysis of the Seven Shock-Like Events

To begin with, let us define two alternate coordinate systems to be used in what follows. They are shown in Figure 5-3. The first one is the so-called RTN coordinate system, in which the R-axis is out from the sun and parallel to the sun-earth line, the T-axis is in the direction of the motion of the earth, and the R-T plane is parallel to the ecliptic

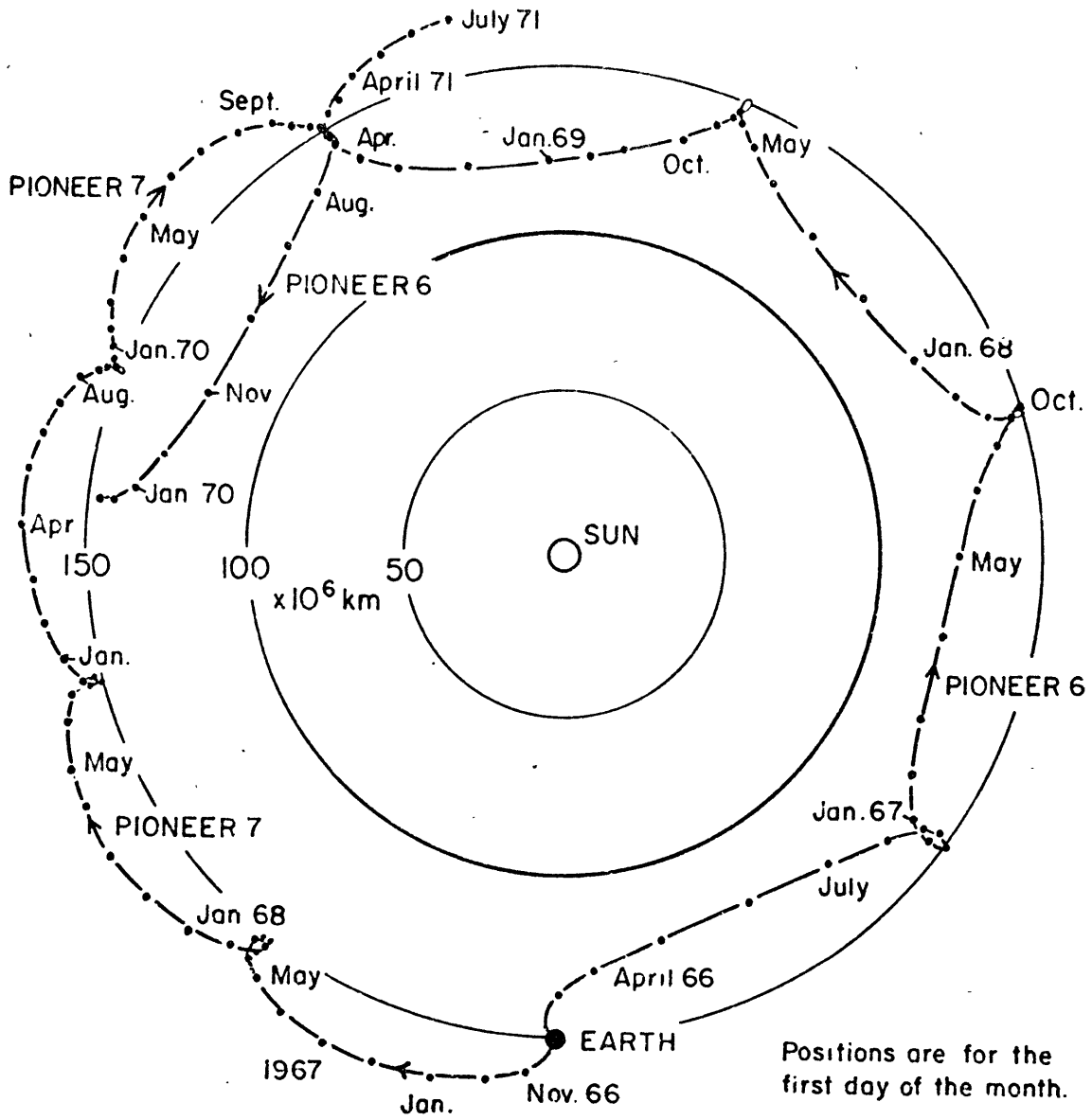


Figure 5-1

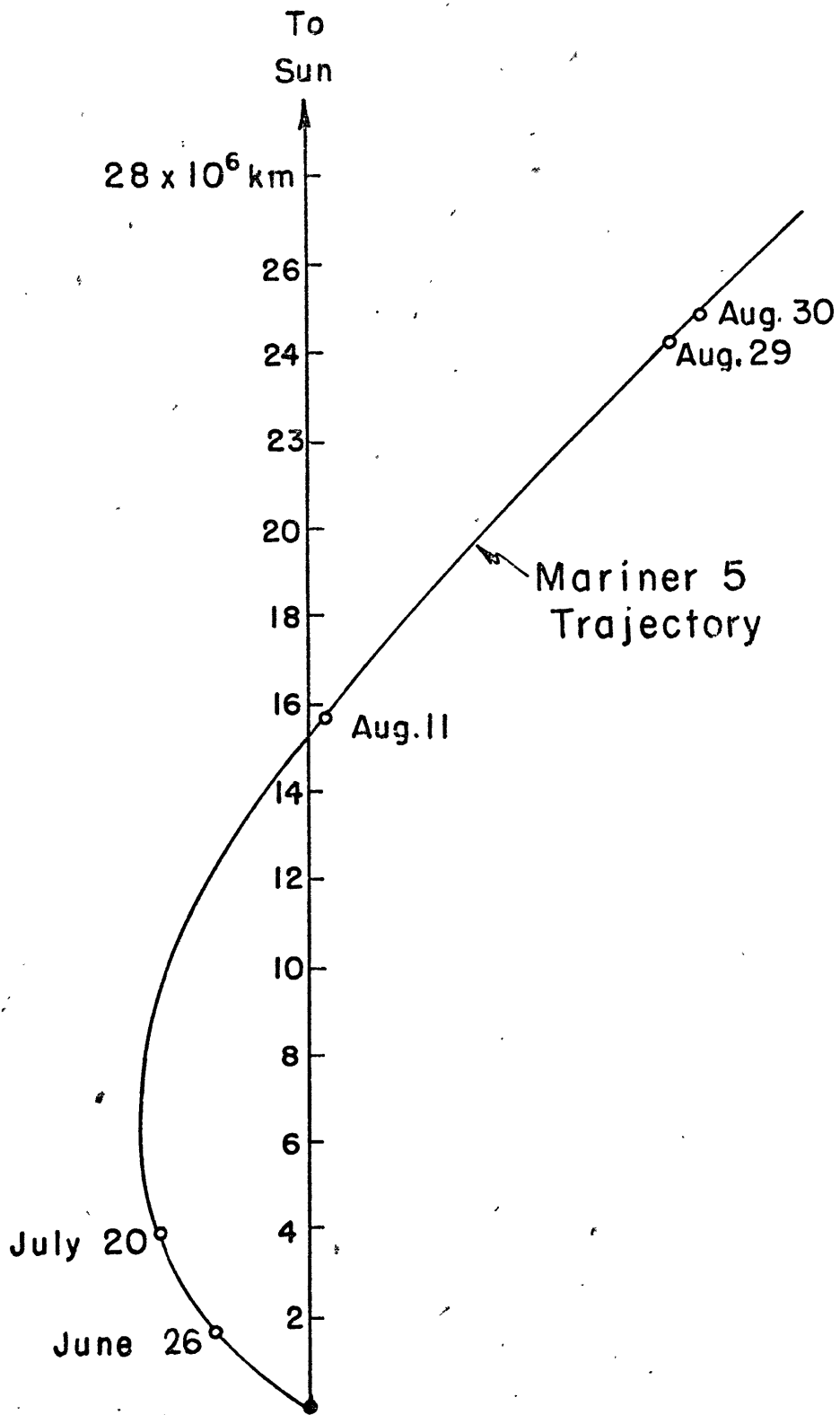
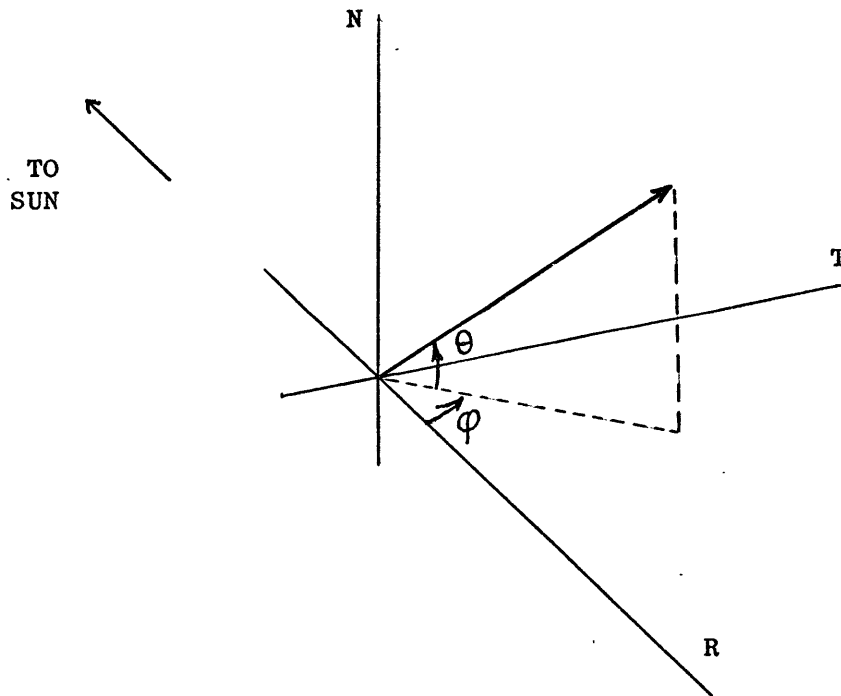


Figure 5-2

plane. The N-axis is perpendicular to the ecliptic plane. The second one is the so-called solar Ecliptic coordinate system, in which the directions of a given vector are identified by the angle, Θ , between the vector and the ecliptic plane, and the angle, φ , between the projection of the given vector onto the ecliptic plane and the R-axis. The angle Θ ranges from 90° to -90° and is positive when the vector points northward from the ecliptic plane. φ equals 90° when the vector is along the T-axis, and ranges from -180° to 180° .

Figure 5-3

The RTN and Solar Ecliptic Coordinates



There are three vectors whose orientation in space is of interest to us: the magnetic field vector, the wind velocity vector and the shock normal. According to the above definition, we can represent the \underline{B} and \underline{V} and \hat{n} vectors alternately as:

$$\underline{B} = B (\Theta_B, \varphi_B) \quad \text{or} \quad \underline{B} = (B_R, B_T, B_N)$$

$$\underline{V} = V (\Theta_V, \varphi_V) \quad \text{or} \quad \underline{V} = (V_R, V_T, V_N)$$

and

$$\hat{n} = (\Theta_s, \varphi_s) \quad \text{or} \quad \hat{n} = (n_R, n_T, n_N)$$

The primed (unprimed) symbols shall refer, as previously, to the post- (pre-) shock conditions.

In this chapter, for the sake of simplicity, we shall analyze all the shocks under the assumption that the plasma pressures are isotropic. This assumption can be justified only a posteriori, i. e., only when the analysis demonstrates a reasonable agreement between observations and theory with $\xi = \xi' = 1$. As we shall see from the quoted results this assumption is quite tenable to the first approximation. As explained in the Appendix C, this simplified assumption leads to three-fold or four-fold overdeterminicity between the measured and computed parameters, depending on whether or not the transit time is available.

With these preliminaries, we are now ready to discuss the individual events.

Fast Shocks of March 22 and March 23, 1966

No geomagnetic storm resulting from the shock of March 22 could

be identified, therefore, there was no transit time available for this particular shock. On the other hand, there was a geomagnetic storm that could be associated with the shock of March 23.

Figures 5-4 and 5-5 show the actual behavior of physical parameters as functions of time within a time interval of 90 minutes involving actual discontinuities.

Each figure contains eight separate graphs. The first column on the left, going from top to bottom, represents, respectively, the thermal velocity (km/sec), the magnitude of the wind velocity (km/sec) and the ion number density (per c. c.). The second column shows the angles φ_V and Θ_V as defined in Figure 5-3, and measured in degrees. Finally the third column, again from top to bottom, shows respectively, the magnitude of the magnetic field (gamma) and the two angles φ_B and Θ_B measured in degrees and identifying the direction of B-vector in the Solar Ecliptic Coordinates. All quantities are plotted vs. time measured in minutes (with arbitrary origin). The data points are connected by straight lines simply to facilitate the following of the temporal trends. The plasma parameters are taken at the rate of 1 minute per measurement. The observed shock jumps occur between two adjacent plasma measurements. In contrast, the curves for the magnetic field refer to intervals between measurements of 30 seconds. The vertical bars on both sides of the discontinuities indicate the combined error (more precisely, the r. m. s. deviation) due both to the experimental uncertain-

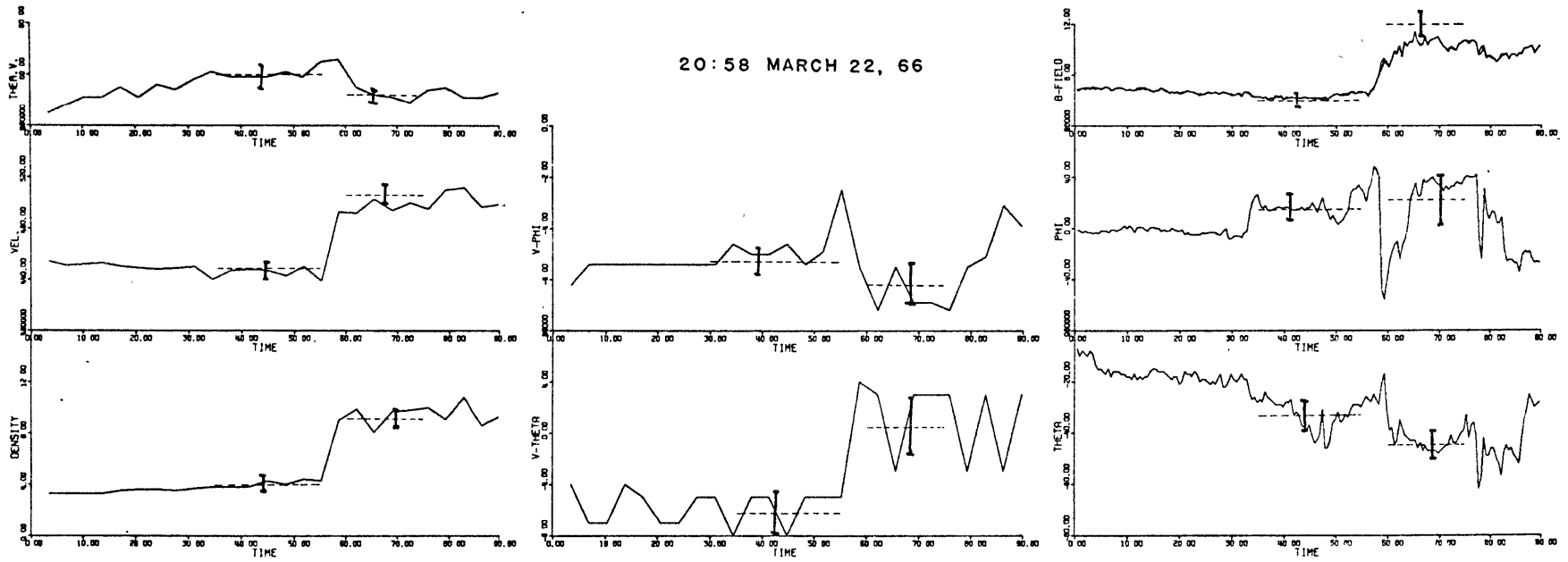
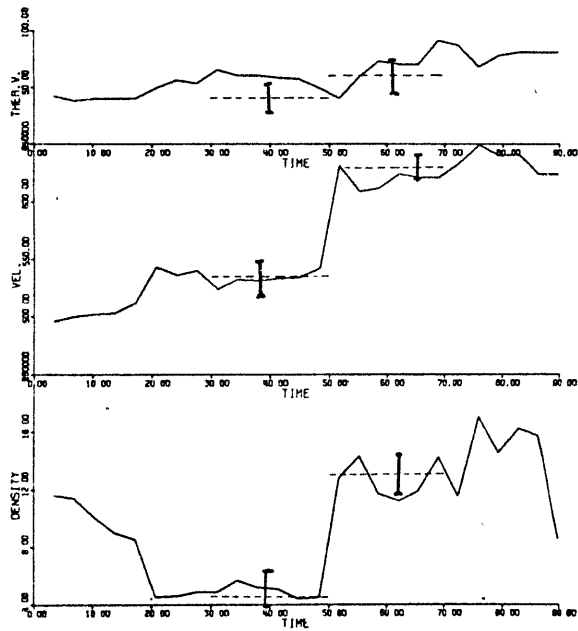


Figure 5-4



04:20 MARCH 23, 66

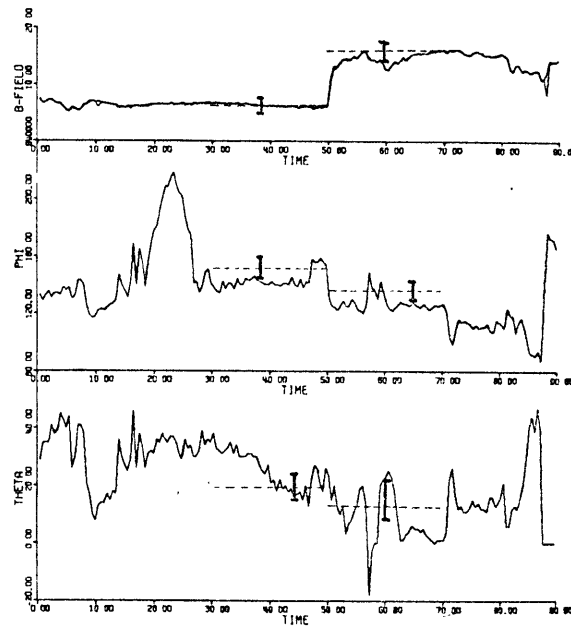
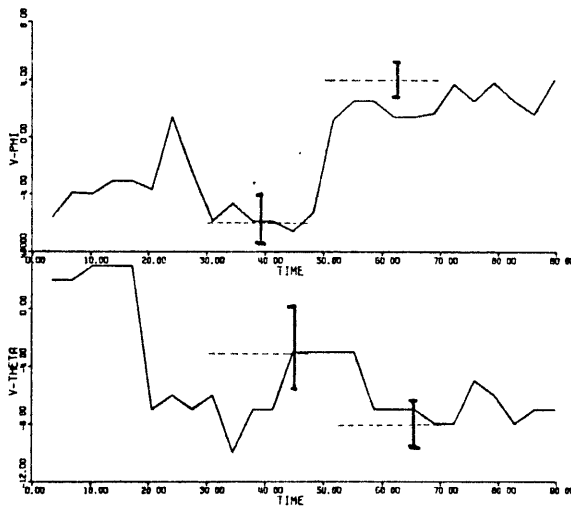


Figure 5-5

ties and to the statistical fluctuations.

Tables 5-2 and 5-3 show the average values of the plasma parameters and the magnetic field on both sides of a given shock, based on the above two figures. The numbers quoted in the tables refer to straight averages involving 30 minutes of data points on either side of the shock.

Making use of the information contained in Tables 5-2 and 5-3, we can now apply our "best-fit matching procedure" for testing these events as MHD shocks. Following the method described in detail in Appendix C, we arrive with the help of digital computers at the results shown in Tables 5-4 and 5-5.

These tables contain the best-fit values of \hat{n} , V_s , \underline{V} , \underline{B} and n , as well as some other computed physical quantities that will be useful in the discussion of our results. V_A and M_A have been defined already in Chapter 2 (see equations (2.50) and (2.51)). $\Theta_{B,n}$ and $\Theta_{V^*,n}$ are the angles formed in Σ^* by \underline{B} and \underline{V}^* with the shock normal, respectively. The underlined numbers are different from the corresponding quantities given in Tables 5-2 and 5-3. However, these differences are small as compared with the r. m. s. deviations of these quantities shown in Figures 5-4 and 5-5. Therefore, we are confident that our measured quantities satisfy the MHD shock conditions.

For the convenience of the reader, the best-fit values of \underline{V} , \underline{B} , and n quoted in Tables 5-4 and 5-5 are also indicated by dashed lines in Figures 5-4 and 5-5.

Table 5-2

Measured Averages of Magnetic Field and Plasma Parameters Across
The Shock of March 22, 1966

<u>Parameter</u>	<u>Pre-Shock</u>	<u>Post-Shock</u>
Bulk Velocity, V in RTN Coordinate, (km/sec)	448 (-5.0 ^o , - 5.0 ^o) (445, - 39, - 39)	501 (1.0 ^o , - 6.5 ^o) (489, - 56, 9)
Magnetic Field in RTN Coordinate, (gamma)	6.0 (-32 ^o , 15 ^o) (4.9, 1.3, - 3.2)	10.0 (- 44 ^o , 20 ^o) (6.8, 2.5, - 7.0)
Ion Density, n , (number / cc)	4.0	9.2
Transit Time, τ , (sec)		none

Table 5-3

Measured Averages of Magnetic Field and Plasma Parameters Across
The Shock of March 23, 1966

<u>Parameter</u>	<u>Pre-Shock</u>	<u>Post-Shock</u>
Bulk Velocity, \underline{V}	535 (-3.0° , -6.0°)	630 (-7.0° , 2.0°)
in RTN Coordinate, (km/sec)	(531, -56, -28)	(625, 22, -78)
Magnetic Field	5.8 (20° , 150°)	150 (14° , 125°)
in RTN Coordinate, (gamma)	(-4.7, 2.7, 2.0)	(-8.4, 11.9, 3.6)
Ion Density, n, (number / cc)	4.4	3.1
Transit Time, τ , (sec)	12561	
Relative Position Vector Between Pioneer 6 and the Earth in RTN Coordinates	(18.7900, -8.4434, 0.3716) $\times 10^6$ km	

Table 5-4

Physical Parameters Associated with March 22, 1966 Shock
and Obtained from the "Best-Fit Matching Procedure"

Transit Time, τ , (sec)	not available	
Shock Normal [(Θ_s, φ_s) and (n_R, n_T, n_N)]	$(32.6^\circ, -6.7^\circ)$	$(0.84, -0.10, 0.54)$
Shock Velocity in RTN Coordinates (km/sec)	$(405, -47, 261)$	

Best-Fit Values of \underline{V} , \underline{B} , n (see dotted lines in Figure 5-4)

	<u>Pre-Shock</u>	<u>Post-Shock</u>
\underline{V}	448 $(-6.2^\circ, -5.3^\circ)$	506 $(0.4^\circ, -6.0^\circ)$
\underline{B}	6.0 $(-32^\circ, 15^\circ)$	13.2 $(-44^\circ, 21^\circ)$
n	4.0	9.2

Physical Quantities Referring to Σ^* and Computed Parameters from the Above

	<u>Pre-Shock</u>	<u>Post-Shock</u>
V_A	24.7	16.3
M_A	5.5	3.6
$\Theta_{B,n}, \Theta_{V^*,n}$	$67.8^\circ, 64.3^\circ$	$80.0^\circ, 77.3^\circ$

Table 5-5

Physical Parameters Associated with March 23, 1966 Shock
and Obtained from the "Best-Fit Matching Procedure"

Transit Time, τ , (sec)	12354	
Shock Normal [(θ_s, φ_s) and (n_R, n_T, n_N)]	$(-26.5^\circ, 43.0^\circ)$	(0.65, 0.61, -0.45)
Shock Velocity in RTN Coordinates (km/sec)	(367, 343, -251)	

Best-Fit Values of \underline{V} , \underline{B} , n (see dotted lines in Figure 5-5)

	<u>Pre-Shock</u>	<u>Post-Shock</u>
\underline{V}	535 $(-3.0^\circ, -6.0^\circ)$	633 $(-8.3^\circ, -4.0^\circ)$
\underline{B}	5.8 $(20^\circ, 150^\circ)$	16.4 $(14^\circ, 135^\circ)$
n	4.4	13.1

Physical Quantities Referring to Σ^* and Computed Parameters from the Above

	<u>Pre-Shock</u>	<u>Post-Shock</u>
V_A	23.9	13.6
M_A	9.2	5.3
$\theta_{B,n}, \theta_{V^*,n}$	$67.0^\circ, 58.0^\circ$	$83.0^\circ, 77.8^\circ$

This surprisingly good matching leads us to believe that plasma was, at least in these two cases nearly isotropic (for a more critical discussion of this conclusion see Chapter 6). This implies that we have a three-fold overdeterminicity among the fourteen numbers for \underline{B} , \underline{V} , and n quoted in Table 5-4. In other words, any three of these numbers can be used as a test for the validity of the MHD shock. The remaining nine numbers have been "used up" for the determination of the shock speed, the shock orientation, etc.

As already mentioned, we have for the shock of March 23, 1966, an additional information, namely that of the transit time. This permits us to employ the results obtained in Chapter 4 for an independent test of this event as a MHD shock.

For this purpose, we take Θ_B and φ_B , defining the direction of the magnetic field in the pre-shock state, and the angles Θ'_V and φ'_V , defining the direction of the solar wind velocity in the post-shock state, as independent variables. For given values of Θ_B , φ_B , Θ'_V and φ'_V , the magnetic field strength B in the pre-shock state and magnetic field vector \underline{B}' in the post-shock state are computed. Various sets of Θ_B , φ_B , Θ'_V and φ'_V -- all close to their measured values, i. e., within the error bars of Figures 5-4 and 5-5 -- are used to compute the corresponding B and \underline{B}' . It was found that the set of Θ_B , φ_B , Θ'_V , φ'_V , B and \underline{B}' given in Table 5-5, is in an excellent agreement with equations (4-21) to (4-23). Hence, the two methods lead to the same iden-

tification of the shock of March 23, 1966.

It is worth noting from Tables 5-4 and 5-5 that the Mach numbers based on the normal Alfvén velocity, M_A , on both sides of the shock are greater than one. This is required from the evolutionary condition for the fast MHD shock. The Alfvén Mach numbers are 5.5 and 3.6 for the pre- and post-shock states, respectively, on March 22, and 9.2 and 5.3 for the pre- and post-shock states, respectively, on March 23. The magnitude of the magnetic fields increases across the shock front (i. e. $B < B'$) as it should.

To visualize more clearly how the wind velocities and magnetic fields change suddenly, both in directions and magnitudes, as viewed by an observer in the shock frame Σ^* , we show the above discussed results also in a graphical form (see Figures 5-6 and 5-7). The solid lines indicate velocities and the dashed lines magnetic fields. The magnetic field vectors and the shock normal lie in the same plane (plane of the page). However, there is a component of the velocity perpendicular to the page on both sides of the shock. As already pointed out in Chapters 2 and 4, this component, labeled in the figures by V_k^* , is continuous across the shock.

So far we have analyzed the shocks utilizing purposefully only those MHD shock equations which do not contain any reference to the plasma pressures. The problem of the pressure jumps and the aniso-

March 22, '66

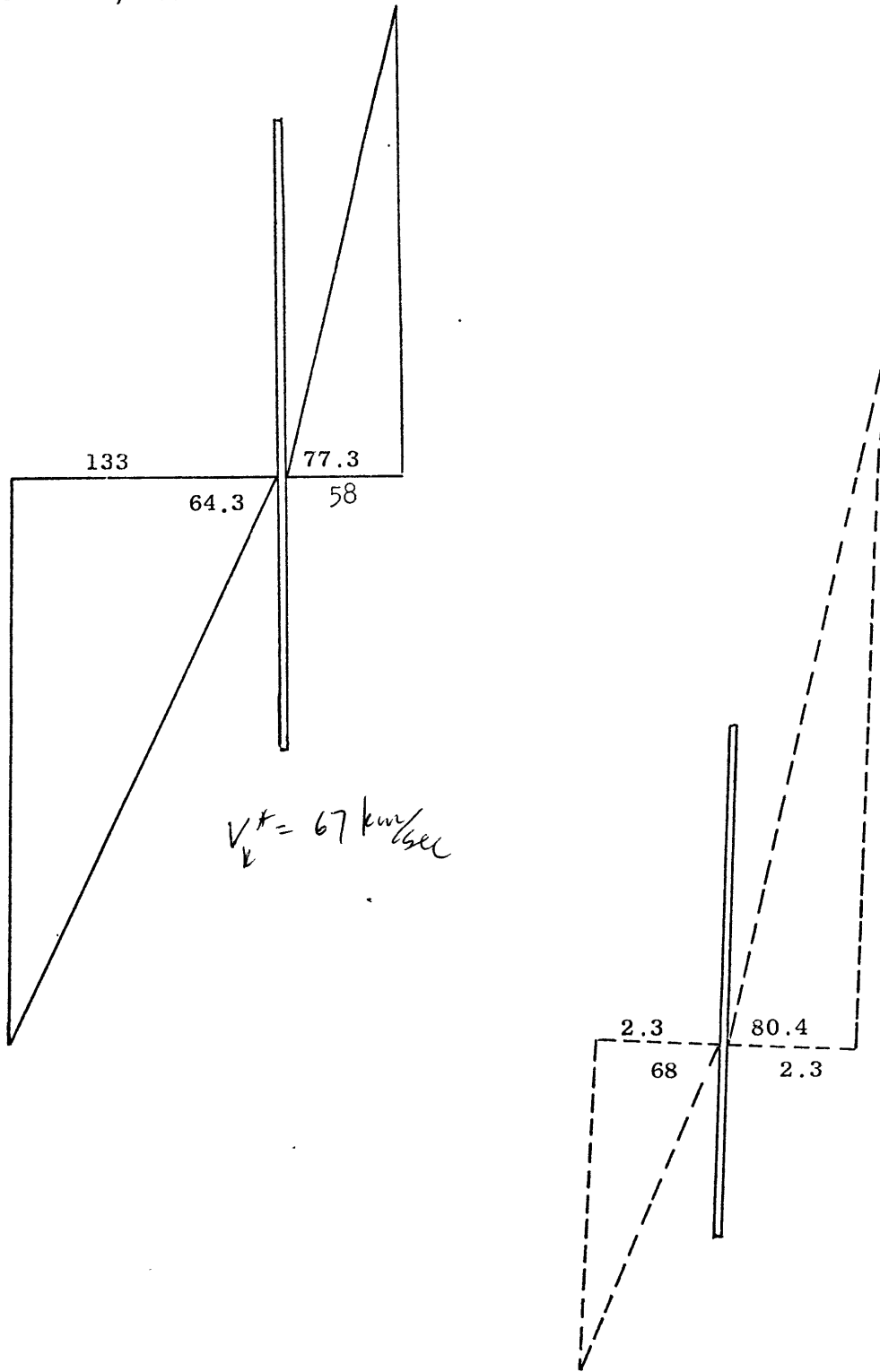


Figure 5-6

March 23, '66

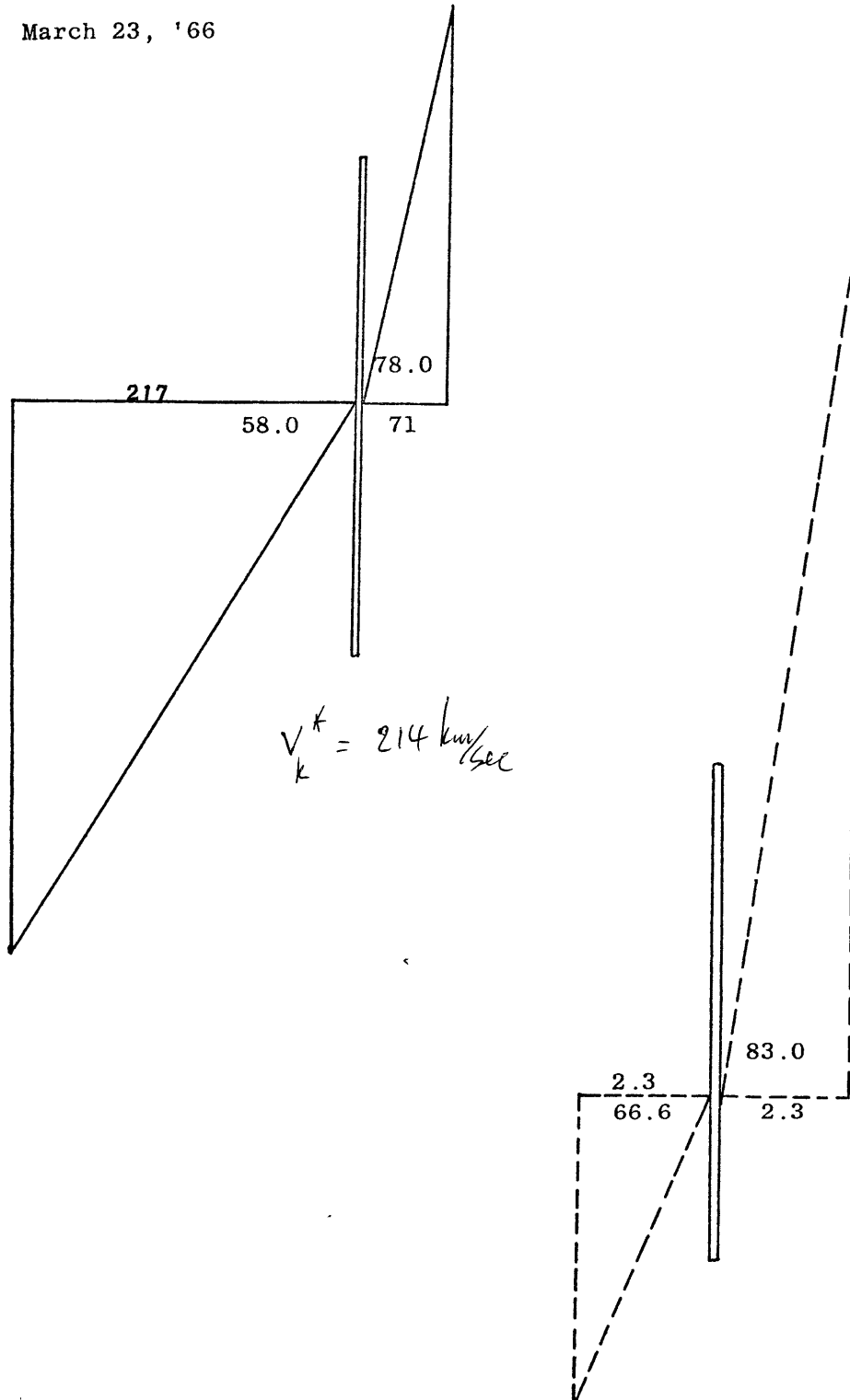


Figure 5-7

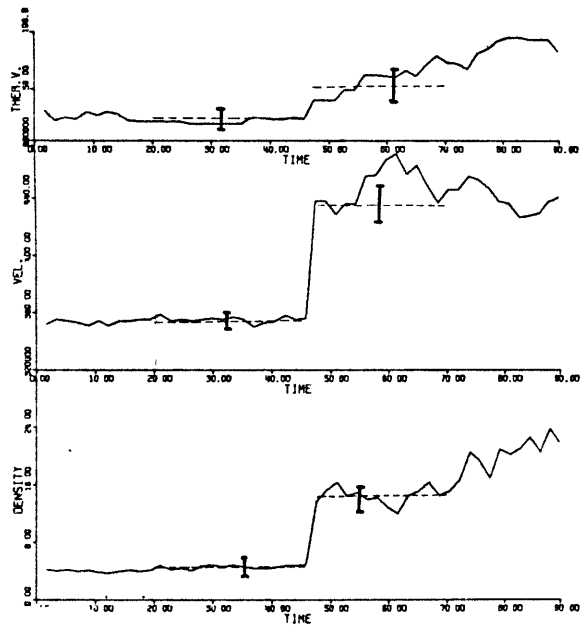
tropy changes across the shock will be discussed in Chapter 6.

We used the shocks of March 22 and 23 as typical examples for detail presentation of our results. The same type of presentation as far as figures and tables are concerned will be adopted for all the remaining shocks.

Fast Shocks of August 29, 1966, June 26, 1967 and August 29, 1967

Figures 5-8, 5-9, 5-10 and Tables 5-6, 5-7, 5-8 display three additional shocks found on Pioneer 7 (August 29, 1966) and Mariner V (June 26, 1967, and August 29, 1967). An analysis of this, data completely analogous to that described for the two previous shocks, revealed that all three events were fast shocks. Tables 5-9, 5-10, and 5-11 show the results of our best-fit matching procedure outlined in Appendix C. A comparison of Tables 5-6 to 5-8 with Tables 5-9 to 5-11 shows a very good agreement between measured and computed quantities, thus giving us confidence as to proper identification of these events as fast MHD shocks.

As indicated previously in Table 5-1, two events of August 29, 1966 and June 26, 1967 were observed also on other satellites (for details, see Tables 5-6, 5-7). This allowed us to use the "method of transit time" outlined in Chapter 4 to double-check our best-fit procedure. Both methods lead to essentially identical results.



14:16 AUGUST 29, 66

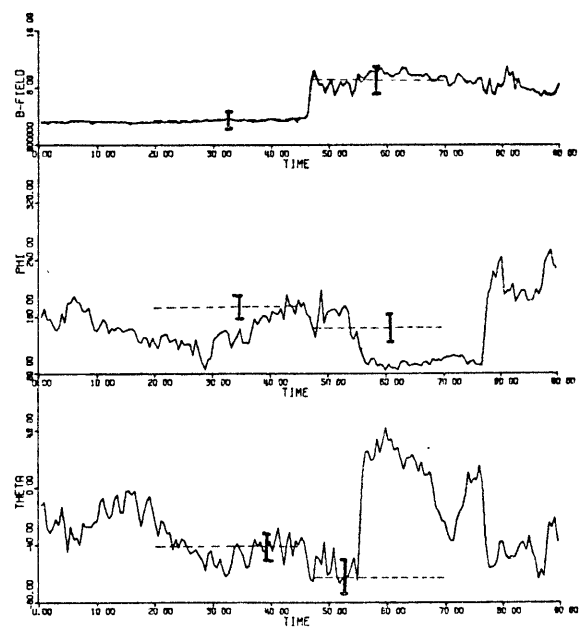
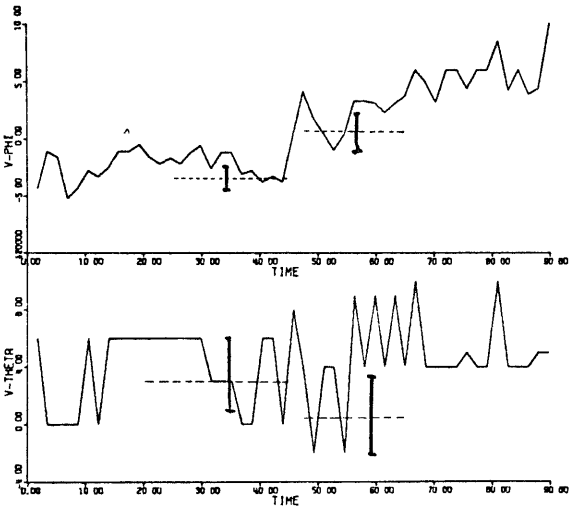


Figure 5-8

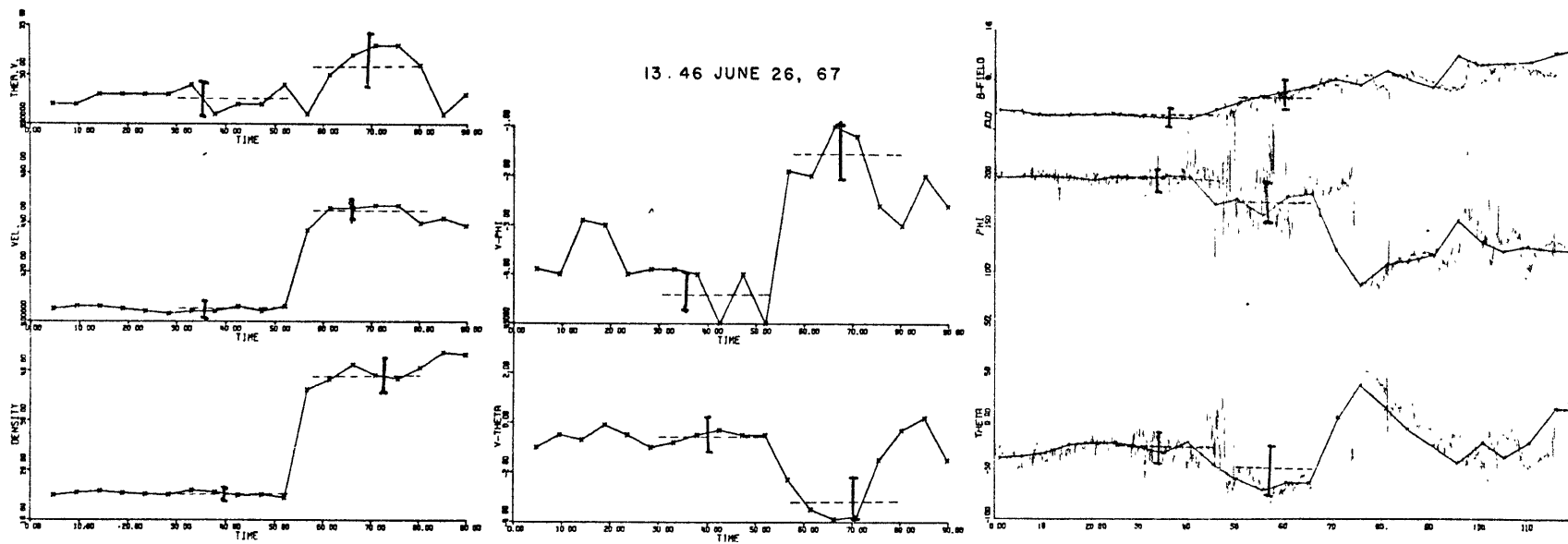


Figure 5-9

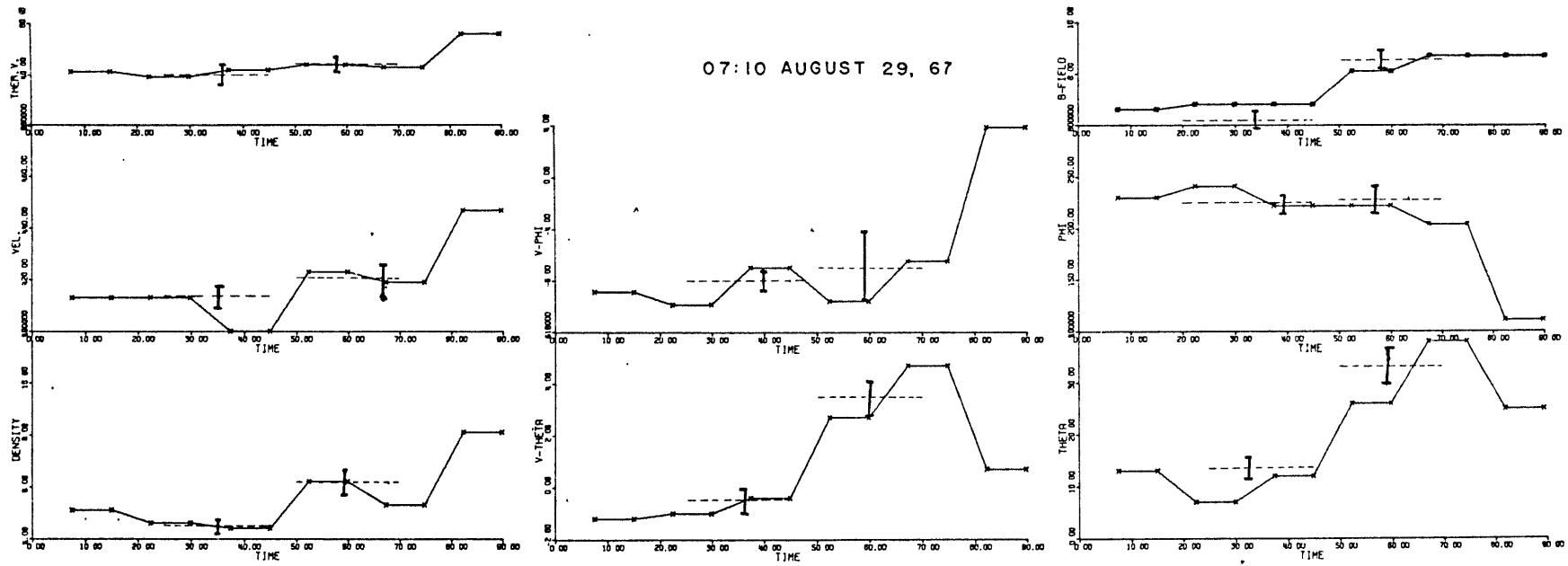


Figure 5-10

Table 5-6

Measured Averages of Magnetic Field and Plasma Parameters Across
The Shock of August 29, 1966

<u>Parameter</u>	<u>Pre-Shock</u>	<u>Post-Shock</u>
Bulk Velocity, \underline{V}	356 (3.0° , -3.5°)	434 (1.0° , 1.0°)
in RTN Coordinate, (km/sec)	(355, -22, 19)	(434, 8, 8)
Magnetic Field	3.7 (-40° , 174°)	9.5 (-60° , 145°)
in RTN Coordinate, (gamma)	(-2.8, 0.3, -2.4)	(-3.9, 2.7, -8.2)
Ion Density, n , (number / cc)	4.7	14.5
Transit Time, τ , (sec)	2970	
Relative Position Vector Between Pioneer 7 and Explorer 33 in RTN Coordinates	(1.2772, 0.5880, 0.0489) $\times 10^6$ km	

Table 5-7

Measured Averages of Magnetic Field and Plasma Parameters Across
The Shock of June 26, 1967

<u>Parameter</u>	<u>Pre-Shock</u>	<u>Post-Shock</u>
Bulk Velocity, \underline{V}	405 (-0.5°, -4.4°)	445 (-3.2°, -1.5°)
in RTN Coordinate, (km/sec)	(404, -31, -4)	(445, -12, -25)
Magnetic Field	2.1 (-25°, -166°)	5.6 (-61°, 175°)
in RTN Coordinate, (gamma)	(-1.8, -0.5, -0.9)	(-2.6, 0.3, -4.8)
Ion Density, n, (number/ cc)	15	38.7
Transit Time, τ , (sec)	4130	
Relative Position Vector Between Mariner V and Explorer 34 in RTN Coordinates	(1.7300 x 10 ⁶ , 2.1386 x 10 ⁶ , 1.3926 x 10 ⁶) km	

Table 5-8

Measured Averages of Magnetic Field and Plasma Parameters Across
The Shock of August 29, 1967

<u>Parameter</u>	<u>Pre-Shock</u>	<u>Post-Shock</u>
Bulk Velocity, \underline{V}	414 (-0.5° , -8.0°)	422 (3.0° , -9.0°)
in RTN Coordinate	(410, -58, -4)	(416, -66, 22)
Magnetic Field	6.6 (12° , -134°)	9.2 (34° , -140°)
in RTN Coordinate, (γ)	(-4.5, -4.6, 1.4)	(-5.8, -4.9, 5.1)
Ion Density, n , (number/cc)	4.5	6.2
Transit Time, τ , (sec)	37320	
Relative Position Vector Between Mariner V and Explorer 34 in RTN Coordinates	(23.7033, -8.7495, 5.7404) $\times 10^6$ km	

Table 5-9

Physical Parameters Associated with August 29, 1966 Shock
and Obtained from the "Best-Fit Matching Procedure"

Transit Time, τ , (sec)	2939	
Shock Normal [(Θ_s, φ_s) and (n_R, n_T, n_N)]	$(-2.5^\circ, 14.5^\circ)$	$(0.97, 0.25, -0.04)$
Shock Velocity in RTN Coordinates (km/sec)	$(453, 117, -21)$	

Best-Fit Values of \underline{V} , \underline{B} , n (see dotted lines in Figure 5-8)

	<u>Pre-Shock</u>	<u>Post-Shock</u>
\underline{V}	356 $(3.0^\circ, -3.5^\circ)$	434 $(0.3^\circ, 0.5^\circ)$
\underline{B}	3.7 $(-40^\circ, 174^\circ)$	9.5 $(-62^\circ, 145^\circ)$
n	4.7	14.5

Physical Quantities Referring to Σ^* and Computed Parameters from the Above

	<u>Pre-Shock</u>	<u>Post-Shock</u>
V_A	25.6	14.6
M_A	4.8	2.7
$\Theta_{B,n}, \Theta_{V^*,n}$	$46.5^\circ, 26.4^\circ$	$74.4^\circ, 50.3^\circ$

Table 5-10

Physical Parameters Associated with June 26, 1967 Shock
and Obtained from the "Best-Fit Matching Procedure"

Transit Time, τ , (sec)	4131	
Shock Normal [(θ_s, φ_s) and (n_R, n_T, n_N)]	$(-23^\circ, 24.9^\circ)$	$(0.84, 0.39, -0.39)$
Shock Velocity in RTN Coordinates (km/sec)	$(349, 162, -164)$	

Best-Fit Values of \underline{V} , \underline{B} , n (see dotted lines in Figure 5-9)

	<u>Pre-Shock</u>	<u>Post-Shock</u>
\underline{V}	405 $(-0.5^\circ, -4.4^\circ)$	445 $(-3.2^\circ, -1.5^\circ)$
\underline{B}	2.7 $(-25^\circ, -166^\circ)$	5.6 $(-47^\circ, 188^\circ)$
n	15.0	38.7

Physical Quantities Referring to Σ^* and Computed Parameters from the Above

	<u>Pre-Shock</u>	<u>Post-Shock</u>
V_A	9.7	6.15
M_A	8.4	5.2
$\theta_{B,n}, \theta_{V^*,n}$	$49.5^\circ, 64.8^\circ$	$71.9^\circ, 79.5^\circ$

Table 5-11

Physical Parameters Associated With August 29, 1967 Shock
and Obtained from the "Best-Fit Matching Procedure"

Transit Time, τ , (sec)	37232	
Shock Normal [(Θ_s, φ_s) and (n_R, n_T, n_N)]	$(20.3^\circ, 43.0^\circ)$	(0.69, 0.64, 0.35)
Shock Velocity in RTN Coordinates (km/sec)	(234, 218, 113)	

Best-Fit Values of \underline{V} , \underline{B} , n (see dotted lines in Figure 5-10)

	<u>Pre-Shock</u>	<u>Post-Shock</u>
\underline{V}	414 $(-0.5^\circ, -8.0^\circ)$	421 $(3.5^\circ, -7.0^\circ)$
\underline{B}	6.1 $(14^\circ, -134^\circ)$	8.54 $(34^\circ, -132^\circ)$
n	4.5	6.2

Physical Quantities Referring to Σ^* and Computed Parameters from the Above

	<u>Pre-Shock</u>	<u>Post-Shock</u>
V_A	51.6	44.0
M_A	1.48	1.26
$\Theta_{B,n}, \Theta_{V^*,n}$	$34.6^\circ, 44.0^\circ$	$54.0^\circ, 42.0^\circ$

The shock of August 29, 1967 requires a special explanation. At the time this shock was observed, Mariner V was at a distance of about 1/8 A. U. from the earth. This distance is so great as to render the assumption on a plane shock propagation at constant speed questionable. Hence, to begin with, the information of this transit time must be considered of secondary importance. Using the shock velocity based on this matching process we still may compute the propagation time for this shock to reach Explorer 34. The detectors on Explorer 34 (Ogilvie & Burlaga, 1969) observed a shock at 17:32 U.T., August 29; 10 hours and 22 minutes after Mariner V "saw" a shock. At that moment Explorer 34 was outside the earth's bow shock and at a distance of about 24 radii from the earth. It turns out that the observed transit time agrees well with the computed one, assuming plane shock propagating from Mariner V to Explorer 34. (No ssc can be associated with this shock.)

The investigators on Explorer 34 have identified independently this event as a shock and quote their measured values of ion densities. Thus, in this case we have an opportunity to compare our number densities (on Mariner V) with their's.

Because of the large distance between Mariner V and Explorer 34 scaling corrections for the plasma density must be employed. If such corrections, based on the $1/r^2$ - law for the heliocentric density decrease are applied to our densities, the measurements on both satellites turn out to be in an excellent agreement. Figures 5-11, 5-12, and 5-13

August 29, '66

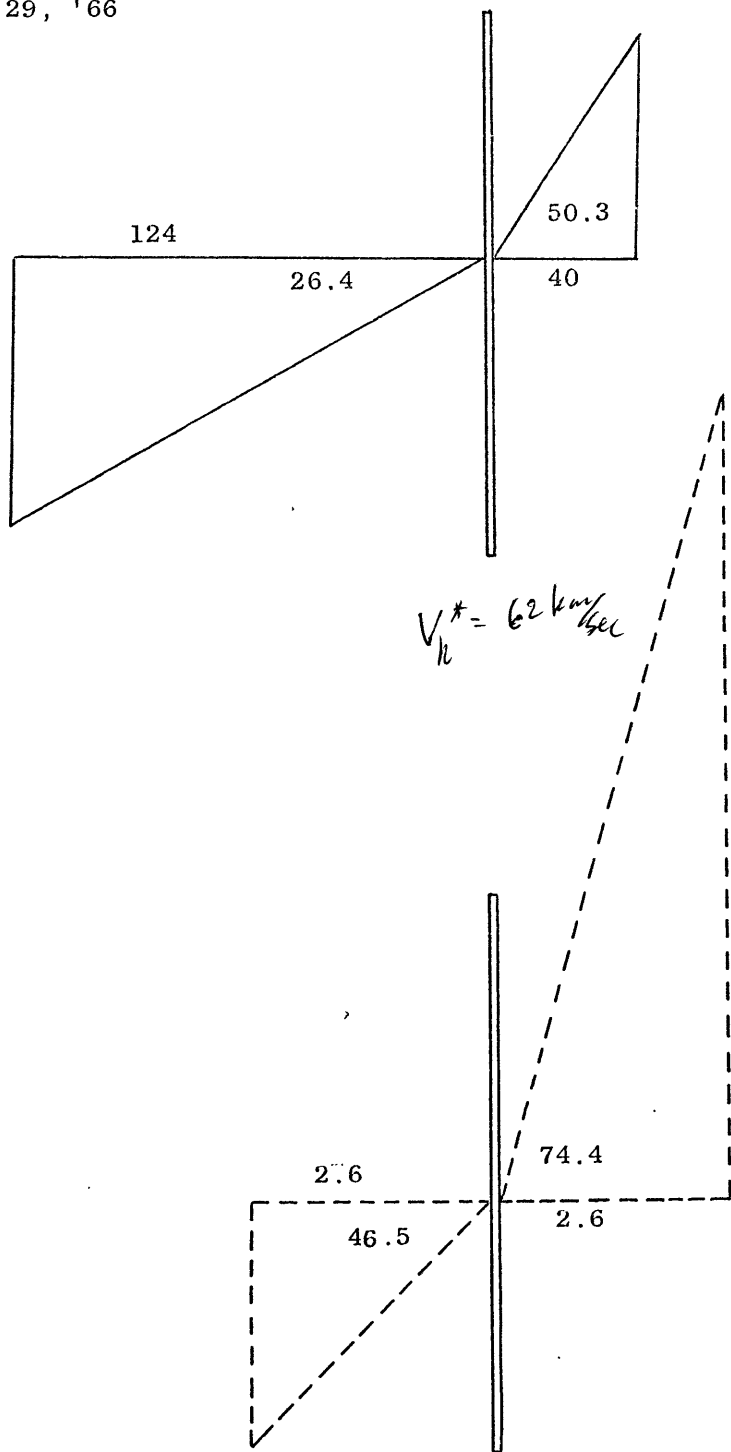


Figure 5-11

June 26, '67

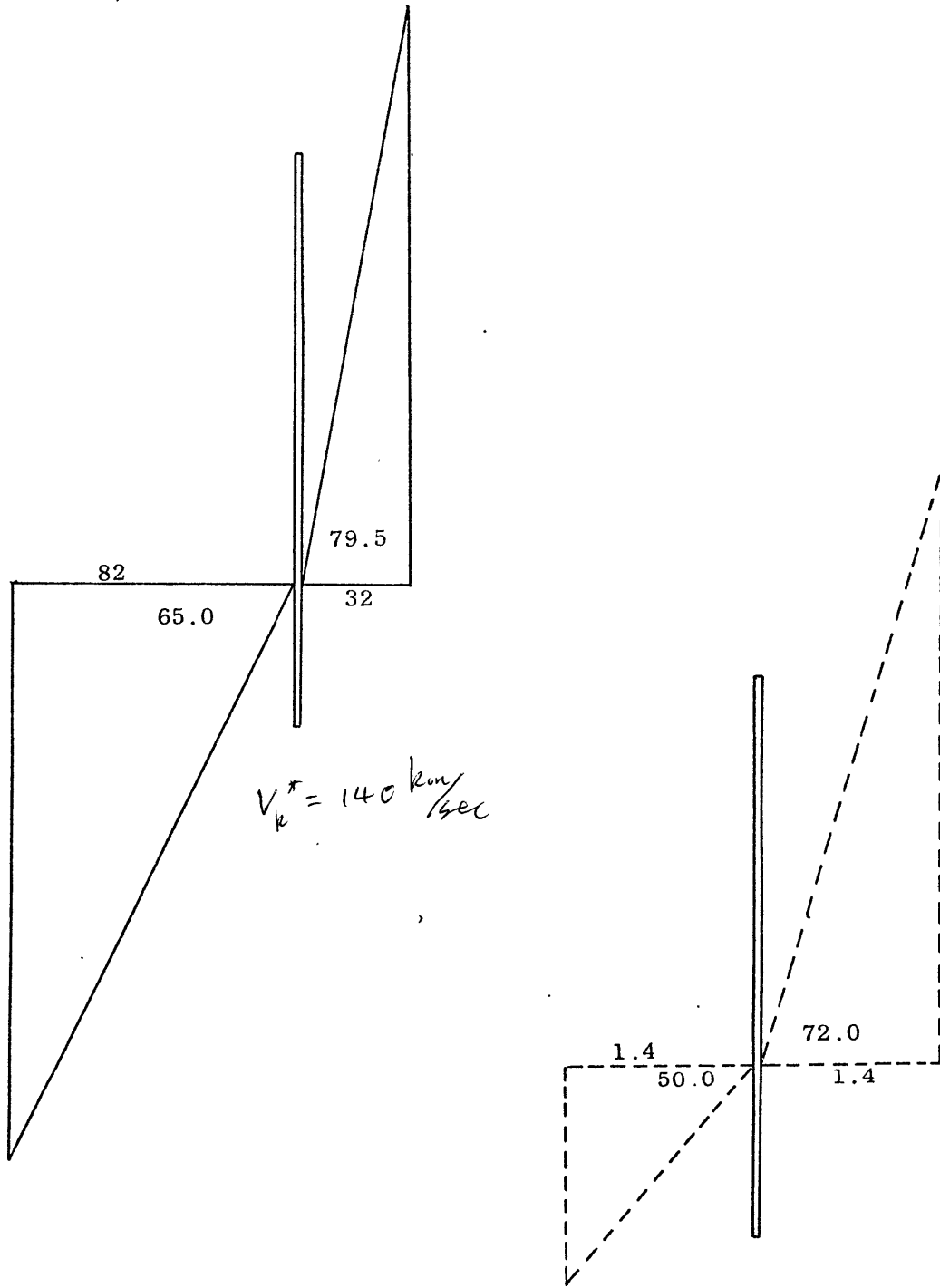


Figure 5-12

August 29, '67

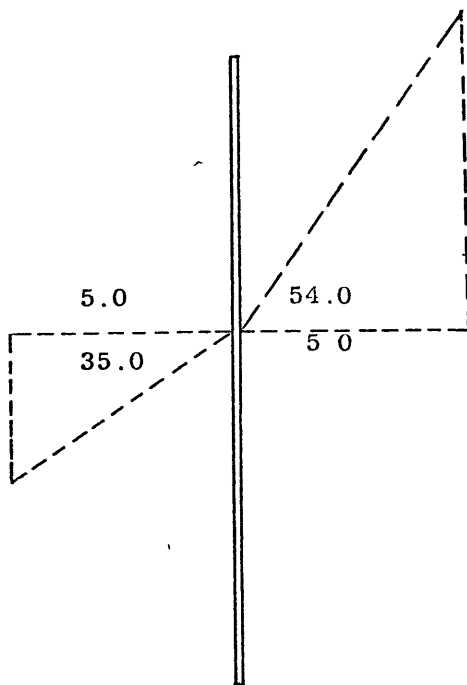
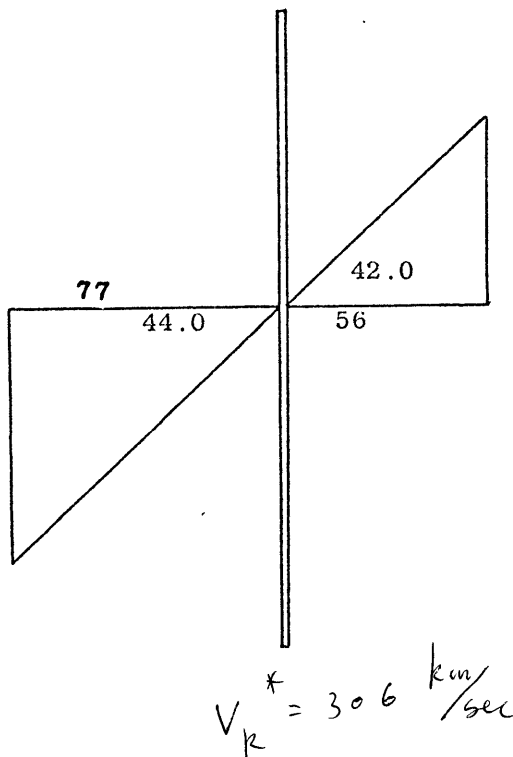


Figure 5-13

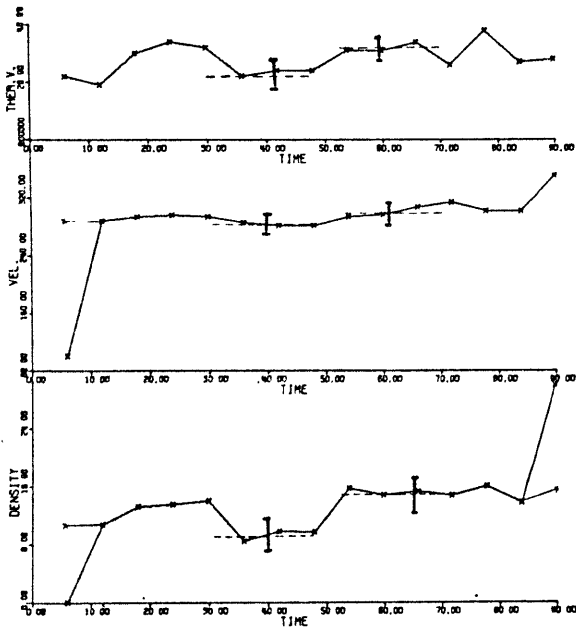
show graphically the behavior of \underline{V}^* and \underline{B} in Σ^* for the three above quoted shocks. Note, in particular, that the behavior of the \underline{B} -field is in accord with that expected on theoretical grounds.

Slow Shocks of July 20 and August 30, 1967

Figures 5-14 and 5-15, together with Tables 5-12 and 5-13, summarize two additional events found on board Mariner V. The analysis of these discontinuities deserves special attention. The behavior of the magnetic field indicates that they are not fast shocks. In fact, the decrease of the field strength across the surface of discontinuity suggests qualitatively that these events may be slow shocks. A careful quantitative analysis supports this contention. Tables 5-14 and 5-15 show the results of our "best-fit matching procedure" to this end. We notice a fairly good agreement between observations and the computations.

Slow shock has been studied extensively theoretically by Kantrowitz & Petschek (1966), Anderson (1963), Bazer & Ericson (1959), and others. However, to the best of this author's knowledge, no slow shocks have been observed experimentally.

In the MHD case, theoretically, a slow shock should satisfy, among others, the following conditions: First, the normal Alfvén Mach numbers, M_A , in both the pre- and post-shock states must be less than unity. Secondly, the magnetic field strength must decrease across the shock front. (The magnetic energy is converted to the thermal energy.) The measured discontinuities associated with the events on



05:25 JULY 20, 67

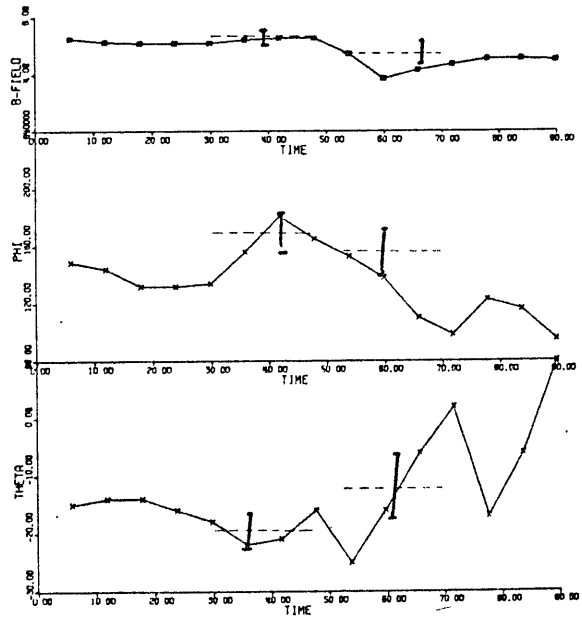
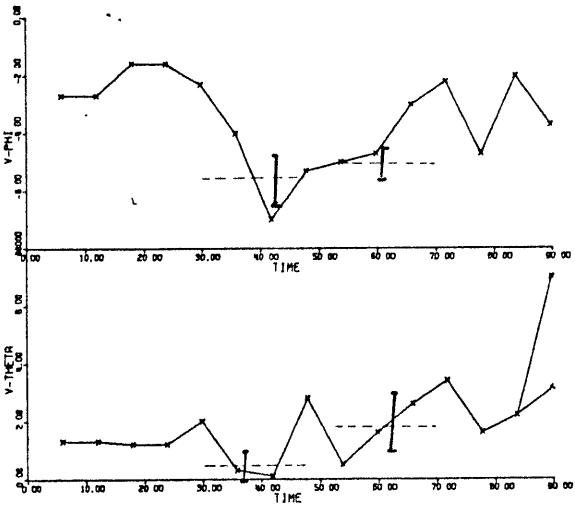
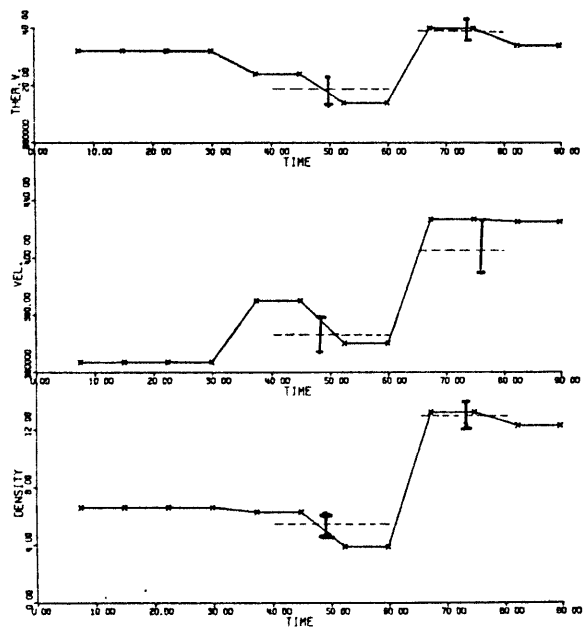


Figure 5-14



13:24 AUGUST 30, 67

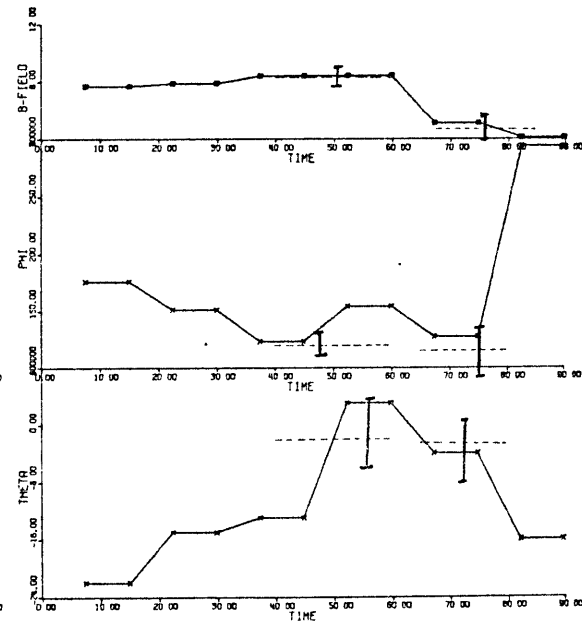
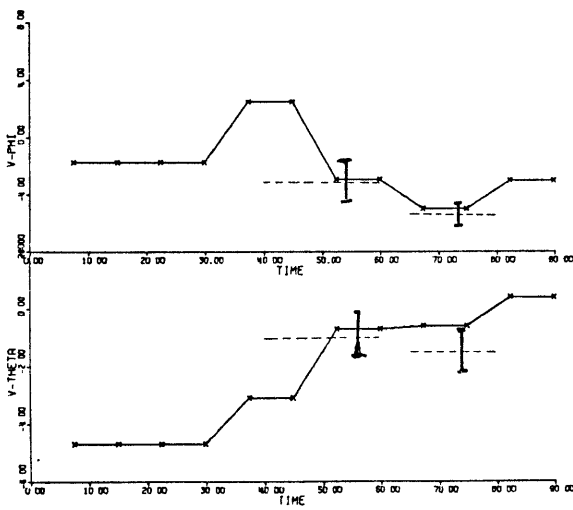
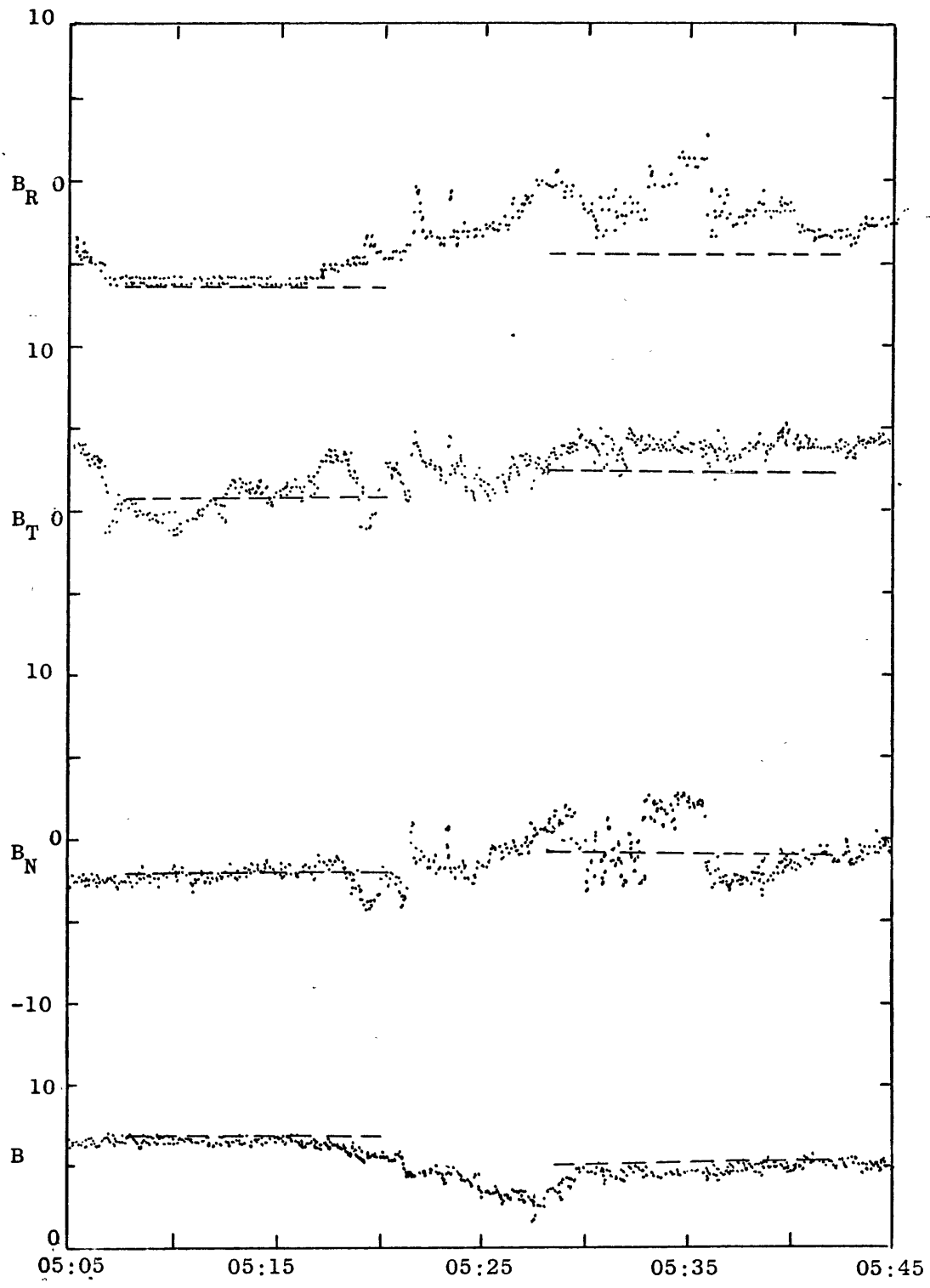


Figure 5-15



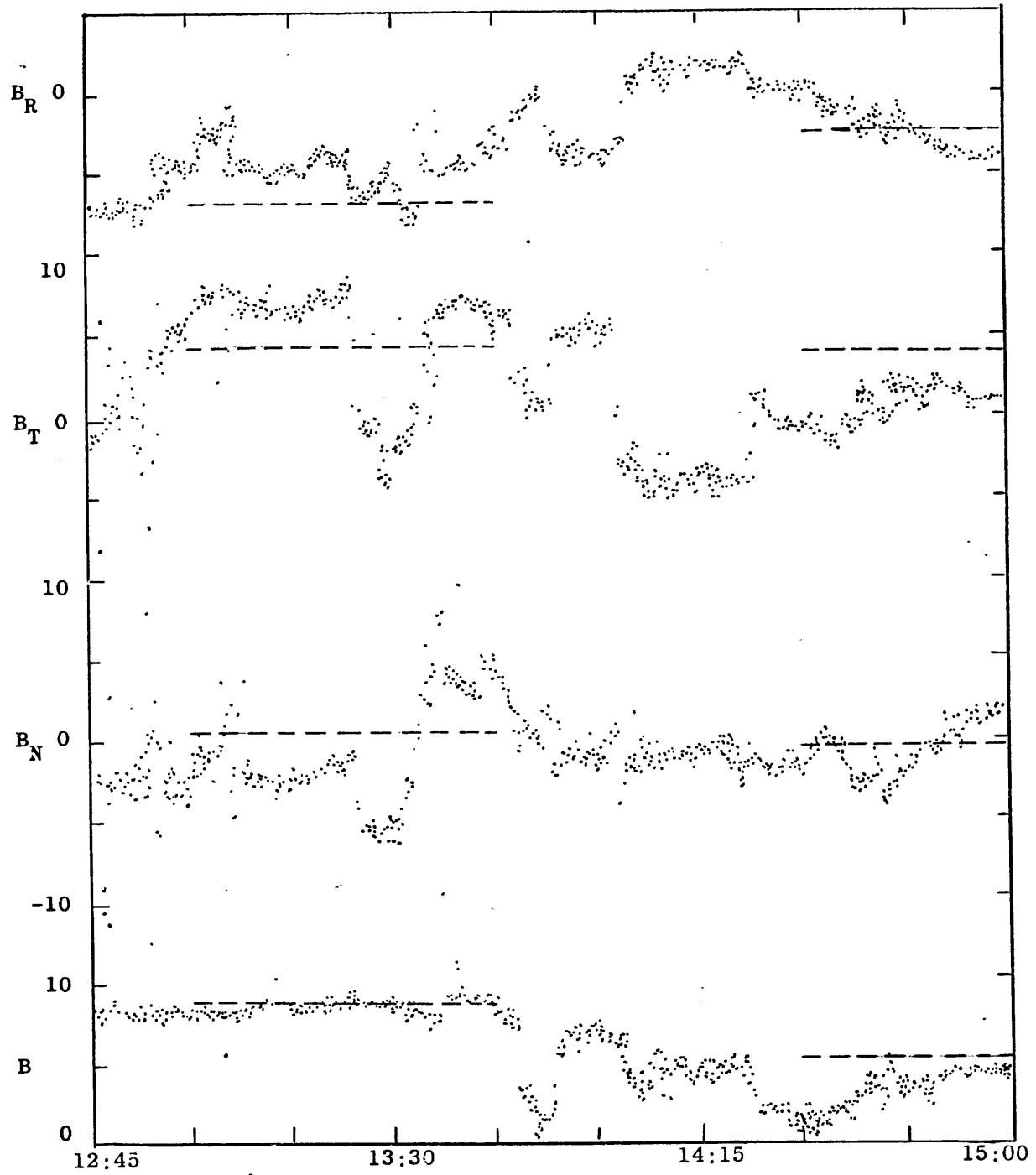


Table 5-12

Measured Averages of Magnetic Field and Plasma Parameters Across
The Shock of July 20, 1967

<u>Parameter</u>	<u>Pre-Shock</u>	<u>Post-Shock</u>
Bulk Velocity, \underline{V}	283 (0.5°, -5.5°)	301 (1.8°, -5.1°)
in RTN Coordinate, (km/sec)	(281, -27, 3)	(300, -26, 10)
Magnetic Field	6.7 (-18°, 171°)	5.0 (-14°, 150°)
in RTN Coordinate, (gamma)	(-6.3, 1.0, -2.1)	(-4.2, 2.4, -1.2)
Ion Density, n, (number / cc)	9.0	15.0
Transit Time, τ , (sec)		not available

Table 5-13

Measured Averages of Magnetic Field and Plasma Parameters Across
The Shock of August 30, 1967

<u>Parameter</u>	<u>Pre-Shock</u>	<u>Post-Shock</u>
Bulk Velocity, \underline{V}	345 (-1.0 ^o , -2.0 ^o)	429 (-0.5 ^o , -5.0 ^o)
in RTN Coordinate, (km/sec)	(345, -12, -6)	(427, -37, -4)
Magnetic Field	8.4 (3 ^o , 150 ^o)	5.0 (-2 ^o , 120 ^o)
in RTN Coordinate, (gamma)	(-7.3, 4.2, 0.4)	(-2.5, 4.3, -0.2)
Ion Density, n , (number / cc)	5.5	13.0
Transit Time, τ , (sec)		not available

Table 5-14

Physical Parameters Associated with July 20, 1967 Shock
and Obtained from the "Best-Fit Matching Procedure"

Transit Time, τ , (sec)	not available	
Shock Normal [(Θ_s, φ_s) and (n_R, n_T, n_N)]	$(-1.6^\circ, -54.8^\circ)$	$(0.58, -0.82, -0.03)$
Shock Velocity in RTN Coordinates (km/sec)	$(107, -152, -5)$	

Best-Fit Values of \underline{V} , \underline{B} , n (see dotted lines in Figure 5-14)

	<u>Pre-Shock</u>	<u>Post-Shock</u>
\underline{V}	283 $(0.5^\circ, -5.5^\circ)$	300 $(1.8^\circ, -5.0^\circ)$
\underline{B}	6.7 $(-18^\circ, 171^\circ)$	5.5 $(-14^\circ, 159^\circ)$
n	9.0	15.0

Physical Quantities Referring to Σ^* and Computed Parameters from the Above

	<u>Pre-Shock</u>	<u>Post-Shock</u>
V_A	32.0	24.8
M_A	0.8	0.6
$\Theta_{B,n}, \Theta_{V^*,n}$	$48.7^\circ, 83.4^\circ$	$36.9^\circ, 86.3^\circ$

Table 5-15

Physical Parameters Associated with August 30, 1967 Shock
and Obtained from the "Best-Fit Matching Procedure"

Transit Time, τ , (sec)	not available	
Shock Normal [(Θ_s, φ_s) and (n_R, n_T, n_N)]	$(4.2^\circ, -87.0^\circ)$	$(0.05, -0.99, 0.07)$
Shock Velocity in RTN Coordinates (km/sec)	$(2, -40, 3)$	

Best-Fit Values of \underline{V} , \underline{B} , n (see dotted lines in Figure 5-15)

	<u>Pre-Shock</u>	<u>Post-Shock</u>
\underline{V}	345 $(-1.0^\circ, -3.0^\circ)$	402 $(-1.5^\circ, -5.45^\circ)$
\underline{B}	8.4 $(-2^\circ, 120^\circ)$	4.7 $(-2^\circ, 110^\circ)$
n	5.5	13.0

Physical Quantities Referring to and Computed Parameters from the Above

	<u>Pre-Shock</u>	<u>Post-Shock</u>
V_A	41.6	27.1
M_A	0.9	0.6
$\Theta_{B,n}, \Theta_{V^*,n}$	$57.0^\circ, 83.5^\circ$	$26.0^\circ, 87.8^\circ$

July 20 and August 30 satisfy the two conditions given above as well as the MHD Rankine-Hugoniot relations used by us in the matching procedure. We thus have a fair degree of confidence (especially for the event of July 20, 1967, that we are dealing, for the first time, with the slow shocks.)

No transit time can be identified for these slow shocks. This circumstance may not be totally accidental. Because the strength of slow shock is much weaker than that of a fast one, it is perhaps not surprising that no ssc on earth and no similar discontinuity on other spacecraft were observed that could be correlated with ours.

Comparing Figures 5-14 and 5-15 with those of the fast shocks, we see that the parameters of the slow shocks are much more fluctuating than those of the fast shocks. Thus, the discontinuities tend to be more obscured in the case of slow shock than that in the case of the fast ones. Such pronounced fluctuations may be understood from the fact that the normal Alfvén Mach numbers are less than unity for both pre- and post-shock states. This, in turn, implies that the Alfvén waves can propagate both up- and downstream of the slow shock and thus enhance the possibility of the occurrence of fluctuations.

We see also from Tables 5-14 and 5-15 that the direction of propagation of these shocks makes a large angle with the direction of sun-earth line. This may mean that these shocks are associated more directly with the inhomogeneities in the interplanetary space such as sector boundaries etc. rather than with the flare events themselves.

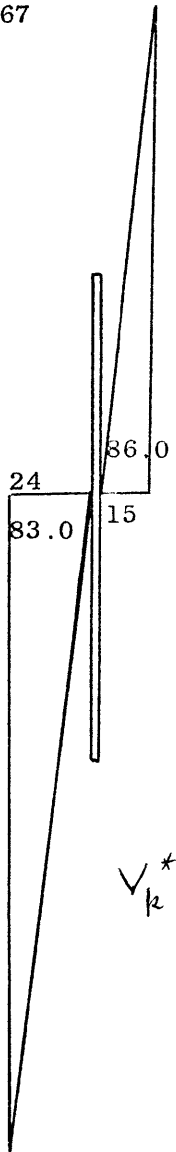
Figures 5-16 and 5-17 show the solar wind velocities and magnetic fields plotted in the frame of the given shock. The magnetic fields display clearly the characteristics of a slow shock.

In this chapter, we have shown that fast and slow shocks do exist in the solar wind. In MHD-approximation, as mentioned in section (2.2.3), there are five kinds of discontinuities: the fast, the slow and the rotational shocks, and the tangential and contact discontinuities. The most important difference between a shock and a discontinuity is that a shock has a mass flow across itself while other discontinuities have not. For the fast shocks presented in this chapter, the mass flows across the shock front at the rate of the order of a hundred kilometers per second. Hence, there is no difficulty in concluding that these events are not tangential or contact discontinuities. On the other hand, for the slow shocks, the mass flows across the shock front only at the rate of 25 and 37 kilometers per second for the July 20 and August 30 shocks, respectively. Fortunately, the experimental uncertainties of the flows across the shock are sufficiently small to render the assumption of no mass flow across the discontinuity as unlikely.

5.3 Spatial Distribution of the Shock Normals

The upper portion of Figure 5-18 shows the projections of the polar angle Θ_s of the shock normals for all seven shocks. The shorter line segments refer to the slow shocks. One sees from this figure that the

July 20, '67



$$V_k^* = 95 \text{ km/sec}$$

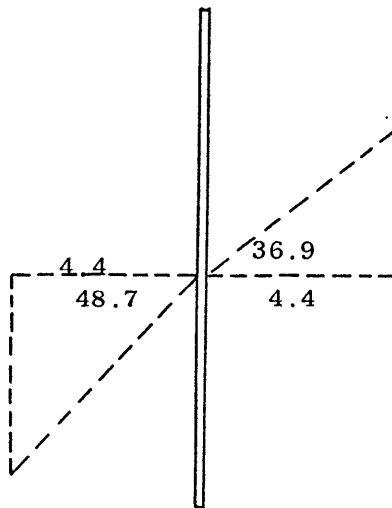


Figure 5-16

August 30, '67

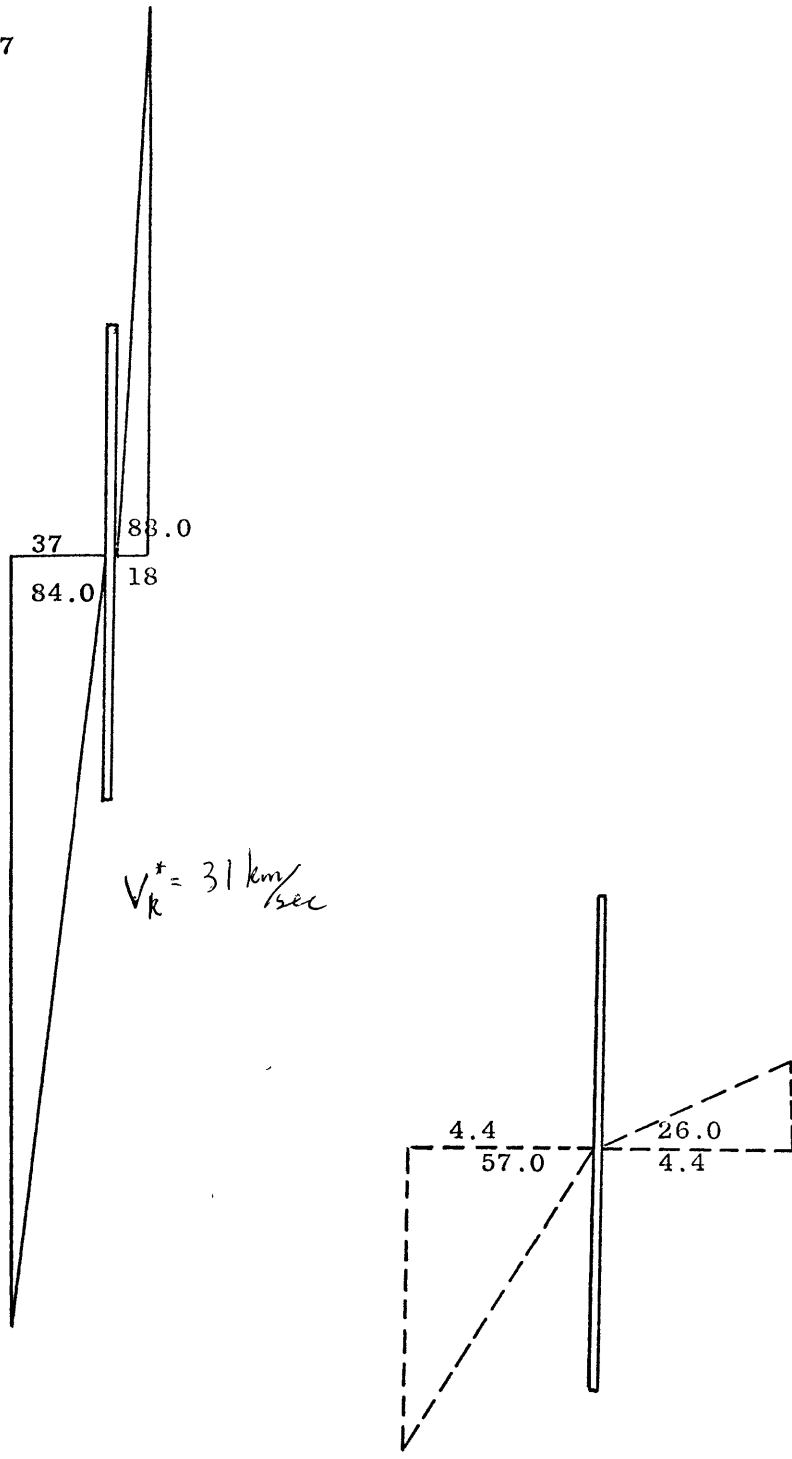


Figure 5-17

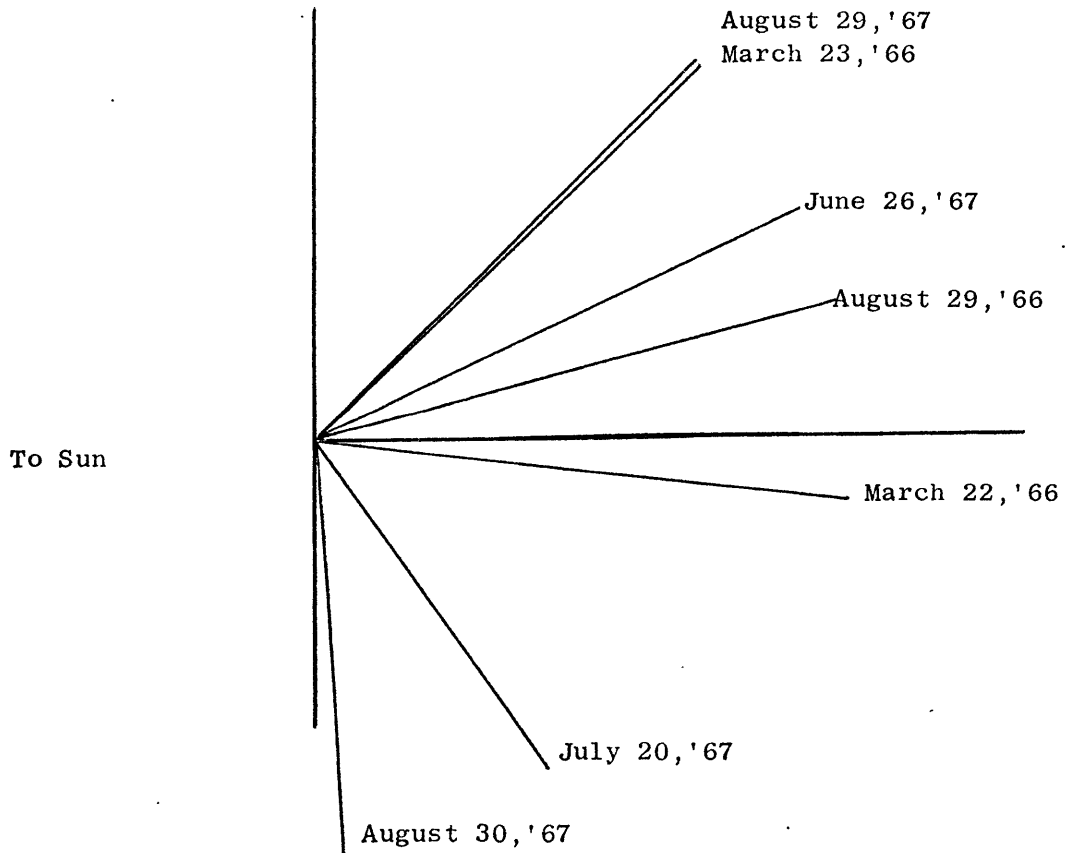
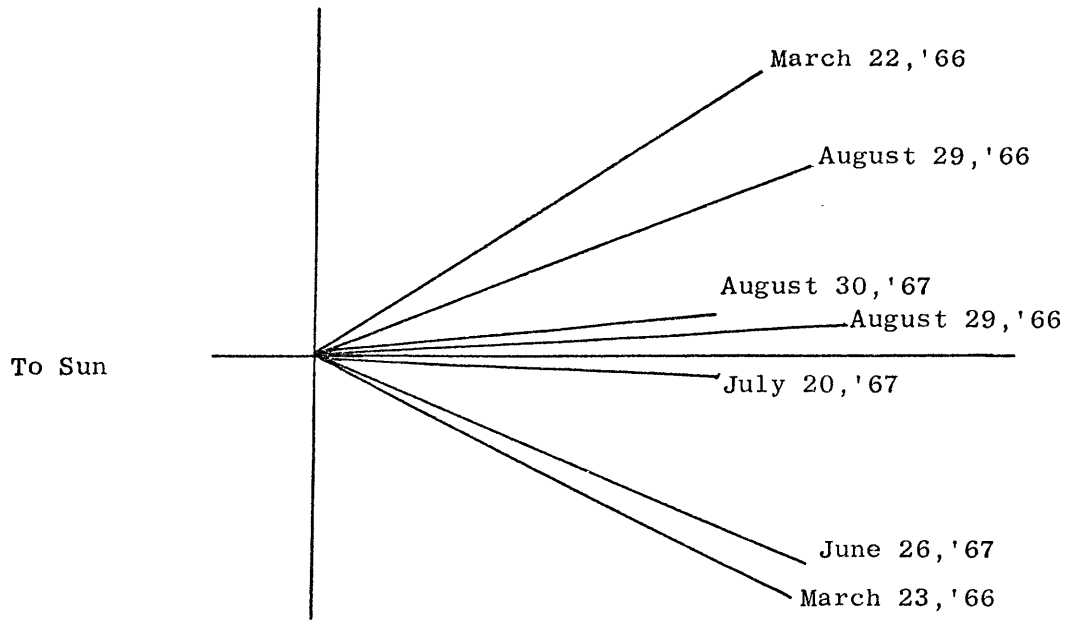


Figure 5-18

Θ_s are evenly distributed in the plane perpendicular to the ecliptic with about as many shocks travelling northward as southward. The lower portion of the figure shows the distribution of the azimuth angles, φ_s , of the shock normals. Here we see that more shocks propagate toward the West (i. e. in the positive T direction) than toward the East of the sun. The normals of the two slow shocks lie close to the ecliptical plane and form large angles with the sun-earth line. In fact, they seem to be at right angles to the azimuths of the fast shock. However, obviously the number of shocks is far too small to draw any statistically significant conclusion from these intriguing results.

Table 5-16 summarizes the distribution of the shock normals and lists solar flares which may be associated with the observed shocks. These flares are identified by the time of their occurrence and their position on the sun. The last column indicates the class of their importance. There seems to be no correlation between the distribution of these flares on the surface of the sun and the distribution of the shock normals. Akasofu and Yoshida (1967) studied the relationship between the positions of the flares and the shock transit time associated with ssc and they also found no correlations.

Table 5-16

Shock Normals and Possible Solar Flares Associated with Them

Shocks Observed	Shock Normal	Possible Flares	Position	Importance
21:00, March 22, '66	(32.6, -6.7)	9:50, March 20	N 20° E 20°	3B
04:20, March 23, '66	(-26.5, 43.0)			
14:16, August 29, '66	(-2.5, 14.5)	15:30, August 28 21:30, August 26	N 21° E 05° N 23° E 26°	4B, 3B 2B
13:46, June 26, '67	(-23.0, 24.9)			
05:25, July 20, '67	(-1.6, -54.8)			
07:10, August 29, '67	(20.3, 43.0)	12:00, August 28	S 23° W 32°	2B
13:34, August 30, '67	(4.2, -87.0)			

Chapter 6

THE TWO-FLUID CHARACTER AND PRESSURE ANISOTROPY OF THE INTERPLANETARY SHOCKS

6.1 General Remarks about Differences between Positive-Ion and Electron Anisotropies

A high temperature and low density plasma, such as that of the interplanetary medium, may be treated as "collisionless" with respect to the binary Coulomb interactions. The "collisionless" plasma is not in thermal equilibrium, because the relaxation times for "isotropization" and "maxwelization" are very long. For a two-species plasma of ions and electrons, neither the electrons nor the ions have Maxwellian distribution. In such a case, we have to treat the plasma starting from the kinetic Vlasov equation. The usual collision mechanism which leads to randomness and allows a description of the system in terms of the hydrodynamic variables, (pressure, density, bulk velocity etc.) is absent. Thus, it would seem that one should use the Vlasov equation to find an adequate description of the motion of the plasma. However, it was shown by Chew, Goldberger, and Low (1956) that when the heat transport is neglected, the presence of a strong magnetic field replaces to some degree the randomizing tendency of collisions, so that fluid concepts may be retained. This set of equations is commonly known as the Chew-Goldberger-Low, double-adiabatic system. The essential assumption of this model is that the Ohm's law be of the form $\underline{E} = - \underline{V} \times \underline{B}$, where \underline{V}

is the macroscopic velocity of the plasma as a whole (or, to a good approximation, the streaming velocity of positive ions).

Buneman (1961) has treated the electrons and ions as separate interpenetrating fluids which interact with each other only via their combined electromagnetic field (collective interaction). A two-fluid model of the collisionless plasma was thus derived. If we study the interplanetary shocks with the "two-fluid" model, detailed information of the ion and electron pressure tensors would be needed for comparison with theory.

Unfortunately, at the present stage of experimental development, we do not have at our disposal such detailed information. In fact, within the frame of this work, we have no information about the behavior of electrons. Consequently, our theoretical test of the interplanetary shocks can not be considered as complete in a strict sense.

The basic equations (2.15), (2.16), (2.22) of Chapter 2 refer to the plasma as a whole. Since these equations express the fundamental laws of mass, momentum and energy, they are of course formally rigorous. However, one has to remember that the physical parameters entering into these equations contain combined effects of both the positive ions and electrons. For example, the pressure tensor P_{ij} stands for the sum of the partial pressures of electrons and ions $(P_{ij}^{(e)} + P_{ij}^{(i)} = P_{ij})$, where $P_{ij}^{(e)}$ and $P_{ij}^{(i)}$ are the pressure tensors for electrons and ions, respectively). If it so happens that we know $P_{ij}^{(i)}$, say, from measurements, then we can derive an information on $P_{ij}^{(e)}$ from the conservation

equations (2.36) and (2.8). As mentioned previously in Chapter 5, we do have some information about the thermal motion of the ions, namely, the so-called "most probable thermal speed" of proton, w_0 (Lazarus et. al, 1966). The meaning of this scalar quantity, available from the MIT data records, would be well understood if protons had Maxwellian distribution in their own frame of reference. Then, we would have

$$w_0 = \sqrt{\frac{2kT_p}{m_p}} \quad (6.1)$$

where T_p is the proton temperature. Unfortunately, we know today that the protons have anisotropic distributions, so that the above statement is only correct to a crude approximation. The information on the anisotropy of the proton distribution has not yet been extracted from the MIT data. In what follows, we shall make the ad hoc assumption that the quoted w_0 is related to the mean kinetic temperature T_p by the same formula as given by (6.1), even in the anisotropic case, provided one interprets kT_p as 1/3 of the trace of the proton pressure tensor.

On the base of the solar corona, the collision frequency of particles of the solar plasma is high enough so that the pressures for both electrons and ions can be assumed to be isotropic. As the solar wind streams outward from the sun, the pressures become anisotropic. If one were to use the CGL double-adiabatic hypothesis to compute the changes in pressure anisotropies, one would obtain much too high anisotropies of both

electrons and ions at the orbit of the earth, as compared with observations. Hundhausen (1968) found that the anisotropy of ions are substantially higher than that of the electrons. He found during the quiet periods of the sun, that the ratio of pressure parallel to the magnetic field to the pressure perpendicular to the magnetic field, $P_{\parallel} / P_{\perp}$, is of the order 2 to 2.4 for ions, and 1 to 1.2 for electrons. On the other hand, the predicted ratio, $P_{\parallel} / P_{\perp}$, according to the CGL hypothesis, would be of the order 80 for both the electrons and ions.

Note that the empirical results of Hundhausen indicate that the electrons are essentially isotropic, i. e., that we can put to a good approximation:

$$P_{\parallel}^{(e)} \approx P_{\perp}^{(e)} \approx P^{(e)} \quad (6.2)$$

Various kinds of fluctuations found in the solar wind are believed to be responsible for the isotropization of the solar plasma. (For most recent comments on this subject, see Nishida, 1969).

Hundhausen (1969) has discussed the role of the heat flux in the solar wind. He found that the observed heat conduction in the solar wind is much smaller than that predicted (Whang, 1965). The problem of the discrepancy between the observed and predicted pressure anisotropies of electrons and ions and the heat conduction of the solar wind at the earth's orbit has not yet been completely resolved.

In the present study, we are not concerned how the pressure aniso-

tropies developed during the solar wind expansion. We are interested in the sudden change of the anisotropy in connection with the shocks. When a shock propagates through the undisturbed solar wind, one should expect it to modify the anisotropy of plasma. In the following sections we shall attempt to investigate semi-quantitatively this question using the experimental data given in the previous chapter.

6.2 Relations Between M_s , P'/P , ξ' and ξ derivable from Equations (2.79), (2.80), (4.27) and Experimental Data of a Given Shock

In the previous chapter, we have shown that the measured parameters, \underline{B} , \underline{V} , and n satisfy the Rankine-Hugoniot relations. However, the study of the pressures and the anisotropies of the solar wind in the pre- and post-shock states have been postponed. We hope to obtain some information about these unknown parameters by making use of the normal momentum and energy equations (see equations (2.35) and (2.36) or the resulting equation (2.80)). Since there are only three equations (see (2.34), (2.35), and (2.36) involving the four parameters ξ , ξ' , P and P' , it is impossible to determine all four parameters at once. We have to assume that one of the four parameters is given or "free". In what follows, we choose ξ as such a "free" parameter.

To begin with, we can gain the information on ξ' , without making any reference to equations (2.35) and (2.36), if we have available a secondary satellite (i. e. the transit time). In this case, we can utilize relations obtained in Chapter 4. As already pointed out in section 4.2,

the observed magnitude of the magnetic field depends on ξ and ξ' .

This dependence comes about via the factor η , defined by (4.27). Note that, considering η as given, (4.27) represents a linear relation between ξ and ξ' , viz.

$$\xi' = \frac{2g\eta + k(k-\beta)\xi}{2g + k(k-\beta)} \quad (6.3)$$

Thus, we can predict ξ' as a function of ξ from the measured value of η .

When the ion pressures are isotropic (i. e. $\xi = \xi' = 1$), η is one. Conversely, when η is one, it does not follow that the pressures are isotropic. As long as ξ and ξ' satisfy the equation (4.27) and $\eta = 1$, our matching procedures employed in Chapter 5 and Appendix C are valid.

It had been found in Chapter 5, that the analyzed events satisfied the shock conditions quite well under the assumption of isotropic pressures. It is more general to state that the observed events satisfy the shock conditions quite well when " $\eta = 1$ ". (The shock of June 26, '67 was the only exception; $\eta = 1.7$ produce better results.)

We would like to point out again that the shock normal, \hat{n} , the normal Alfvén Mach number, M_A , and the angles $\Theta_{B,n}$ and $\Theta_{V^*,n}$ determined by the method given in Chapter 4 are independent of the anisotropy parameters.

Let us return to (2.80) and let us assume again that ξ is "free". Substituting (6.3) in to (2.80), we find an equation that contains the measured parameters, the anisotropy parameter ξ , and the sound Mach number, M_S , defined by (2.61). Solving this equation for M_S , we can look upon M_S as a function of ξ alone for a given shock, because all the other parameters entering into the equation for M_S are uniquely determined by the measurements (and thus can be treated as fixed numbers known for each shock). Next, substituting the equation for M_S and (6.3) into the equation for normal momentum (2.76), we can derive P'/P as a function of ξ (and a given set of measured parameters such as M_A , $\Theta_{B,n}$, and y).

In the three cases, when the transit time was not available, the equations given in Chapter 4 are not applicable, and the procedure discussed above is not useful. However, also in these cases, we were able to determine the shock velocities by the "best-fit matching procedure". Using these results and the formulas in Chapter 4 we can derive an artificial transit time, τ , and the related position vector \underline{y} . Once we have a relative position vector and an artificial transit time, an equation similar to (6.3) can be constructed. Therefore, the curves of M_S vs. ξ and P'/P vs. ξ can also be produced in these three cases.

6.3 Results of Numerical Computations of ξ' , M_S and P'/P as Functions of ξ

Following the above outline procedures and using the results quoted in Chapter 5, we can plot, for each shock, three separate curves, namely, P'/P (or T'/T) vs. ξ , M_S vs. ξ , and ξ' vs. ξ (we thus have all together 21 curves). These plots are shown in Figures 6-1 through 6-7, each figure referring in a chronological order to a given shock.

The ordinates and the abscissas are self-explanatory. As to the behavior of these curves we should like to make the following comments:

(1) In all seven cases, for a fairly wide range of ξ which we may consider as empirically reasonable, P'/P is very insensitive to the assumed values of ξ . In other words, the pressure ratios seem to depend very weakly on the degree of anisotropy of plasma in the pre-shock state.

(2) The dependence of M_S on ξ seems to be more pronounced than that of P'/P ; in fact one notices that in some cases M_S may change by even more than a factor^{or} of two within a relatively narrow range of ξ .

(3) We believe that the results for ξ' vs. ξ are most informative. We note that in all cases except for the shock of August 30, '67, the predicted values of ξ' are larger than the corresponding values of ξ , for wide range of ξ . In other words, we arrive at the important conclusion that all shocks (with the exception of the case of August 30, '67) cause the interplanetary plasma to change suddenly from the state of higher anisotropy to the state of lower anisotropy. This result is very

satisfying because on theoretical grounds, one would expect physical shocks to lead to strong randomization of plasma. Let us recall that the shocks are manifestations of highly irreversible, dissipative physical processes. As far as the exceptional case of the slow shock of August 30 is concerned, we should like to comment that both ξ and ξ' may very well be close to unity. In other words, we might deal in this case with an isotropic plasma on both sides of the shock.

6.4 Attempts to Estimate the Electron Temperature from Available Data

As we have mentioned in the beginning of this chapter, in addition to all physical parameters used thus far, we have available the thermal speed of protons on both sides of the shock. Table 6-1 shows the average values of the most probable thermal speed of proton, w_0 and w'_0 on both sides of the shock. The table contains also the corresponding values of the proton pressures (measure in terms of the magnetic pressure). The last column of the table indicates the empirical values of the parameter η (see 4.27) found to produce the best-fit in our matching procedure.

Using the above quoted values for proton pressure we should be able, in principle, with the help of Figures 6-1 through 6-7, to determine the electron pressures on both sides of the shock as functions of ξ . We simply have to recall that:

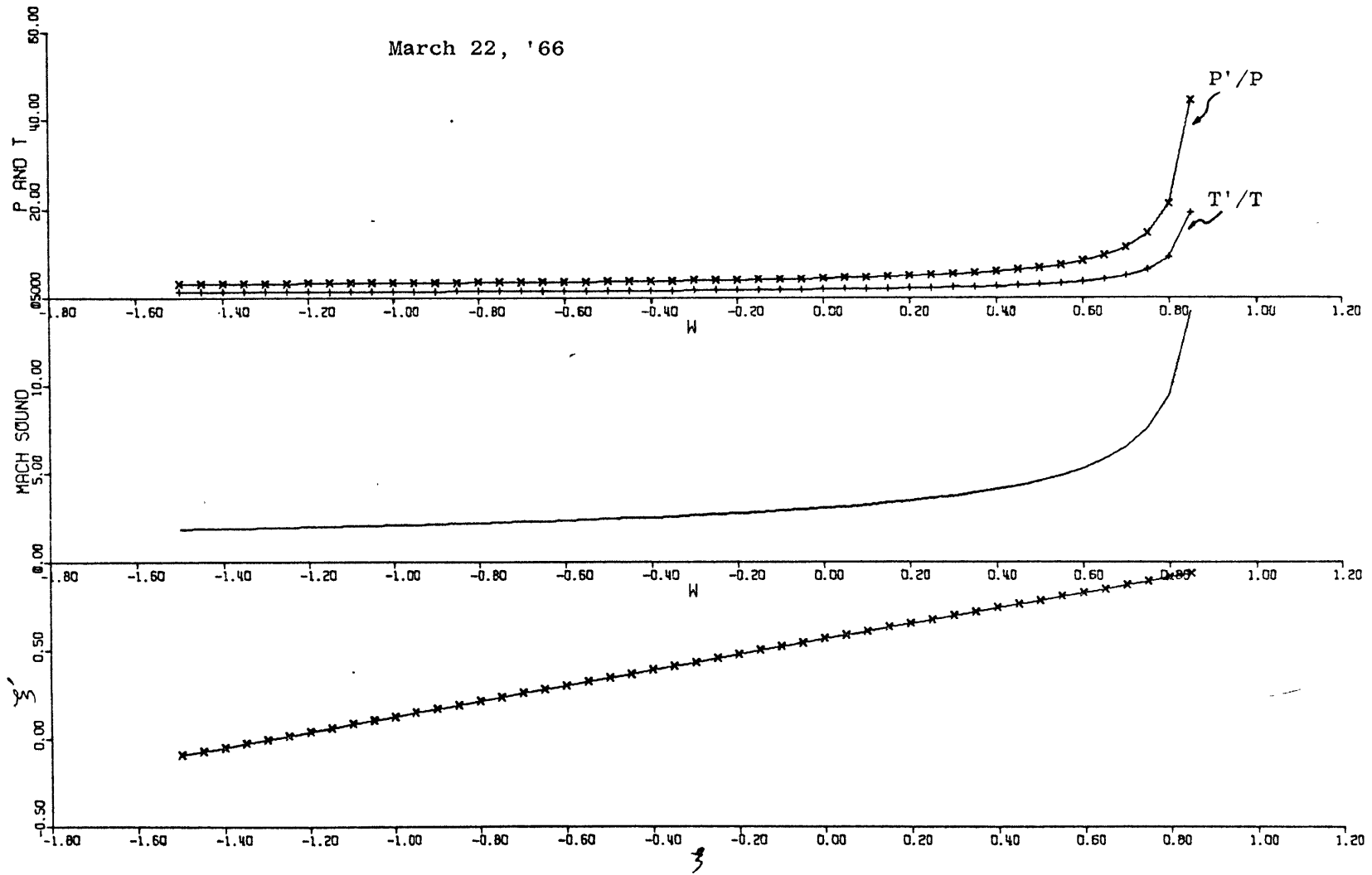


Figure 6-1

March 23, '66

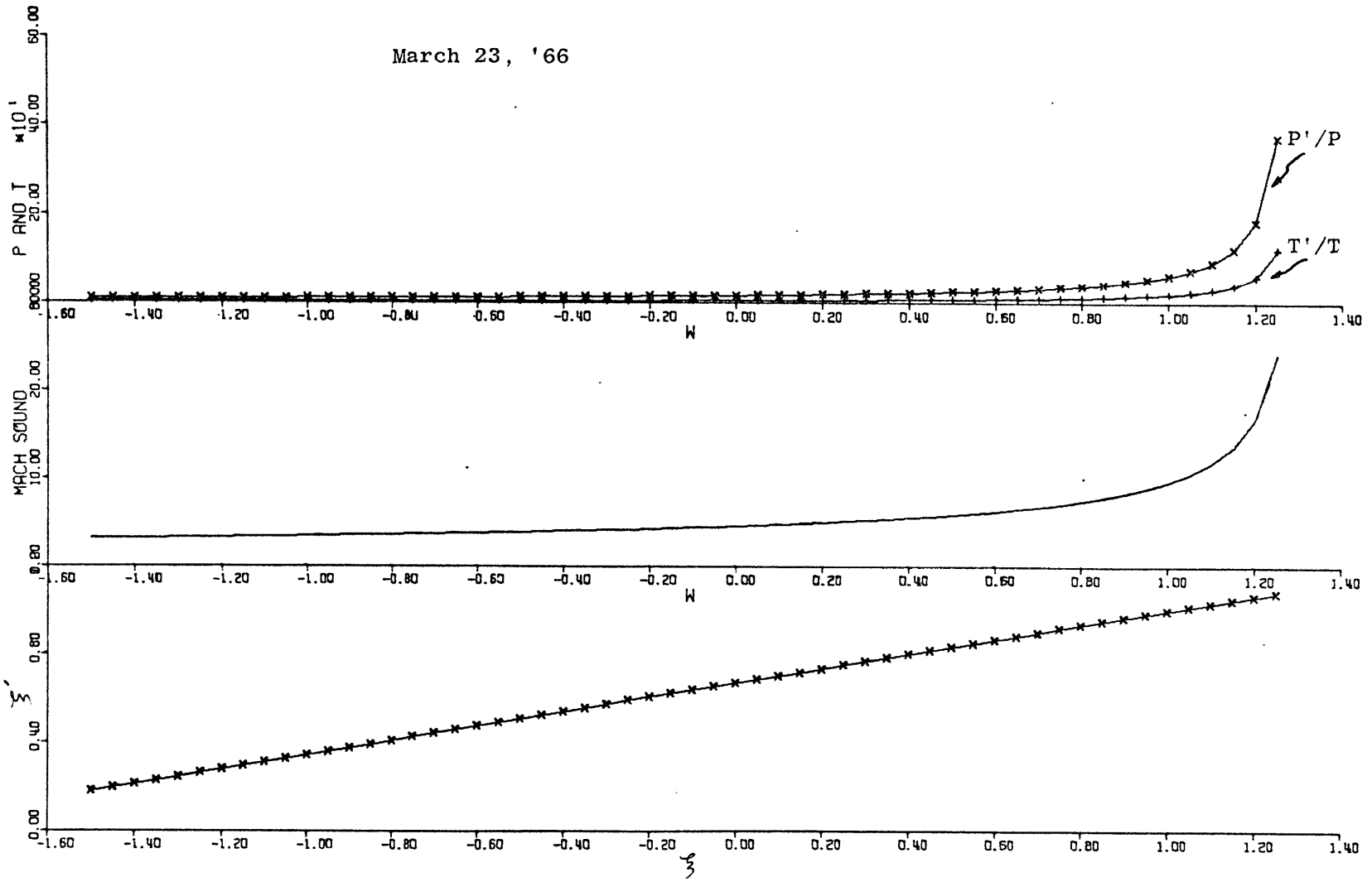


Figure 6-2

August 29, '66

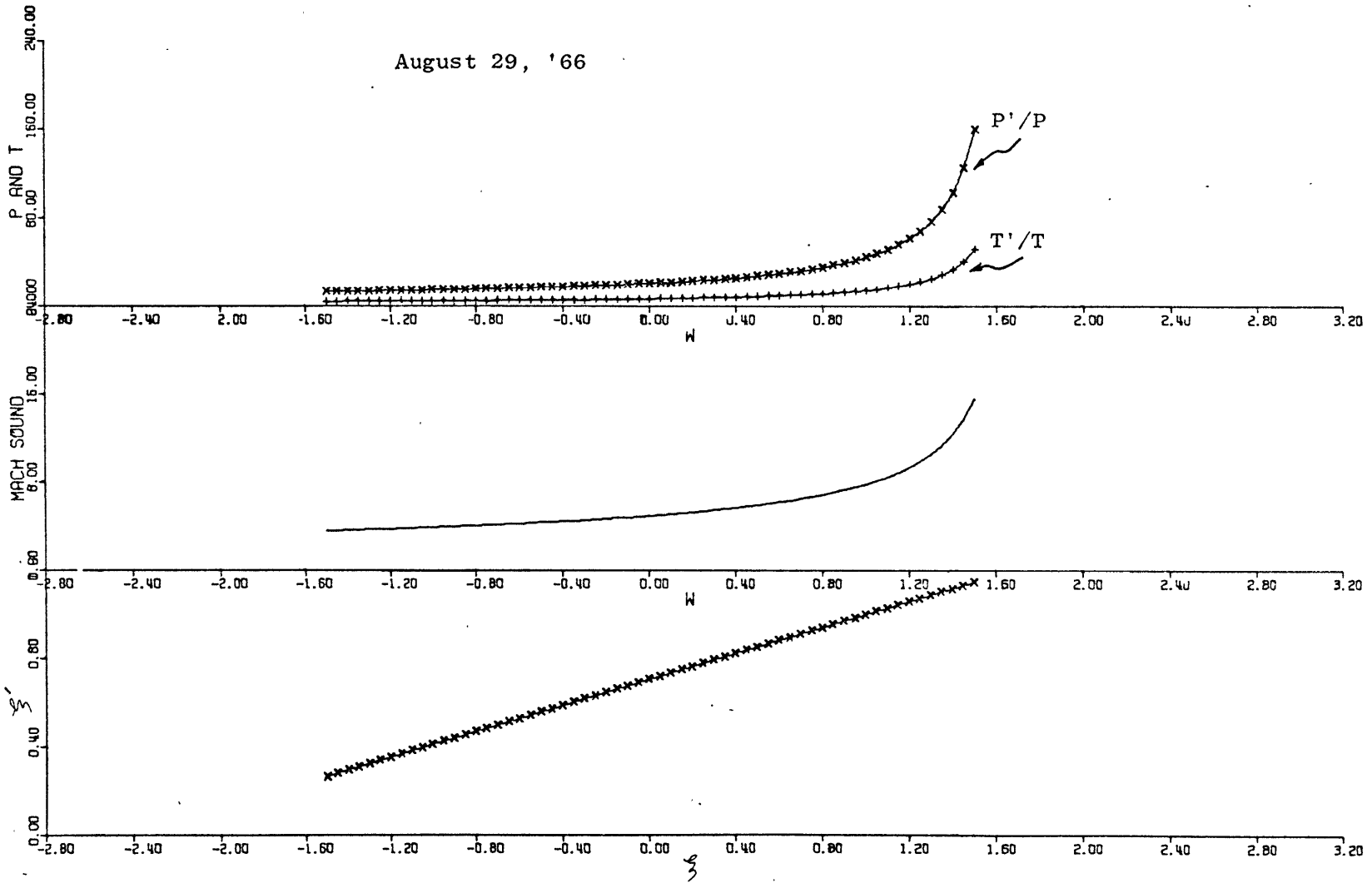


Figure 6-3

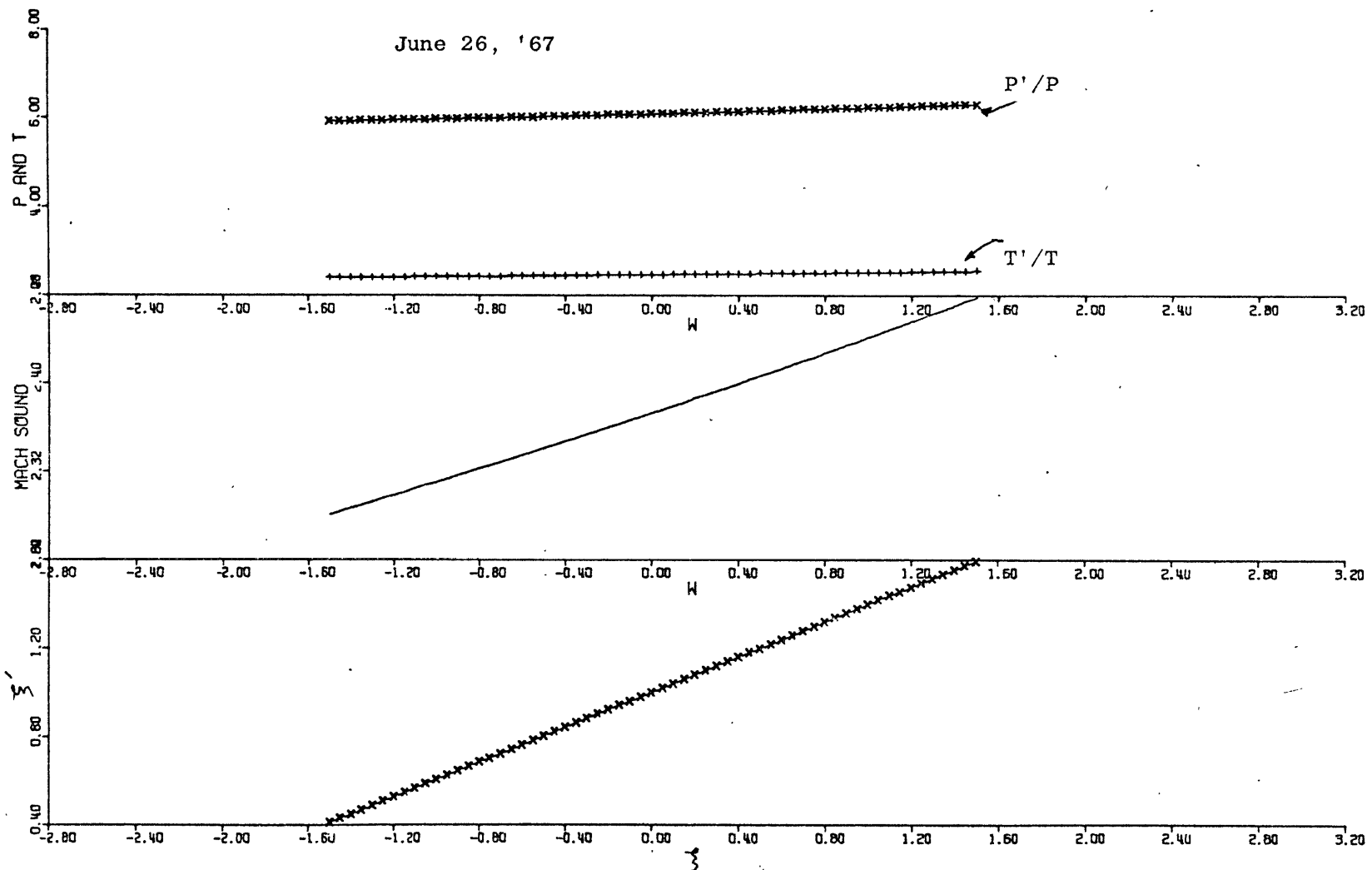


Figure 6-4

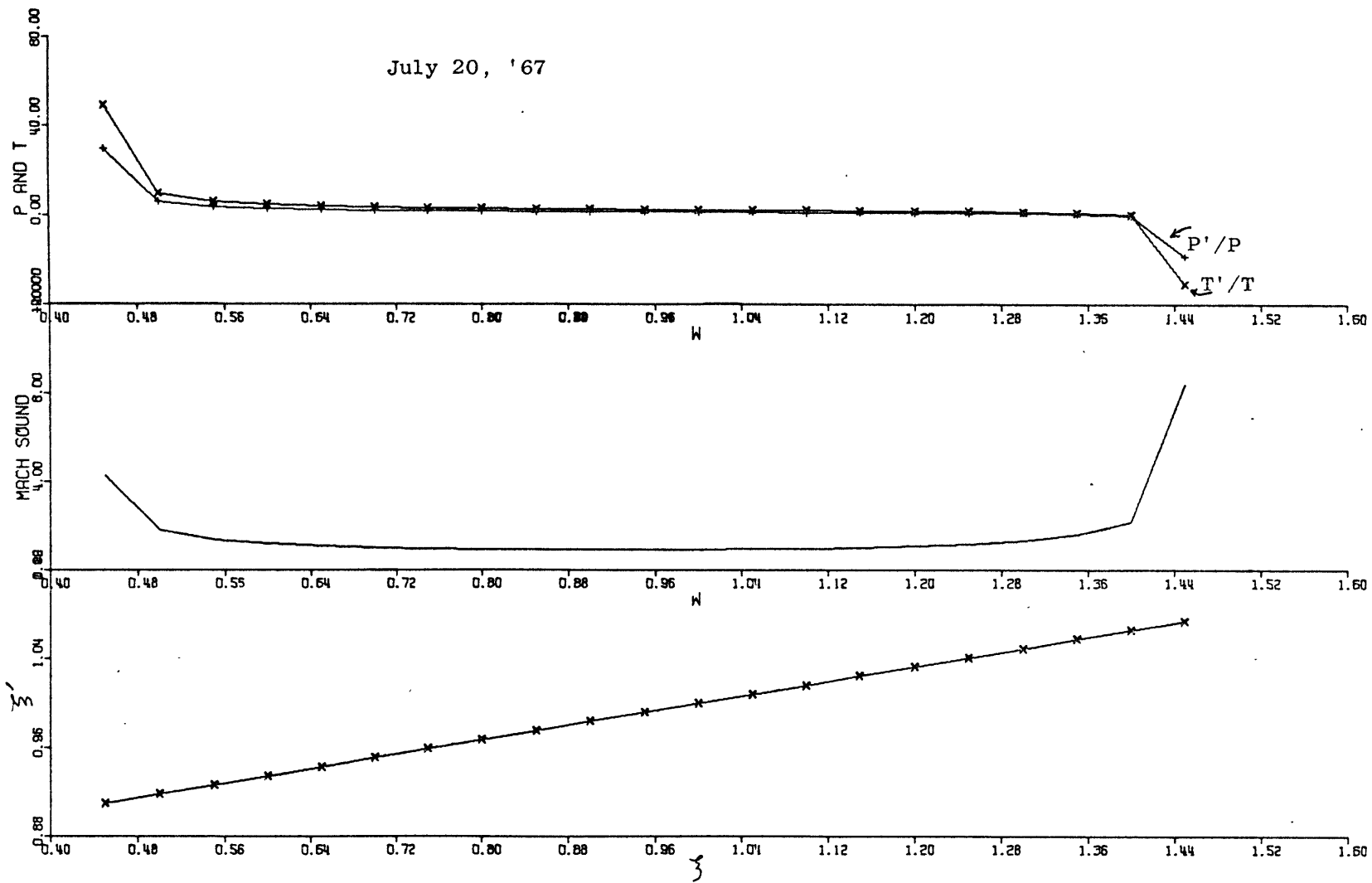


Figure 6-5

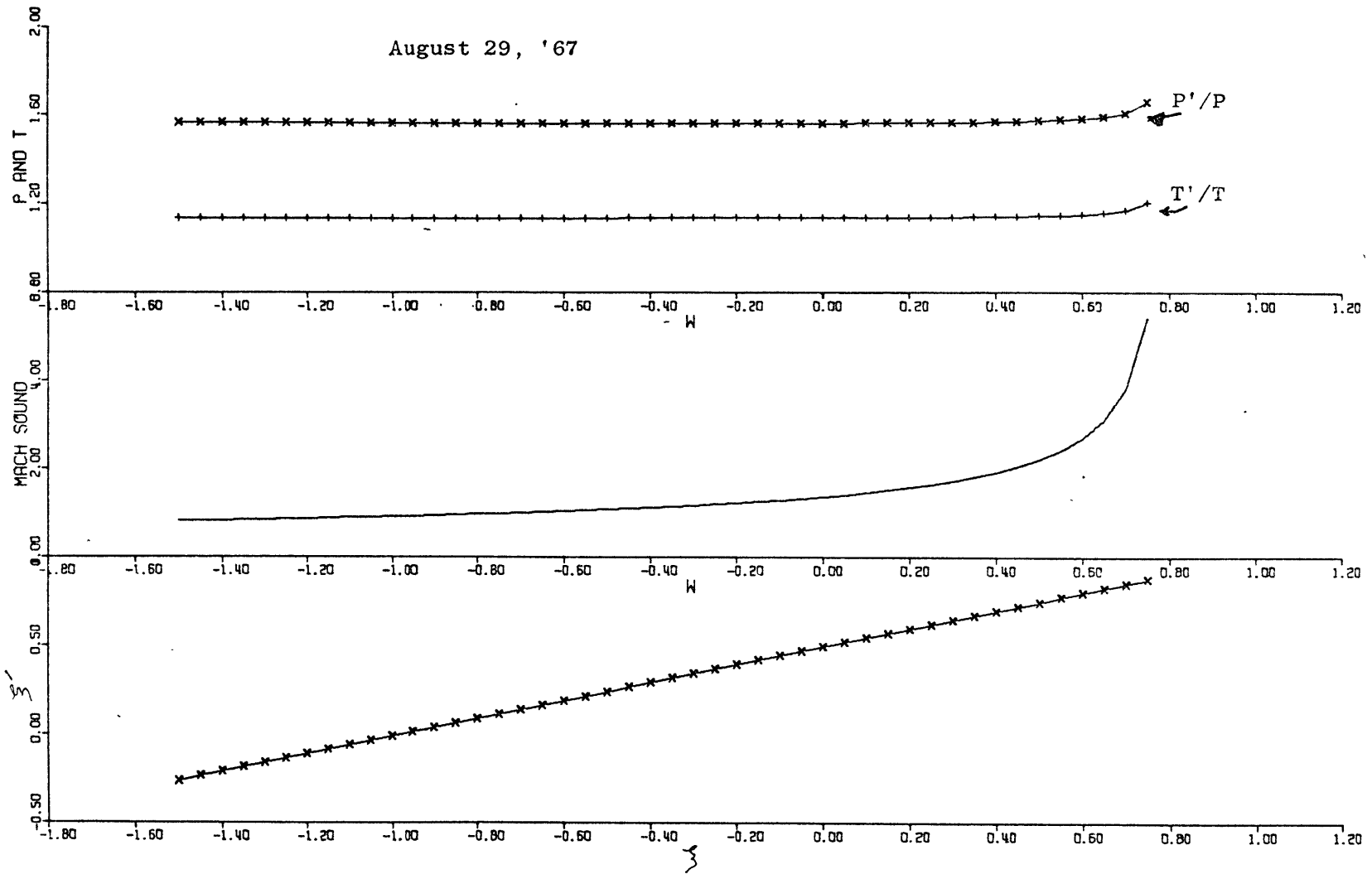


Figure 6-6

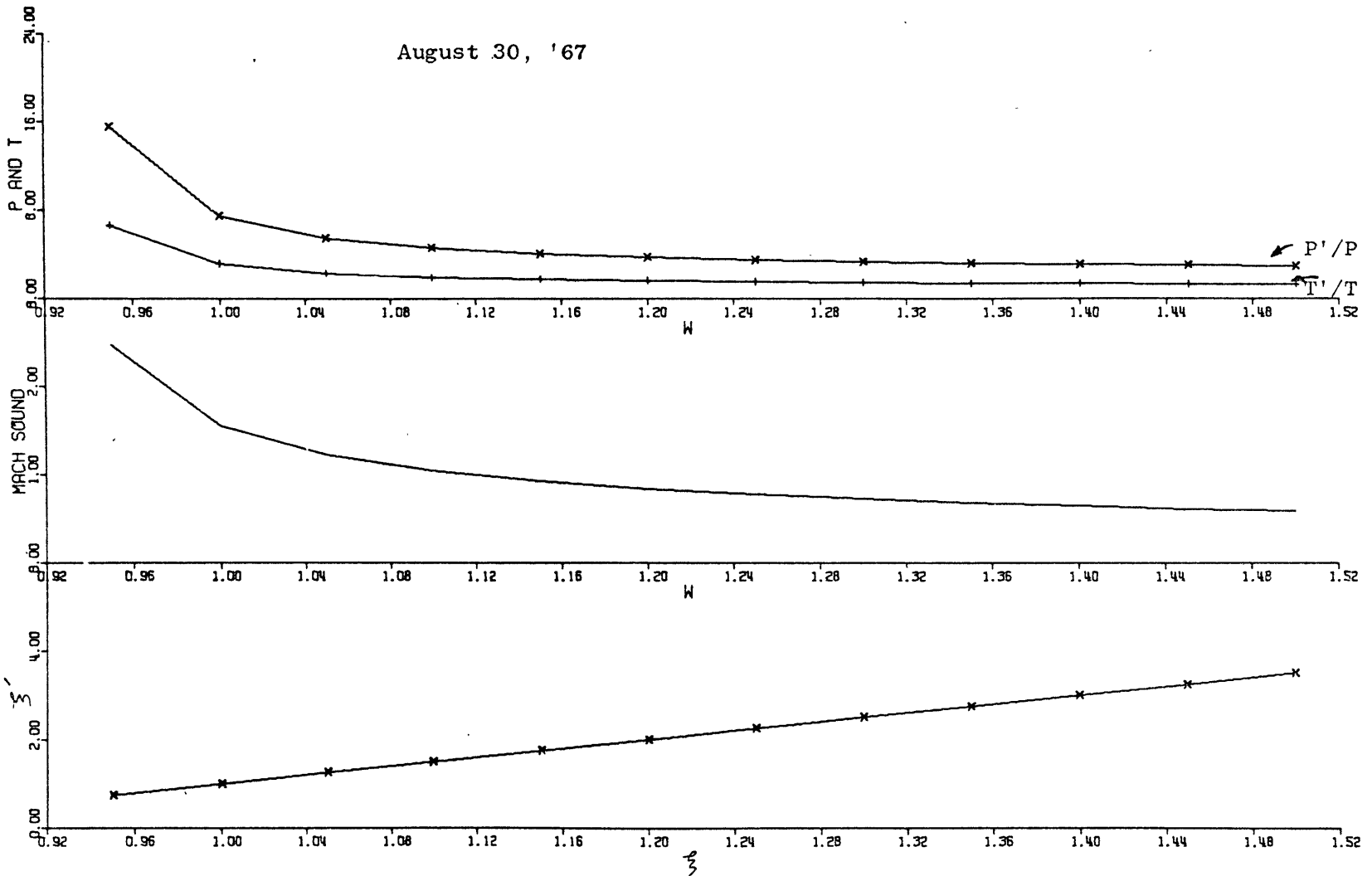


Figure 6-7

Table 6-1

Best-Fit Values of η and the Measured Parameters, w_0 and $P^{(i)}/(B^2/2\mu_0)$

Shocks (denoted by the date measured)	Most Probable Thermal Speed (km/sec)		$\frac{P^{(i)}}{(B^2/2\mu_0)}$	$\frac{P^{(i)'}}{(B^2/2\mu_0)}$	η
	Pre-Shock	Post-Shock	Pre-Shock	Post-Shock	
	w_0	w_0			
March 22, '66	60	52	0.2	0.1	1
March 23, '66	50	75	0.1	0.1	1
August 29, '66	24	50	0.1	0.2	1
June 26, '67	28	31	1.4	1.0	1.7
July 20, '67	22	32	0.05	0.3	1
August 29, '67	40	47	0.08	0.1	1
August 30, '67	19	39	0.02	0.4	1

$$P^{(e)} = \frac{3}{5} \rho \frac{V_n^{*2}}{M_s^2} - P^{(i)} \quad (6.4)$$

and

$$P^{(e)'} = \frac{3}{5} \rho \left(\frac{P'}{P} \right) \frac{V_n^{*2}}{M_s^2} - P^{(i)'} \quad (6.5)$$

We have performed such calculations of $P^{(e)'}$ and $P^{(e)}$ for various values of ξ , and β , to our surprise, we have found that in all cases (except the shock of June 26, '67), that the obtained values of $P^{(e)'}$ and $P^{(e)}$ turn out to be very small in comparison with the corresponding values of ion pressures. The exceptional case of June 26, '67 leads to values of electron pressure comparable to that of ions.

Because of these unexpected results we concerned ourselves with the questions whether our interpretation of w_0 was tenable and how sensitive were our results to w_0 . For this purpose, as a tentative exercise, we have reduced all the observed values of w_0 by 30% and then repeated the processes of the electron pressure estimates. Under this ad hoc assumption the electron pressures in the pre-shock state could be brought to be equal to ion pressures in the pre-shock state for reasonable values of ξ . The results of this exercise are shown in Table 6-2. The first column shows the ratio of measured ion

Table 6-2

The Ion and Electron Temperature Ratios
 (under the assumption that $P^{(e)} = P^{(i)}$)

Shocks	$T^{(i)'}/T^{(i)}$	$T^{(e)'}/T^{(e)}$ (with w_0 reduced by 30%)	ξ	ξ'
March 22, '66	0.8	2.6	-0.4	0.4
March 23, '66	2.3	9.6	0.1	0.7
August 29, '66	4.5	12.2	0.5	0.8
July 20, '67	2.1	0.5	1.3	1.0
August 29, '67	1.4	0.9	0.5	0.7
August 30, '67	4.2	4.3	1.0	0.9

temperatures across the shock. The remaining columns show, respectively, the ratio of the electron temperatures, ξ and ξ' , all quantities being computed with the value of w_0 reduced by 30% and under the assumption that $P^{(e)} = P^{(i)}$. The results in Table 6-2 seem to be physically reasonable.

We should not like to attach any precise physical significance to the results obtained in Table 6-2. All they demonstrate is the fact that the estimates of the electron temperature by our procedure are quite sensitive to the assumed values of w_0 . A glance at Figures 5-4, 5-5, 5-8, 5-9, 5-10, 5-14, and 5-15 shows that the fluctuations of w_0 are quite severe. It is not obvious that the average values of physical quantities, rather than the instantaneous values at the occurrence of the shock, should be used in analyzing the shock.

Chapter 7

SUMMARY OF THE RESULTS

7.1 Critical Review of Observational Findings

Let us review first the results obtained in Chapters 5 and 6.

We found seven events which have been identified as shocks: five fast and two slow shocks.

The experimental data were taken from three satellites: Pioneer 6, 7 and Mariner V. The rate of data collection was different for different physical quantities (and different satellites). The plasma data rates associated with the shocks found on Pioneer 6 and 7 happened to be the same: at about one minute intervals. The magnetic field measurements were taken at a faster rate but have been averaged over 30 second intervals. The measurements of Mariner V were taken at a slower rate than those on Pioneer 6 and 7. The data for the June 26 and July 20 shocks were taken at a rate of one measurement per five minutes. When the satellite was further away from the earth, the data rate, such as during the August 29 and 30 shocks, was one point per twenty minutes.

Our confidence in the shock identification depends on the rate the data are taken. Therefore, the August 29 and 30 shocks of Mariner V should be treated with less confidence than the other shocks. The fitting results for these two shocks do not appear as good as for the

others.

The June 26 and July 20 shocks display better fits than the August 29 and 30 shocks of Mariner V, but not as good as the fits for Pioneer 6 and 7. (The latter shocks have higher data collection rates.)

The data rate for the study of interplanetary shocks should be greater than one point per 5 minutes to achieve a more precise agreement between the measured and computed parameters, than we have obtained.

The strength of the slow shocks is weaker than that of the fast shocks. The normal Alfvén Mach number of slow shocks in both the pre- and post-shock states is less than one. Hence, the Alfvén waves may propagate both up- and downstream from the shock. The pre- and post-shock states appear to fluctuate more. This may be the main reason why the fitting of slow shocks is not as good as that of the fast shocks. In order to obtain a better fitting and more trust worthy results for slow shocks, we suggest that the data rate used should be no less than one point per 2 minutes.

The errors of the measured parameters result from a combination of the instrumental uncertainties and actual fluctuations of these parameters in space and time. The instrumental errors in the case if the fields are much smaller than their fluctuations; the latter often are quite severe. As far as the plasma data are concerned, the instrumental uncertainties and fluctuations are comparable; however, the plasma

fluctuations are substantially smaller than those of the magnetic fields.

There are four shocks (June 26, August 29 of Mariner V, March 23 of Pioneer 6 and August 29 of Pioneer 7) which have the additional information on the transit time, (secondary satellite available). These shocks should be taken as more significant than those without a transit time. However, information concerning transit time is useful only when the distance between two satellites or between the satellite and the earth is less than $\sim 1/10$ A. U. but larger than 10^6 km. When the separation between the primary and the secondary vehicles is outside this range, the transit time information should be considered of secondary importance.

In spite of the above quoted restrictions, we found the information on the transit time very valuable. It permitted us to impose upon the data an additional quantitative test for their shock properties. We believe that any data that survive this test and satisfy the MHD Rankine-Hugoniot relations given by equations (2.64), (2.65), (2.66), indeed demonstrate unambiguously the existence of MHD shocks in collisionless plasma. More specifically, we believe that we have demonstrated, for the first time, the existence of slow shocks.

In Chapter 6 we have attempted to gain some information on the changes of the thermal anisotropies across the shock. Although the conclusions that we could draw were only qualitative, we believe that they are valuable: our analysis showed that, as anticipated on physical

ground, the anisotropy of plasma pressure decreases suddenly when the plasma passes from pre- to post-shock state, (i. e. $\xi' > \xi$).

We also attempted in Chapter 6 to estimate the partial pressures for electrons on both sides of the shock, using all available shock equations and experimental information on positive ions. We are perplexed with our findings. Except for the shock of June 26, 1967 where the computed electron pressures appear to be "reasonable", the fitting of the data on all other spacecraft seem to require very cold electrons. We fear that such a conclusion may be fallacious; however, we cannot either prove it or disprove it. We are mindful of the surprising results obtained in IMP-1 (Olbert, 1968) where it was found that the electrons behind the earth's bow shock failed to heat up to any appreciable degree as compared with protons. The difficulties here are enhanced by the fact that we are not certain if our interpretation of w_0 is valid. The entire issue of the meaning of w_0 and the behavior of electron pressures across the shock should be investigated more carefully in the future.

7.2 Resumé of Analytical Investigations

To summarize our analytical effort of Chapters 2 to 4, we should like to bring out the following points:

(1) In Chapter 2, we have derived the shock equations for plasma with anisotropic pressures. These equations represent the generalization of

the known MHD Rankine-Hugoniot relations for isotropic plasmas.

(2) We have shown that the coplanarity theorem for the magnetic field and the continuity theorem for the velocity component perpendicular to the (\hat{n}, \underline{B}) plane still hold for anisotropic plasmas.

(3) In Chapter 3, we have investigated extensively the dependence of the shock relations on the assumed values of the anisotropic parameters ξ and ξ' . The results are presented in graphical form.

(4) In Chapter 4 we took advantage of occasional presence of secondary satellites capable of detecting the passage of the shock. We have shown that in this case we could derive simple analytical expressions determining the orientation of the shock in the interplanetary space. The results of Chapter 4 played an important role for an independent test whether the observed events were indeed MHD shocks.

Appendix A

SHOCK EQUATIONS FOR ANISOTROPIC PLASMAS

By virtue of the coplanarity theorem derived in section 2.2.1, we always can orient the shock coordinate system in such a way that B_2 vanishes on both sides of the shock. From (2.32) and (2.33), we obtain $V_2^* = V_2^{*'}$. And from (2.29), we obtain $B_1 = B_1'$. Therefore, eight equations (2.29) to (2.36) reduce to five equations, namely, (2.30), (2.31), (2.34), (2.35) and (2.36). We have now six unknowns: ρ' , $V_1^{*'}$, B_3' , V_3^* , P' and ξ' .

Equation (2.30) can be written as:

$$\rho V_1^* = \rho' V_1^{*'} \quad (\text{A.1})$$

If we divide (A.1) by $\rho V_1^{*'}$, we obtain equation (2.76).

Equation (2.31) can be written as:

$$V_3^* B_1 - V_1^* B_3 = V_3^{*'} B_1 - V_1^{*'} B_3 \quad (\text{A.2})$$

If we divide (A.2) by $V_3^{*'} B_3$ and use the fact that $\tan \theta_B = \frac{B_3}{B_1}$ and $\tan \theta_{V^*} = \frac{V_3^{*'}}{V_3^*}$, and obtain:

$$\xi \equiv \frac{V_3^{*'}}{V_3^*} = \frac{\tan \theta_B}{\tan \theta_V} (uy - 1) + 1 \quad (\text{A.3})$$

Equation (2.34) can be written as:

$$\rho V_1^* V_3^* - \xi \frac{B_1 B_3}{\mu_0} = \rho' V_1^{*'} V_3^{*'} - \xi' \frac{B_1 B_3'}{\mu_0} \quad (\text{A.4})$$

If we divide (A.4) by $\rho V_1^* V_3^*$ and use (A.3) and (2.50) and obtain equation (2.78). Substituting (2.78) into (A.3), we obtain equation (2.77).

Equation (2.35) can be written as:

$$\begin{aligned} \rho V_1^{*2} + P + \frac{1}{3} \left(\xi + \frac{1}{2} \right) \frac{B^2}{\mu_0} - \xi \frac{B_1^2}{\mu_0} = \\ \rho' V_1^{*2} + P' + \frac{1}{3} \left(\xi' + \frac{1}{2} \right) \frac{B'^2}{\mu_0} - \xi' \frac{B_1'^2}{\mu_0} \end{aligned} \quad (\text{A.5})$$

If we divide (A.5) by ρV_1^{*2} and use (2.61) we obtain equation (2.79).

Equation (2.36) can be written as:

$$\begin{aligned} \left[\frac{1}{2} \rho V^{*2} + \epsilon_T + P + \frac{1}{3} (\xi + 2) \frac{B^2}{\mu_0} \right] V_1^* - \xi \frac{B_1 B_3}{\mu_0} V_3^* = \\ \left[\frac{1}{2} \rho' V^{*2} + \epsilon_T' + P' + \frac{1}{3} (\xi' + 2) \frac{B'^2}{\mu_0} \right] V_1^{*'} - \xi' \frac{B_1 B_3'}{\mu_0} V_3^{*'} \end{aligned} \quad (\text{A.6})$$

where according to (2.39), (2.74) and (2.75), we have:

$$\epsilon_T = \frac{3}{2} P \quad (\text{A.7})$$

$$\epsilon_T' = \frac{3}{2} P' \quad (\text{A.8})$$

If we divide (A.6) by ρV^{*2} and multiple by $(M_A^2 y - \xi')^2$, and obtain with the help of (2.76) through (2.79), equation (2.80).

Appendix B

PROOF FOR COMMON INTERSECTION POINT IN
THE FAMILY OF CURVES SHOWN IN FIGURES (3.1) TO (3.5)

We should like to prove analytically, that the family of curves for y vs. ξ' for various values of Θ_B (at fixed values of M_A , M_S and ξ) pass through a common point. This can be shown by using (2.80) to (2.85).

The coefficients C_i 's can be written as:

$$C_i = \bar{C}_i + C_{iT} \tan^2 \Theta_B \quad (i = 1, 2, 3, 4) \quad (B.1)$$

where, neither \bar{C}_i nor C_{iT} depend on Θ_B

Substituting the relations (B.1) into (2.80), we obtain:

$$\begin{aligned} & (\bar{C}_4 y^4 + \bar{C}_3 y^3 + \bar{C}_2 y^2 + \bar{C}_1 y + \bar{C}_0) + \tan^2 \Theta_B (C_{3T} y^3 \\ & + C_{2T} y^2 + C_{1T} y + C_{0T}) = 0 \end{aligned} \quad (B.2)$$

where we made use of the fact that $C_{4T} = 0$. Note that the coefficients \bar{C}_i and C_{iT} are functions of ξ , ξ' , M_A and M_S only. Let us investigate the case when the factor multiplying $\tan^2 \Theta_B$ vanishes, i. e.,

$$C_{3T} y^3 + C_{2T} y^2 + C_{1T} y + C_{0T} = 0 \quad (B.3)$$

If we solve (B.3) for y in terms of ξ' , ξ , M_A and M_S and substitute it into the first parenthesis of (B.2), we obtain an expression

of the form

$$\begin{aligned} & \bar{C}_4 y^4(\xi'; \xi, M_A, M_S) + \bar{C}_3 y^3(\xi'; \xi, M_A, M_S) + \bar{C}_2 y^2(\xi'; \xi, M_A, M_S) \\ & + \bar{C}_1 y(\xi'; \xi, M_A, M_S) + \bar{C}_0 = 0 \end{aligned} \quad (\text{B.4})$$

which for fixed values of ξ , M_A and M_S may be considered as a function of ξ' alone. In general, one expects that there exists at least one value of ξ' , which make the function given by (B.4) vanished. Explicit numerical calculations show (see Figures 3.1 to 3.5) that in most cases studied there is only one such special value of ξ' for a fixed set of ξ , M_A and M_S . The range of the numerical values for this special ξ' is surprisingly narrow ($0 < \xi < 0.5$).

If the anisotropy parameter ξ' equals the value associated with the intersection point, the jump parameters x , y and u are independent of Θ_B i. e., of the orientation of the \underline{B} -field in Σ^* .

Appendix C

THE "BEST-FIT" PROCEDURE FOR MATCHING
THE MHD SHOCK RELATIONS WITH THE DATA

There are eight shock equations: (2.29) through (2.36). Five of these equations are based on the conservation laws: one equation from the law of mass conservation, three equations from the law of momentum conservation, and one equation from the law of energy conservation. The remaining three equations are derived from the requirements of Maxwell's equations that, across the shock, the tangential component of the electric field be continuous (2 equations) and that the normal component of the magnetic field be continuous (1 equation). Together, these eight equations, if written out in an arbitrary frame of references, contain twenty-one parameters. Fifteen of these parameters refer to the following vectors: the magnetic field and the solar-wind velocity, in the pre- and post-shock states, as well as the shock velocity. The remaining six are scalar parameters, namely, the density, the pressure, and anisotropy parameters on both sides of the shock.

Out of the twenty-one parameters only fourteen are measured; the measured parameters are: \underline{B} , \underline{V} , and n , (on both sides of the shock). Thus, in general, by using the eight conservation equations, one should be able to predict any eight out of twenty-one parameters, provided the remaining thirteen are known. Thus, in our case, one of

the fourteen measured parameters is overdetermined and its predicted value can be tested against observations.

If we have the additional information on the transit time of the shock wave from one satellite to another or if the shock wave causes a storm sudden commencement on earth, the number of the overdetermined parameters increases to two. In more specialized case when the pressures are isotropic (i. e. $\xi = \xi' = 1$), the number of overdetermined parameters increases to four.

Let us turn our attention to the details of our best-fit procedure. We shall restrict our discussion to the isotropic case (i. e. $\xi = \xi' = 1$). The method described below can be readily generalized to the case when the anisotropy parameters ξ and ξ' differ from unity, however, this more involved case is beyond the scope of our thesis.

As the first step, we find the shock normal \hat{n} by means of (4.1). As already pointed out, the results based on this equation will be, in general, very inaccurate. In order to improve this accuracy, we make use of the equations (2.55), (2.77) and (2.78) which are part the basic shock relations. In other words, we require, first of all, that according to (2.55):

$$\underline{V}_2 = \underline{V}'_2 \tag{C.2}$$

Recalling the definition of our Cartesian coordinates in Σ^* , the above equation can be also written as:

$$\delta \equiv (\underline{V}' - \underline{V}) \cdot (\hat{n} \times \underline{B}) = 0 \tag{C.2}$$

Secondly, we require that, (for $\xi = \xi' = 1$) according to (2.77) that

$$\zeta = \frac{\tan_{B,n}}{\tan_{V,n}} \left(\frac{1-y}{M_A^2 y - 1} \right) + 1 \quad (C.3)$$

and recall that according to the definition of ζ (see Eq. (2.63))

$$\zeta = \frac{[(\hat{n} \times \underline{B}) \times \hat{n}] \cdot \underline{V}'}{[(\hat{n} \times \underline{B}) \times \hat{n}] \cdot \underline{V}} \quad (C.4)$$

Thirdly, we require that, according to (2.78) (for $\xi = \xi' = 1$)

$$u = \frac{M_A^2 - 1}{M_A^2 y - 1} \quad (C.5)$$

and recall that according to the definition of u (see Eq. (2.63))

$$u = \frac{[(\hat{n} \times \underline{B}) \times \hat{n}] \cdot \underline{B}'}{[(\hat{n} \times \underline{B}) \times \hat{n}] \cdot \underline{B}} \quad (C.6)$$

Note that the quantities ζ , ζ and u defined by (C.1), (C.4) and (C.6) can be looked upon as given from experimental data. Since they depend on \hat{n} , they, in general, will be burdened with large errors. Consequently, their values computed from the data and (4.1) will not, as a rule, satisfy (C.2), (C.3) and (C.5) rigorously. Labeling these first-step experimental values of ζ , ζ , u , respectively, by ζ_{exp}

z_{exp} , and u_{exp} , we can define the following differences between their measured and the theoretically expected values:

$$d_z = \left| z_{\text{exp}} - \left[\frac{\tan \Theta_{B,n}}{\tan \Theta_{V^*,n}} \left(\frac{1-\gamma}{M_A^2 \gamma - 1} \right) + 1 \right] \right| \quad (\text{C.7})$$

$$d_u = \left| u_{\text{exp.}} - \frac{M_A^2 - 1}{M_A^2 \gamma - 1} \right| \quad (\text{C.8})$$

$$d_\delta = \left| \delta_{\text{exp}} - 0 \right| \quad (\text{C.9})$$

These differences can be obtained in their entirety from the available data, provided one first computes not only \hat{n} but also the shock speed V_S (see 4.8). (Note that one has to transform first various data to the shock frame of reference Σ^* in order to obtain Θ_{V^*} and M_A).

Our task is to minimize d_z , d_u , and d_δ in order to obtain the best fit values of the physical parameters. For this purpose, we have employed standard minimization procedures with the aid of the computer. The method involves simultaneous variation of the experimental parameters within the allowed range of observation uncertainties. It is essentially an iteration process in which, as the first step, the average values of the physical parameters on both sides of the shock are used.

REFERENCES

- Abraham-Shrauner, B., *J. Plasma Physics*, 3, 361, 1967.
- Akasofu, S.I., and S. Yoshida, *Planet. Space Sci.*, 15, 39, 1967.
- Anderson, J.E., *Magnetohydrodynamic Shock Waves*, MIT Press, Cambridge, Mass., 1963.
- Axford, W.I., *J. Geophys. Res.*, 67, 3791-3796, 1962.
- Bazer, J. and W.B. Ericson., *Ap. J.*, 129, 758, 1959.
- Buneman, O., *Physics of Fluids*, 4, 669, 1961.
- Burlaga, L.F., *Solar Physics*, 4, 67, 1968.
- Burlaga, L.F. and N.F. Ness, *Solar Physics*, 9, 467, 1967.
- Chew, G.F., M.L. Goldberger, and F.E. Low, *Proc. Roy. Soc.*, A 236, 112, 1956.
- Colburn, D.S. and C.P. Sonett, *Space Science Rev.*, 5, 430, 1966.
- Gold, T., *Gasdynamics of Cosmic Clouds*, (ed. by H.C. Van de Hulst and J.M. Burgers) North-Holland Publ. Co., 1955.
- Gosling, J.T., J.R. Asbridge, S.J. Bame, A.J. Hundhausen, and I.B. Strong, *J. Geophys. Res.*, 7, 3357, 1967.
- Hirshberg, J., *J. Geophys. Res.*, 68, 6201, 1963.
- Hughes, W.F. and F.J. Young, *The Electromagnetodynamics of Fluids*, John Wiley & Sons, Inc., 1966.
- Hundhausen, A.J., H.E. Gilbert and N.F. Ness, *J. Geophys. Res.*, 72, 5265, 1967.
- Hundhausen, A.J., *Space Phys. Rev.*, 8, 690, 1968.
- Hundhausen, A.J., *J. Geophys. Res.*, 74, 5810, 1969.
- Kantrowitz, A. and H.E. Petschek, *MHD Characteristics and Shock Waves in "Plasma Physics in Theory and Application"*, (ed. W.B. Kunkel) McGraw-Hill, 1966.

- Kulikovskiy, A.G. and G.A. Lyubimov, Magnetohydrodynamics, Addison-Wesley Pub. Inc., Reading, Mass., 1965.
- Landau, L.D., and E.M. Lifshitz, Fluid Mechanics, Addison-Wesley, Reading, Mass., 1959.
- Lazarus, A.J., H.S. Bridge, and J. Davis, J. Geophys. Res., 71, 3787, 1966.
- Lynn, Y.M., The Phys. of Fluids, 10, 2278, 1967.
- Ness, N.T., and J.M. Wilcox, Solar Phys., 2, 351, 1967.
- Nishida, A., J Geophys. Res., 69, 5155, 1969.
- Nishida, A., Satellite Information on the Origin of Geomagnetic Variations (to be published).
- Ogilvie, K.W. and L.F. Burlaga, Hydromagnetic Shocks in the Solar Wind, GSFC Report, X-616-69-29, Jan., 1969.
- Olbert, S., Summary of Experimental Results from M.I.T. Detector on IMP-1, in Phys. of the Magnetosphere, Ed. by R.L. Carovillano et al, D. Reidel Publisher, 642, 1968.
- Parker, E.N., Interplanetary Dynamical Processes, Interscience Publishers, 1963.
- Rossi, B., and S. Olbert, Introduction to the Physics of Space, McGraw-Hill, 1970.
- Scarf, F.L., Planet. Space Sci., 17, 595, 1969.
- Shercliff, J.A., A Text Book of Magnetohydrodynamics, Pergamon Press, N.Y., 1965.
- Shercliff, J.A., J. Fluid. Mech., 9, 481, 1960.
- Sonett, C.P., D.S. Colburn, L. Davis Jr., E.J. Smith, and P.J. Coleman, Phys. Rev. Letters, 13, 1964.
- Spitzer, L., Physics of Fully Ionized Gases, Pergamon Press, N.Y., 1965.

Spreiter, J.R., and B.R. Briggs, Theoretical Determination of the Form of the Boundary of the Solar Corpuscular Stream Produced by Interaction with the Magnetic Dipole Field of the Earth, NASA TR R-120, 1961.

Taylor, H.E., Sudden Commencement Associated Discontinuities in the Interplanetary Magnetic Field Observed by IMP-3, GSFC Report X-616-68-239, 1968.

Vasyliunas, V.M., Deep Space Plasma Measurements to appear in "Methods of Experimental Physics," IX (Plasma Physics), Ed. by H.D. Griem and Lovberg, Academic Press, N.Y.

Whang, Y.C. and C.C. Chang, J. Geophys. Res., 70, 4175, 1965.

Wilcox, J.M., Space Phys. Rev., 8, 258, 1968.

Wilkerson, T.D., Solar Rphysics, 644, 1969.

ACKNOWLEDGEMENTS

I would like to thank Professor S. Olbert, my major thesis supervisor, for guidance and friendship throughout the course of this study. His diligence in working with me on the final form of this thesis and the many other generousities towards me, are gratefully acknowledged.

I am particularly indebted to Dr. A. Lazarus for his assistance and encouragement during the entire course of this study. I appreciate the opportunity to use the plasma data before their final publication.

I also would like to take this opportunity to thank the members of my Advisory Committee, Professors N. Phillips, R. Newell for helping me in carrying through the graduate study program.

I am indebted to Professors H. S. Bridge, V. Starr and V. Vasyliunas for their encouragement, suggestions and their interest to this work.

I would like to express my deep appreciation to my fellow graduate students, William Burke, Bruce Goldstein and Herbert Howe for many discussions about the physics of this thesis and also for their help in the final preparation of this work. I would also like to thank M. Heine-
mann for his assistance in computer techniques. Dr. J. Binsack kindly provided Explorer 33 plasma data prior to publication.

I would also like to thank Dr. N. F. Ness and his group at GSFC

for permission to use Pioneer 6 and 7 magnetic field data prior to publication.

This work was supported in part by the National Aeronautics and Space Administration under contracts: NGR 22-009-372 and NGR 22-009-289.

I would like to thank the entire Cosmic Ray Group at MIT for the hospitality shown me during my stay with them.

The first year and half of my graduate studies at MIT was supported by the Meteorology Department and I thank them for their many kindness.

Finally, I cannot express enough gratitude for all the patience and understanding given to me by my wife, who typed the first draft and a part of the final form of this thesis. I would like to thank Mrs. C. Webster who typed the final form of this thesis.

BIOGRAPHICAL NOTE

The author was born on April 3, 1940, in Kwin-Ming City, China, but moved with his family to Taiwan in 1949. He matriculated at the National Taiwan University in September 1958 and was awarded the Bachelor of Science degree in Physics in June of 1962. Subsequently he served one year as a second lieutenant in the Chinese Army. He joined the Geophysical Institute, University of Alaska as a graduate student and research assistant where, in June 1965, he received his Master of Science degree. The thesis dealt with the Mie scattering theory applied to noctilucent cloud particles. The fall semester of 1965 was spent teaching at the Geophysical Institute of the National Central University and for the Physics Department of the National Taiwan University. In February 1966, the author began his graduate work at the Massachusetts Institute of Technology toward the doctorate in the Meteorology Department. Shortly thereafter he joined the space plasma group of the Physics Department at the Center for Space Research under the supervision of Professor S. Olbert. Since then, he has been primarily concerned with the propagation of shocks in the interplanetary medium.